1-1-2013

Modeling And Characterization Of High Carbon Nanobainitic Steels

Gaganpreet Sidhu
Ryerson University

MODELING AND CHARACTERIZATION OF HIGH CARBON

NANOBAINITIC STEELS

by

Gaganpreet Sidhu,

B Tech, Punjab Technical University, 2002

M E, Panjab University, 2004

A dissertation

presented to Ryerson University

in partial fulfillment of the

requirement for the degree of

Doctor of Philosophy

in the Program of

Mechanical Engineering

Toronto, Ontario, Canada, 2013

Author's Declaration

I hereby declare that I am the sole author of this dissertation. This is a true copy of the dissertation, including any required final revisions, as accepted by my examiners.

I authorize Ryerson University to lend this dissertation to other institutions or individuals for the purpose of scholarly research.

I further authorize Ryerson University to reproduce this dissertation by photocopying or by other means, in total or in part, at the request of other institutions or individuals for the purpose of scholarly research.

I understand that my dissertation may be made electronically available to the public.

Abstract

MODELING AND CHARACTERIZATION OF HIGH CARBON

NANOBAINITIC STEELS

Doctor of Philosophy, 2013

Gaganpreet Sidhu

Mechanical Engineering

Ryerson University

Analytical models have been developed for the transformation kinetics, microstructure analysis and the mechanical properties in bainitic steels. Three models are proposed for the bainitic transformation based on the chemical composition and the heat treatment conditions of the steel as inputs: (1) thermodynamic model on kinetics of bainite transformation, (2) improved thermo-statistical model that eliminates the material dependent empirical constants and (3) an artificial neural network model to predict the volume fraction of bainite. Neural networks have also been used to model the hardness of high carbon steels, subjected to isothermal heat treatment. Collectively, for a steel of given composition and subjected to a particular isothermal heat treatment, the models can be used to determine the volume fraction of bainitic phase and the material hardness values.

The models have been extensively validated with the experimental data from literature as well as from three new high carbon experimental steels with various alloying elements that

were used in the present work. For these experimental steels, data on the volume fraction of phases (via X-ray diffraction), yield strength (via compression tests) and hardness were obtained for various combinations of isothermal heat treatment times and temperatures. The heat treated steels were subjected to compression and hardness tests and the data have been used to develop a new correlation between the yield stress and the hardness. It was observed that while all three experimental steels exhibit a predominantly nanostructured bainite microstructure, the presence of Co and Al in one of the steels accelerated and maximized the nano-bainitic transformation within a reasonably short isothermal transformation time. Excellent yield strength (>1.7 GPa) and good deformability were observed in this steel after isothermal heat treatment at a low temperature of 250°C for a relatively short duration of 24 hours.

Acknowledgements

Resume

Education

PhD,	**Mechanical & Industrial Engg.**	(2008-present)
	Ryerson University	
M E,	**Industrial Materials & Metallurgy**	(2002-2004)
	Panjab University	
B Tech,	**Materials Science & Engg.**	(1998-2002)
	Punjab Technical University	

Honors & Awards

Ontario Graduate Scholarship in Science and Technology   Sep 2008-Sep 2009

Ryerson Graduate Student Award   Sep 2009-Sep 2012

Research Student Stipend   Sep 2009-Sep 2012

Gold Medalist at the Center for Pedagogical Studies in Mathematics   Jun 1995

Peer Reviewed Publications

1. G. Sidhu, S.D. Bhole, D.L. Chen, E. Essadiqi, Development and Experimental Validation of a Neural Network Model for Prediction and Analysis of the Strength of Bainitic Steels, *Material and Design,* Vol. 41 (2012) 99-107.

2. G. Sidhu, S.D. Bhole, D.L. Chen, E. Essadiqi, An improved model for bainite formation at isothermal temperatures. *Scripta. Materialia.* Vol. 64 (2011) 73-76.

3. G. Sidhu, S.D. Bhole, D.L. Chen, E. Essadiqi, Reply To Comments on An improved model for bainite formation at isothermal temperatures. *Scripta. Materialia.* Vol. 65 (2011) 373-375.

4. G. Sidhu, S.D. Bhole, D.L. Chen, E. Essadiqi, Determination of volume fraction of bainite in low carbon steels using artificial neural networks. *Computational Material Science*. Vol. 50 (2011) 3377-3384.

Publications Under Review

1. G. Sidhu, S.D. Bhole, D.L. Chen, E. Essadiqi, A Fourier Method to Analyze Experimental Data of New Nanobainitic Research Steels (submitted to *Journal of Materials Science*).

2. G. Sidhu, S.D. Bhole, D.L. Chen, E. Essadiqi, Compression behaviour of high carbon nanobainitic steels (*under internal review*)**.**

3. G. Sidhu, S.D. Bhole, D.L. Chen, E. Essadiqi and F. Fazeli, Impact of isothermal transformation temperature on compression properties for high carbon nanobainitic steels (*under internal review*).

4. G. Sidhu, S.D. Bhole, D.L. Chen, E. Essadiqi, A thermodynamic and chemical composition based model for bainite transformation in steels (*under internal review*).

 Presentations

1. G. Sidhu, S.D. Bhole, D.L. Chen, Low Temperature Nanobainitic Steels: Processing and Structures. *24th Can. Mat. Sci. Conf.*, June 5-7, 2012, London, Ontario.

2. G. Sidhu, S.D. Bhole, D.L. Chen, Modeling of bainite formation at isothermal transformation temperatures. *23rd Can. Mat. Sci. Conf.*, June 22-24, 2011, Kelowna, BC.

3. G. Sidhu, S.D. Bhole, D.L. Chen, A displacive model for isothermal bainitic transformation. *23rd Can. Mat. Sci. Conf.*, June 22-24, 2011, Kelowna, BC.

Dedication

In loving memory of my brother, Parry (APS Virk)

Table of Contents

List of Tables

List of Figures

xvi

List of Illustrations

List of Appendices

Nomenclature

f	Volume fraction
f_s	Sampling frequency
h	Planks constant
k	Boltzman constant
m	Rate parameter
nH	Hidden layer
$\mathbf{o}$	Output vector of the neural network
o_i	ith element of $\mathbf{o}$
$s(x)$	Activation function
t	Time
t_p	Plate thickness
u	voulme of bainte sub-units
w_{ij}	Elements of the $\mathbf{W}$ matrix
ΔG_m	Driving pressure
ANN	Artifical Neural Network
B_s	Bainite start temperature
B	Model constant
C	Material constant
$\mathbf{D}$	Intermediate matrix containing the output of neural network
DFT	Discrete fourier transform
DSC	Differential scanning calorimetry
E	Error
G_n	Universal nucleation function
HV	Hardness
I	Integrated intensity of XRD peak
IP	Image processing
IRP	Incomplete Reaction Phenomenon
K_1	Constant of proportionality
L	Length period
$\bar{L}$	Mean linear intercept

LMBP	Levenberg-Marquardt backpropagation
M_s	Marteniste start temperature
N_i	Number density of nucleation sites
N	Number of pixels
NN	Neural network
OM	Optical microscope
Q^*	Activation energy
SEM	Scanning electron microscope
T	Temperature
T_h	Maximum temperature at which bainite take place
TTT	Time-Temperature-Transformation
V	Average volume
$V\alpha$	Volume fraction of bainite
$V\gamma$	Volume fraction of retained austenite
W	Weight matric in neural network
W_i	weight content of the ^{i}th alloying element
XRD	X-ray Diffraction
Z	Geometrical factor

Greek Symbols

λ	Autocatalytic parameter
γ	Austenite phase
Γ	Constant
β	Weight coefficients
θ	Weight coefficients, lattice spacing
σ_y	yield strength
ε_y	yield strain

Subscripts

aus	Austenitization
b	Bainite sub-units
calc	Calculated
expt	Experimental
i	Initially or potential
i, j, k	indices
iso	Isothermal temperature or time

max	Maximium
n	Strain hardening coefficient
nn	Neural network
C_i	Individual alloying elements

Chapter 1
Introduction

1.1 Background and Motivation

The ultimate goal of steel researchers is to obtain a product that is cheap to manufacture but at the same time meets certain requirements on mechanical properties. This can be achieved by the addition of alloying elements to the steel accompanied with an appropriate heat treatment. Collectively these two actions will influence the microstructure of the steel and thereby its properties. Of course, the engineering challenge is in determining the appropriate alloying elements and their proportions in the steel to give a positive outcome. Here, appropriateness implies alloying elements that not only aid in achieving the goals on the strength, ductility and toughness of the material but that are also less expensive to add.

With respect to the heat treatment of steels, it is well known that, starting from an initial austenite phase, depending upon the heat treatment conditions, microstructures such as allotriomorphic ferrite, pearlite, Widmanstatten ferrite, bainite and martensite can be obtained. These steels vary in their microstructure and morphological features due to the variations in their nucleation and growth kinetics. Among these, bainitic steels, of interest in this thesis, evolve from the austenitic phase by cooling at rates that are fast enough to avoid the diffusion-controlled transformations such as pearlite and at the same time sufficiently slow to avoid the diffusionless transformation into martensite [1]. Thus, the formation of bainite in steels occurs at a temperature between pearlite formation and martensite-start temperatures.

The focus on bainitic steels is because of their wide range of applicability. For example, transformation-assisted steels are used in automotive applications, inoculated acicular ferrite steels are used in the construction of oil platforms, high-strength alloys are used in the defense and aerospace industries, ultra-low carbon bainitic steels are used in the construction industries, etc. [1].

A more recent application includes railways, where tough rail steels are being manufactured that are extremely resistant to wear [2]. The microstructure of conventional rails is based on a mixture of cementite and ferrite in the form of pearlite. Cementite is hard and therefore provides wear resistance, but is at the same time brittle. On the other hand bainitic rail steel it has a much higher toughness while at the same time being harder due to the fine grain size and the presence of some martensite and retained austenite. Tests show that it has remarkable wear resistance and reduces wear on the wheels (see Figure1.1).

Medium-strength steels with the same microstructure but lower alloy content have applications in the automobile industry as crash reinforcement bars to protect against sidewise impact. There is also an application of bainitic forging alloys in components such as cam shafts [3]. Creep-resistant bainitic steels have been used successfully in the power generation industry. The alloys utilize chromium and molybdenum, which enhance hardenability. Further, heat treatment results in the precipitation of alloy carbides thereby improving the creep resistance.
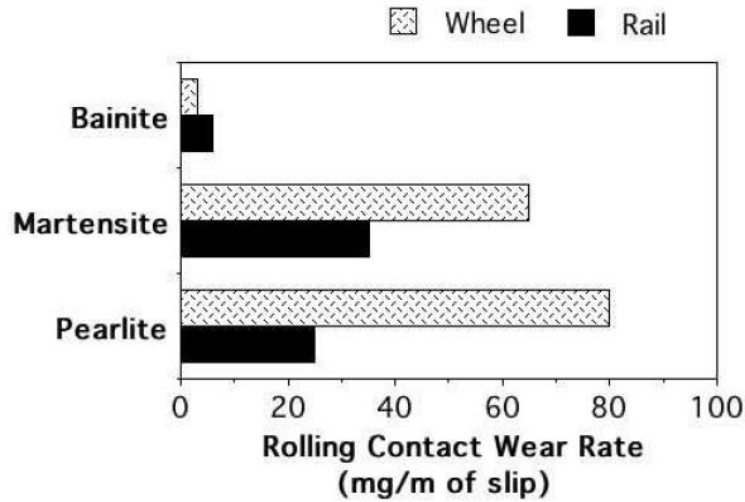
Figure 1.1: Test of whole-wheel showing wear resistance of carbide-free bainitic rail steels (source of image is Ref. [1]).

By inoculating molten steel with controlled additions of non-metallic particles, bainite can be induced to nucleate intragranularly on the inclusions, rather than from the austenite grain surfaces. This intragranularly nucleated bainite is called acicular ferrite. Inoculated steels are commercially used in demanding structural applications such as the fabrication of oil rigs for hostile environments.

Advances in rolling technology have led to the ability to cool the steel plate rapidly during the rolling process, without causing undue distortion. This has led to the development of accelerated cooled steels which have a bainitic microstructure, and can be highly formable and compete with conventional control-rolled steels [3].

Thus, depending upon the application, steels with different properties can be obtained via addition of various alloying elements accompanied by an appropriate heat treatment. Due to such

3

increased uses of bainitic steels, a lot of research, numerical as well as experimental, is focused in designing and developing (via alloy compositions and heat treatment) bainitic steels. As outlined in the following section, in this thesis, both approaches have been pursued, i.e., computational as well as experimental, to understand and design better bainitic steels.

1.2 Objectives

In pursuit of identifying high carbon nanobainitic steels with desired mechanical properties of high strength and deformability, a combined approach of modeling and experiments has been undertaken with an aim of developing modified models, validating them with respect to the experimental data and furthering the understanding of the structure-property relationship.

The specific objectives of the present research include the following:

a) Development of numerical models that can be used to predict more accurately the volume fraction of bainite for a given steel at a particular isothermal transformation temperature. In developing such a model the following goals must be achieved:

   i. It should take into account the incomplete reaction phenomenon which normally prevents 100% transformation of austenite into bainite.

   ii. It should involve as few model constants as possible.

   iii. It should account for the effects of the chemical composition of the steel.

   iv. It should be valid for a wide range of isothermal transformation temperatures and chemical compositions of the material.

b) Development of a numerical model to predict the hardness of the steel. Once again, the model should meet the following objectives:

   i. It should account for the effects of the chemical composition of the steel.

   ii. It should be valid for a wide range of isothermal transformation temperatures and chemical compositions of the material.

c) To ensure the validity of the models, three experimental steels have been produced and subjected to heat treatment, material characterization and mechanical testing to obtain the experimental data for evaluating the model performance. The specific steps in the last two tasks include:

   i. The characterization of the materials using two methods. In the first method, scanning Electron Microscope (SEM) is used to obtain the images of the microstructures and compare them with the standard reference bainitic microstructures to verify the formation of nanostructured bainite. In the second method, high temperature X-ray diffraction (XRD) is used on the material to identify and quantify the different phases.

   ii. Mechanical properties of the material are determined by conducting micro-hardness, macro-hardness and compression tests. Collectively, these can be used to understand the material properties such as strength and deformability.

This thesis has been structured as follows:

Chapter-2 presents a literature survey that contains a concise review of kinetics, transformation and effect of alloying elements on the bainitic steels.

Chapter-3 presents the theoretical background or framework on the thermo-statistical model for bainite transformation with different evaluation criterion.

Chapters-4 and 5, describe two models for the determination of the volume fraction of bainite and hardness, respectively, via neural network.

Chapter-6 describes the experiments carried out, including heat treatment parameters, material characterization and mechanical testing. The experimental results are presented along with the discussion of their significance in relation to the kinetics of bainitic steels in Chapter-7.

Chapter-8 summarizes the current work and points to the potential projects for continuing with this research.

Chapter 2
Literature Survey

The bainitic microstructure was first identified by Davenport and Bain [4] following the analysis of a series of heat treatment experiments at various isothermal transformation temperatures. In particular, the authors reported the discovery of an '*acicular, dark etching aggregate*' formed after isothermal holding between the temperatures for pearlite and martensite formation. The microstructures in Figure 2.1 were unlike martensite or pearlite observed in the same steel, and were found to be represented by their own 'C–curve' on the time–temperature–transformation (TTT) diagrams which they introduced as a convenient way to represent the time dependence of
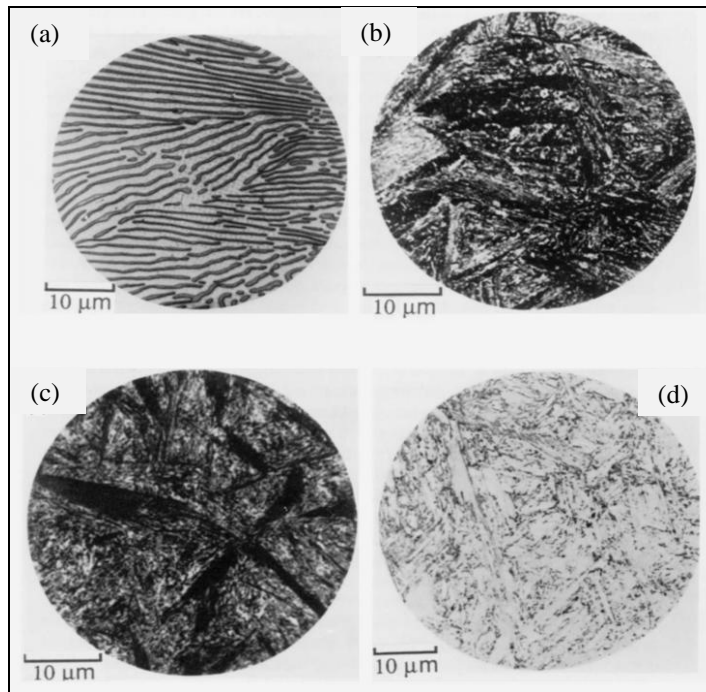
Figure 2.1: Microstructures in a eutectoid steel. (a) Pearlite formed at 720°C (b) bainite formed at 290°C (c) bainite formed at 180°C (d) martensite. (Image reproduced from Ref. [5]).
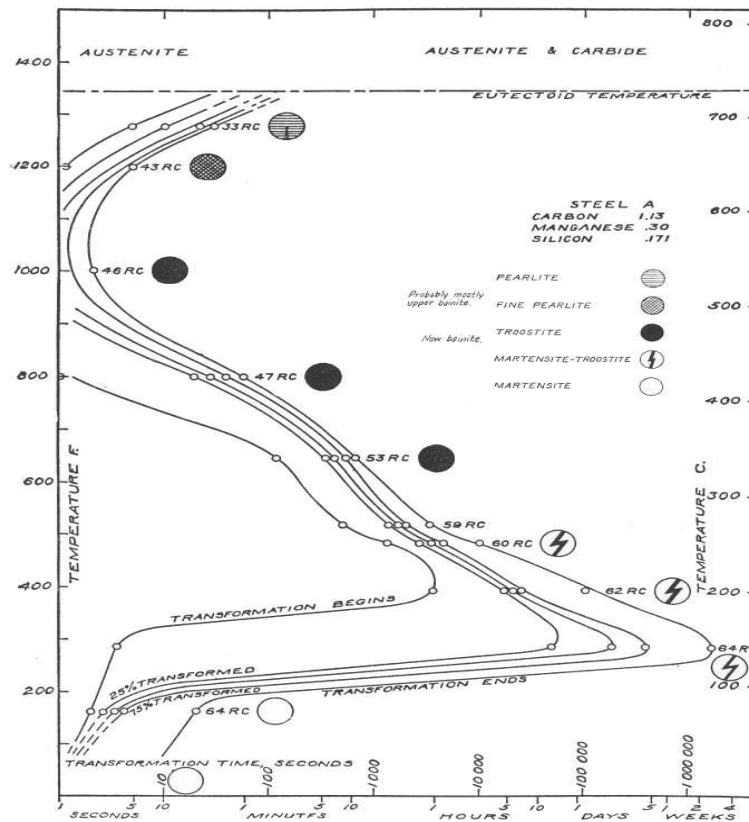
Figure 2.2: An illustration of the time temperature transformation diagram obtained using optical microscopy and dilatometry by Davenport and Bain [4]. (Image reproduced from Ref. [4])

transformation at different temperatures. Figure 2.2 shows an example TTT diagram reported by Davenport and Bain [4] for a high carbon alloy.

Before the coining of the name 'bainite', Hultgren [6] described the bainitic structure, as 'needles of troostite' that initially form as martensite needles and subsequently self–temper, being able to reject carbon. In doing so, they form carbides due to the higher temperature of transformation than that associated with martensite.

Following these initial discovery, several independent studies were made by researchers to understand these structures. Robertson [7] investigated the transformation rate of the microstructures that formed upon quenching from austenite and proposed that the slow growth of the ferrites constituent of bainite is best explained by transformation being controlled by carbon diffusion. Other work emphasised the similarity to martensite, and it was understood that bainite formed with a supersaturation of carbon [8-11]. Vilella [12] and Bain [13] proposed that transformation involved the formation of flat plates which form abruptly, before decarburising at a rate depending on the temperature. The process to reject carbon from the 'quasi–martensite' was proposed to take millionths of a second.

In general, it was recognized that the form of bainite was different in different temperatures ranges and as such, bainitic microstructures can be described as non-lamellar aggregates of carbides and plate-shaped ferrite.

2.1 Morphology of Bainite

While the above definition of bainite is quite general and valid for the entire bainitic range of temperatures, it has been noted that the morphology of the heat treated steel will be different in this bainitic range. Consequently, bainite can be classified according to morphology as *upper* and *lower* bainite (see Figure 2.3).

Upper bainite consists of aggregates of ferrite laths (sub-units) with the precipitation of coarse carbide in the austenite between the sub-units. On the other hand, in lower bainite, in addition to
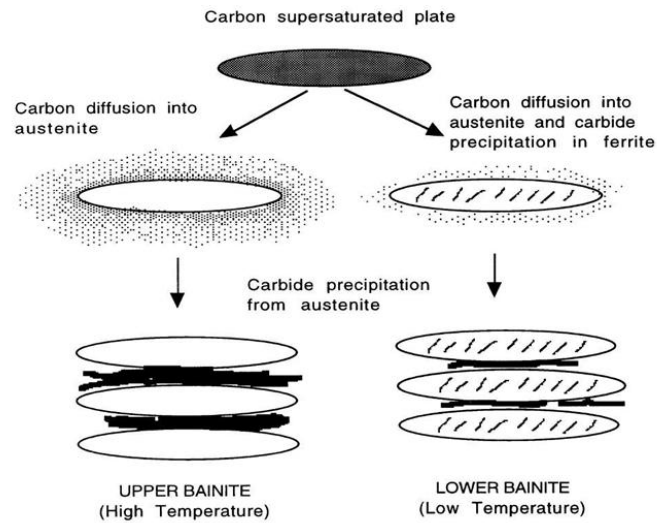
Figure 2.3 Illustration of upper and lower bainite showing the main differences in carbon partitioning and precipitation behaviors. (Image reproduced from Ref. [1]).

the inter-lath carbide, there is carbide precipitation inside ferrite laths also [14]. While it is accepted that bainite grows without diffusion, due to the relatively high transformation temperatures involved, the excess carbon is partitioned into the residual austenite [14, 15].

To describe the bainite formation in a little more detail, at high transformation temperatures, if the steel contains a sufficient quantity of silicon, the carbon remains within and stabilizes the austenite. Further, a large quantity of austenite might be retained to ambient temperature, with some transforming to high-carbon martensite [16, 17]. If the transformation temperature is low such that the carbon cannot partition rapidly, some of the excess carbon in the supersaturated ferrite might precipitate in the form of carbide, in which case a lower bainitic microstructure is obtained. Otherwise, upper bainite dominates the microstructure [17]. In either form of bainite,
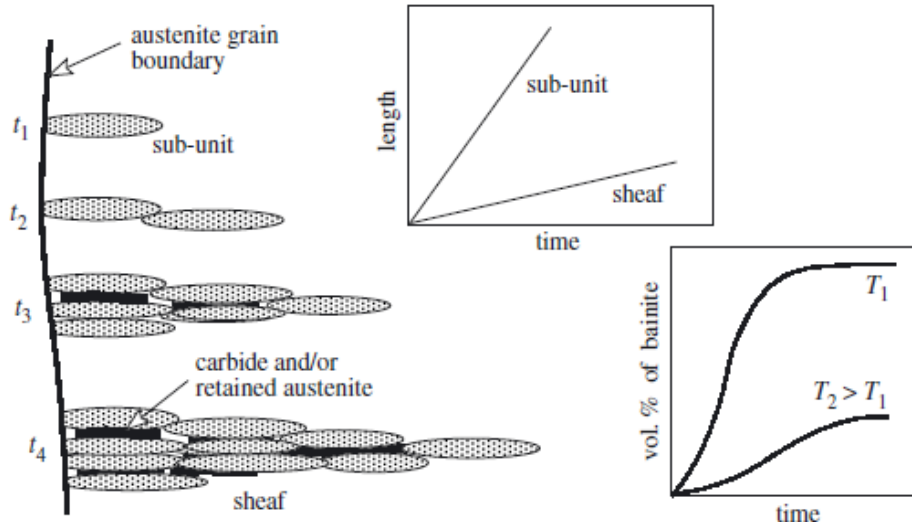
Figure 2.4: An illustration of the sheaf structure of bainite. (Image reproduced from Ref. [1]).

thin plates called subunits that are about 10 μm long and 0.2 μm thick [1], grow in clusters known as sheaves as shown in Figure 2.4.

2.2 Bainite Transformation Mechanism

The mechanism of the bainite transformation has been a subject of controversy, and discussing different schools of thought in detail is beyond the scope of the present work. However, a brief discussion is necessary so as to understand some relevant aspects of mechanisms which are discussed in the literature.

In general, there are two theories of bainite transformation, viz., the *diffusional* mechanism [18-21] and the *displacive* mechanism [1, 22-24]. The diffusional growth model is related to the

11
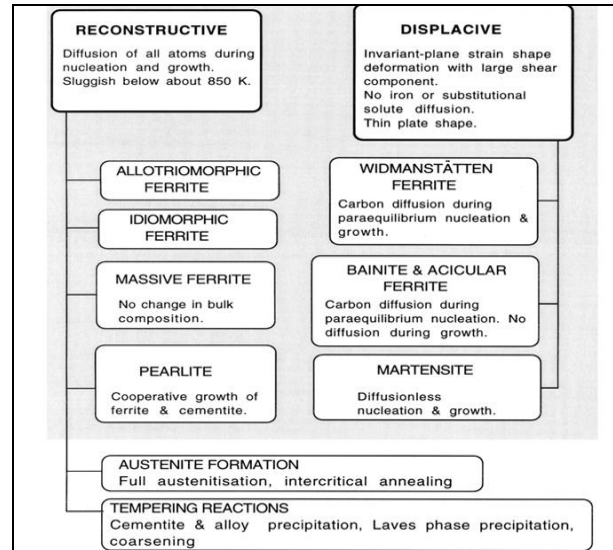
Figure 2.5: Flowchart summarizing the characterizing of transformations in steels. (Image reproduced from Ref. [1]).

reconstructive growth of both ferrite and carbides. As per the displacive mechanism, pioneered mainly by the research group of Bhadeshia at the University of Cambridge, the bainite sub-unit grows without partitioning of alloying elements, analogous to the martensitic transformation [1, 22-24]. A summary of these growth mechanisms and their byproducts is shown in Figure 2.5.

Apart from these, an intermediate theory was proposed by Speer *et al.* [25, 26] who suggest that bainite may initially grow by a martensite-like growth mechanism which is diffusionless followed by, or along with, carbon partitioning into austenite, with overall kinetics controlled by carbon diffusion. In other words, the authors suggest that the growth mechanism is both 'fully' displacive and `fully' diffusional. This growth mechanism was also proposed by Muddle and Nie [27], and Saha *et al.* [28].

2.3 T_o Concept and the Incomplete Reaction Phenomenon

While it is agreed widely in the literature that using appropriate heat treatment parameters, bainite transformation takes place via displacive mechanism, it is well known that the volume fraction of bainitic ferrite in the isothermally heat treated material is lower than 100%. This is attributed to the '*incomplete reaction phenomenon*' (IRP), the thermodynamics of which was founded by Zener [29, 30] and later refined by Wever and Lange [31].

The IRP is best explained by considering the graph of the carbon content of austenite and the corresponding limiting temperature (T_o) at which bainite reaction takes place (see Figure 2.6). Hence, this is also popularly known as the T_o concept in this area. As per this concept, a plate (or sub–unit) of bainite forms with supersaturation of carbon which is then rejected into the residual austenite. Subsequent to this, the next plate of bainite has to grow from the carbon enriched austenite. Eventually, this process ceases when the austenite carbon concentration reaches the T_o curve, since the nucleation of the next ferrite plate is thermodynamically unfavorable. More precisely, as long as the free energy of austenite is greater than the free energy of ferrite, the bainite transformation takes place. During the course of bainitic reaction, as carbon is partitioned into the austenite, the free energy of austenite decreases. Upon reaching the T_o line, there is no further carbide precipitation and the volume fraction of the bainitic phase, V_b can be roughly estimated using the relation

13
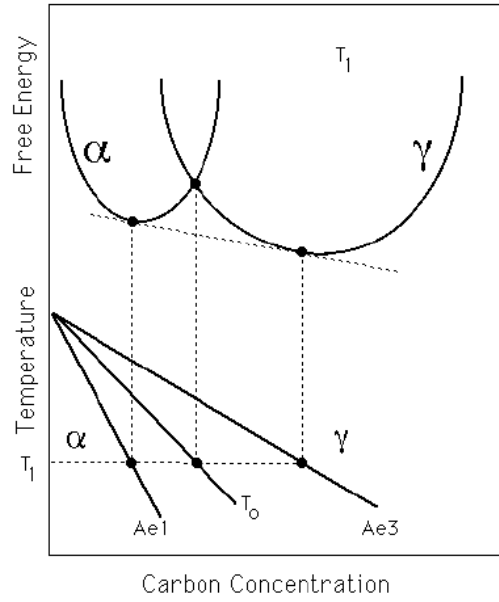
Figure 2.6: Schematic illustration of the T_o curve [1]. T_1 is the temperature corresponding to the free energy curves. (Image reproduced from Ref. [1]).

$$x_\gamma = \bar{x} + V_b \left(\frac{\bar{x} - x_\alpha}{1 - V_b} \right) \qquad (2.1)$$

where $\bar{x}$ is the average carbon content of the alloy, x_γ is the carbon content of the austenite and x_α is the final carbon content of the ferrite.

It should be noted that if the bainitic reaction occurred with diffusion, the ferrite would continue to grow until the carbon para-equilibrium carbon concentration and the transformation would then go on until the carbon concentration of austenite reached the Ae_3 curve, i.e., much larger volume fraction would be realized than what has been observed experimentally.

An important observation from this IRP is that greater volume fractions of bainite can be achieved by conducting transformation at lower temperatures. Also, the remaining austenite is available for further transformations, or can be retained after the sample is cooled to room temperature. With respect to this retained austenite, it should be noted that it can either be present in the form of large volumes where little bainite has formed, referred to as 'blocky austenite', or as thin films present in-between the bainitic ferrite plates. The final form of the retained austenite is important for the mechanical properties of the steel and can also affect the martensite content in the final quenched material.

2.4 Modeling of the Bainite Transformation Kinetics

While the theory behind bainite transformation kinetics is somewhat well formed, modeling the transformation kinetics is more challenging due to the complex nature of the transformation process. The focus of the present thesis is restricted to the displacive mechanism of bainite formation since it is now well accepted in the literature. Over the last couple of decades, a few models based on the displacive mechanism have been developed, some of which are discussed here for the sake of completeness.

Following a series of continuously evolving models [32-35], Matsuda and Bhadeshia [36] presented a theory of bainite evolution as a function of time, temperature and chemical composition and austenite grain size. Their model incorporated the details of the mechanisms of transformation such as: (a) nucleation begins at the austenite grain boundary, (b) growth of sheaf occurs by the repeated nucleation of small platelets. Evaluation of this model with respect to the

experimental data of three steels showed only a reasonable performance of the model at several temperatures.

Recently, Van Boheman and Sietsma [37] presented a displacive model of bainite transformation in which the nucleation rate was considered to be dependent on the number of potential nucleation sites, autocatalytic factor and activation energy. Subsequently, the authors also employed this model to medium carbon steels. They also showed that for a given composition, once the model parameters are obtained using the experimental data, the model performs satisfactorily in predicting the bainite transformation kinetics [38]. The authors presented a validation of this model for lean silicon steels to demonstrate a satisfactory performance of this model. However, the problem with their model is that they normalize the predicted volume fraction and so the transformation curves always predict a 100% transformation at steady state. To calculate the actual volume fraction of bainite, which is normally lower than 100% due to the incomplete reaction phenomenon, the predicted transformation profiles will have to be multiplied by the experimental value of the maximum volume fraction of bainite.

Santofimia *et al*. [39] proposed a geometrical conception of the transformation thereby avoiding the use of autocatalysis factor. In this model, the kinetics of nucleation at the austenite grain boundaries and on the previously formed subunits has been separated via a coupled equation formulation. In the second part of this study they applied the model to medium-carbon-high-silicon steels and demonstrated a mixed performance of this model for several steels [40]. In fact, this is the only study where a much larger number of steels are considered for the model evaluation. However, the model predictions are good only for a few steels.

A pertinent review of these relevant displacive models is also summarized in the work of Santofimia *et al.* [41]. In general, it has been observed that in all these models for bainitic transformation, while the underlying principle is a displacive growth mechanism, they vary in their expressions for the nucleation rate. However, these models perform well only with respect to a few selected steels. Also, most of these models involve a large number of tuning constants that can be adjusted to match the experimental data. As a result, applying them to new steels becomes increasingly difficult. Keeping these points in mind, the main objective of the present thesis is to develop models that have fewer model constants and that are applicable to more steels. Furthermore, for the model development studies pertaining to this thesis, the displacive method of growth of bainitic sheaves has been considered due to the fact that this theory is well established and widely accepted in the literature.

2.5 Experiments on Bainitic Steels

In steel research, on the experimental front, attention is given to the design and development of steels with certain desired properties. This goal can be achieved using a combination of heat treatment parameters and addition of alloying elements.

The major purpose of heat treatment of a material is to reduce the brittleness imparted by excessive hardening and to introduce the degree of ductility and strength necessary for a given application. In doing so, it is desirable to preserve the strength and hardness of the material. Specifically, the choice of isothermal heat treatment is particularly attractive due to the following reasons:

1. Conducting an isothermal heat treatment at a constant temperature is much easier than the continuous cooling transformations in which the cooling rate must be carefully controlled.

2. Unlike the continuous cooling transformations where one is more likely to see heterogeneous microstructures with not only different phases but also different plate sizes, for instance, in bainitic phase, in isothermal transformation, by maintaining the material at a fixed temperature, a uniform microstructure can be obtained. In case of bainitic steels, this means uniform plate thickness and thereby material properties. Of course, there is still the element of time duration for which this isothermal heat treatment is done, that can influence the overall microstructure and phase content of the material. In fact, by regulating the transformation time, i.e., the duration for which the material is isothermally heat treated, it is possible to obtain a desired phase fraction in the material, thereby affecting the material strength and deformation properties.

3. Another advantage of heat treatment of steels is that severe internal stresses that may reside in the material due to rapid cooling from the austenite phase can be relieved by isothermal heat treatment.

As will be discussed in the ensuing sections, by adding appropriate alloying elements, one can control the thermodynamic behavior of the transformation as well as the subsequent microstructure. Thus, certain alloying elements that increase the transformation kinetics are desirable to reduce the time needed for the complete bainitic transformation at a certain temperature. On the other hand, certain alloying elements are likely to aid in improving the mechanical properties of the material, and are therefore desirable in the composition. Thus, an

optimal chemical composition in conjunction with the isothermal heat treatment at an appropriate temperature can yield steel with good strength, toughness and ductility properties. While there is a plethora of work in the literature relating to this, some of the key studies relevant to the present thesis are discussed below.

C. Garcia-Mateo *et. al* [42], demonstrated that in a high carbon steel where carbide precipitation is suppressed, extremely thin bainite plates can be obtained by isothermal transformation at temperatures as low as 200°C. However, the time taken for nucleation at this temperature can be many days. To overcome this delay, the authors proposed the addition of cobalt and aluminum in a subsequent study. Additionally, the authors also suggested that by refining the austenite grain size a further acceleration of bainite formation can be achieved [43].

The authors also conducted an investigation to characterize the important mechanical properties, including the tensile strength, ductility and the toughness of these alloy steels. For this the authors generated the microstructure via isothermal transformation temperatures in the range 200°C-300°C. From their study, the authors reported yield strength as high as 1.5 GPa and an ultimate tensile strength between 1.8 to 2.2 GPa, depending on the isothermal transformation temperature. They also concluded that the high strength is frequently accompanied by ductility and respectable levels of fracture toughness. They attributed these unusual combinations of properties to the exceptionally fine scale of the carbide-free bainitic microstructure and the associated retained austenite [44].

Experimental investigations on the low temperature bainite formation were also successfully conducted by F. G. Caballero *et al*. [45-48]. The authors were able to obtain very fine bainite plates that were about 30-40 nm in thickness resulting in a microstructure with high strength and high toughness.

Bhadeshia and coworkers [43, 45, 49] have demonstrated the development of steels with an ultimate tensile strength of 2500 MPa, a hardness of 600–670 HV and toughness in excess of 30–40 MPa-m$^{1/2}$. To achieve this, their group used slow cooling techniques so that residual stresses are avoided, even in large pieces of steels. In fact, this led to several new terms being coined from this approach:

a) Cold-bainite because of the low temperature growth regime.

b) Hard-bainite because the hardness of the microstructure is almost close to that of the hardest untempered martensite.

c) Strong-bainite because of the tensile strength in excess of 4.5 GPa.

d) Fast-bainite for the steels containing cobalt and aluminum that accelerate the transformation process.

Thus, at this time it can be said that low isothermal transformation temperature in conjunction with accelerator elements can aid in developing bainitic steels with good mechanical properties and at the same time reduce the energy required for the production of such steels.

2.6 Effect of Alloying Elements

In pursuit of appropriate alloying elements to obtain good strength and ductility, a literature search reveals several elements that can used to meet the desired properties:

Silicon is known to decrease the lower-bainite start temperature [50]. When added in excess of 1%, Si aids in the enrichment of carbon in the austenite by preventing carbide precipitation. The final microstructure, obtained in such silicon- rich steel, consists of fine plates of bainitic ferrite separated by carbon enriched regions of austenite. This would give rise to good mechanical properties.

Gordine and Codd [51] and Owen [52] suggested that silicon postpones the final stage of tempering because, in the presence of sufficient silicon (>1wt %), the tempering reaction is controlled by the diffusion of silicon instead of carbon.

Silicon is also added in bainitic steels to suppress cementite precipitation [53, 54]. When cementite forms under paraequilibrium conditions, the silicon is trapped inside the cementite lattice, reducing the free energy and ultimately the kinetics of precipitation [55]. Thus, carbon that is partitioned into the residual austenite after bainitic transformation does not precipitate as cementite. Instead it remains there making the austenite stable at ambient temperature [16, 56, and 57].

On the other hand, under equilibrium conditions the solubility of silicon in cementite is negligible due to the partitioning into the austenite and its concentration hardly affects the phase fraction. Hence, at elevated temperatures, in transformations involving cementite, small fractions of Si do not have any detrimental effects [55]. Additionally, in view of the fact that the driving force for the reaction is large even for paraequilibrium precipitation, silicon is also ineffective in retarding the precipitation of cementite if the parent phase is significantly supersaturated with carbon. Finally, Si harms the surface quality of steels and limits their use in galvanised products, where Al or P is preferred instead [58].

Aluminium is a good carbide-suppressing element. However, it does not contribute to the strengthening of ferrite. Results obtained in TRIP-aided steels (Table 2.1) containing various levels of Al and Si have shown that for the same holding time, the amount of untransformed retained austenite was less in the Al-steel compared with Si-steel. However, Al-Si steel exhibits the lowest amount of retained austenite [59].

Further, full or partial substitution of Si with Al neither decelerates bainite transformation nor affects the carbon content of retained austenite.

Table 2.1: Chemical composition of steels investigated by Jacques et al. [59].

wt%	C	Mn	Si	Al	P	S	N
Al 1	0.11	1.55	0.059	1.5	0.012	0.007	0.017
Si 1	0.11	1.53	1.5	0.043	0.008	0.006	0.0035
Al-Si	0.0115	1.51	0.49	0.38	0.003	0.009	0.03

Perhaps the greatest benefit of the addition of Al to the steel is its ability to accelerate the transformation speed. Mertens *et al.* [60] demonstrated the pronounced effect of Al in accelerating bainite transformation kinetics in comparison with Si.

Molybdenum is effective as a ferrite solid-solution strengthening element which inhibits carbide precipitation [61, 62]. Molybdenum decreases the bainite start temperature. This will refine the microstructure thereby resulting in a material with improved hardness and strength. Addition of Mo, will help to suppress the formation of pearlite and polygonal ferrite and yield more bainitic microstructure [5].

Manganese plays an important role during steelmaking, via helping in deoxidation of the melt by forming MnO [63]. It also aids in converting the sulphides into MnS [63]. It is important in enhancing the hardenability of the steel [65]. Addition of Mn, in amounts greater than 0.8wt% increases the hardness of the steels by decreasing the plate width in the microstructures [1]. Specifically, plate widths of the order of 20-40 nm can be achieved [47]. These finer microstructures increase the hardness of the material [43].

Manganese refines the grain size and thereby improves the tensile strength [64]. Manganese is also very effective in lowering the M_s temperature [3] and is known to promote the retention of austenite [66]. However, a negative effect of high manganese content is that it decreases ductility as well as weldability.

In the context of the bainitic transformation, addition of Mn shifts the T_o temperature, favoring a higher volume fraction of transformation [67]. Manganese also decelerates the pearlite reaction because of its slow diffusivity even through the moving interface [54].

Cobalt is added primarily for low-temperature bainite transformations that generally proceed at a very slow rate [43]. The difference in the free energy of austenite and ferrite is the driving force for transformation. Both nucleation and growth rates, that are a function of this driving force, can be increased by addition of cobalt [68]. This faster nucleation and transformation will result in finer microstructures that will in turn increase the strength and hardness of the material [43].

Chromium is included in steels that are needed in the hydrogen rich environment, e.g., coal conversion plants, where hydrogen can cause a lot of damage and eventual wearing of the steel [1]. The addition of chromium will lead to a microstructure that it quickly replaces the cementite with various carbides, thereby shielding the steel from the severe hydrogen attack. In other words, it increases the wear resistance of the steel. Additionally, Cr is known to suppress the bainite start temperature. This will result in microstructure refinement that will increase hardness and strength.

Vanadium enhances acicular ferrite microstructure and improves the toughness of the material. Essentially, the microstructure consists of fine interlocking ferrite plates [69]. Vanadium carbides in the microstructure are more resistant to tempering. As a result of this, the material becomes increasingly creep resistant. Additionally, the resulting material also has a superior hardenability [1].

Thus, it can be stated that to obtain a steel with a good combination of strength and ductility, isothermal heat treatment in the bainitic range of temperatures is desirable. Additionally, the steel must contain some favorable alloying elements that not only enhance the transformation speed but also result in improved mechanical properties of the steel. To this end, it is desirable to get a lower bainitic microstructure, i.e., thin bainitic plates, ideally of the order of nanometers.

Finally, for a good working range of bainitic temperatures, it is necessary to work with high carbon steels. In fact, in high purity Fe–C alloys, lower bainite is not obtained when carbon concentration is less than around 0.4 wt %. On the other hand, by employing high carbon steels, the gap between the B_s and the M_s temperature widens. This is because high carbon content helps to suppress the M_s temperature. This means, depending upon the desired microstructure it is possible to develop lower as well as upper bainitic steels.

In summary, from the literature survey of the research pertaining to bainitic steels the limitations in the current state of the models can be summarized as follows:

1. Some of the models for the bainitic transformation kinetics assume a 100% transformation. This is contrary to the physics of the bainitic transformation, i.e., the incomplete reaction phenomenon is completely neglected. The models that do not assume 100% transformation and that account for the incomplete reaction phenomena are only valid for a limited number of compositions and a small range of isothermal transformation temperature.

2. The models in the literature involve several tuning constants that require to be adjusted to match the experimental data.

3. With respect to understanding the mechanical properties of the steel, some correlations are present in the literature that relates hardness to the yield strength of the steel. However, all these correlations are valid only for a limited number of steels.

In this thesis, the above deficiencies in the current state of computational/analytical research in bainitic steels are addressed. Specifically, improved bainitic transformation models are proposed that take into account the incomplete reaction phenomena, thereby avoiding the prediction of 100% volume fraction of bainite. The proposed models, with fewer model constants, take into account the effects of alloying elements and are valid for a wide range of high carbon steels. Apart from these, understanding the bainitic transformation as well as the mechanical properties using the principles of artificial neural networks has also been explored in this thesis.

Finally, by undertaking the experimental investigation on newly designed high carbon nanobainitic research steels, our current understanding of the bainitic transformation kinetics is deepened. Further, the new data are also used for the validation of the models proposed in this thesis as well as for the development of an improved mechanical property correlation.

Chapter 3

Thermodynamic and Thermo-statistical models for Bainitic Kinetics

3.1 Introduction

In this chapter, pursuing the displacive theory of bainite formation, a modified form of the thermodynamic model of Van Bohemen *et al*. [37], is presented. The displacive theory of bainite transformation is well established and sufficiently proven experimentally. However, there is still scope for a more comprehensive thermodynamic formulation that is applicable to a wide range of steels. The model development has been presented in two stages.

In the first stage (Model 1), a model is proposed for the low carbon steels with several alloying elements. As will be discussed in the following section, the model includes the effects of alloying elements and it incorporates several constants that must be determined experimentally.

This issue is addressed in Model-2 that is presented in Section 3.3, were fixed constants, independent of the steel compositions, are used. Further, this enhanced model is applicable for low-carbon as well as high-carbon steels and is validated more extensively with respect to several criteria to establish its validity, which is a second stage.

3.2 Model-1: Background and Theoretical Framework

The key features of this model include:

(1) a temperature dependent expression for the number density of potential nucleation sites N_i, and

(2) a temperature dependent scaling function in the expression for volume fraction of bainite (f) to account for the incomplete reaction of austenite into bainite [1]. This differentiates the current model from that of Van Bohemen, whose expression for f predicts 100% transformation requiring the experimental data to be normalized.

The model has been validated with the experimental data taken from Refs [33, 36, and 40] of three steels containing high levels of silicon whose compositions have been summarized in Table 3.1.

The starting point of this model is the equation for the rate of change of the volume fraction of bainite that is given according to Van Bohemen *et al.* [37] as

$$\frac{df}{dt} = \frac{dN}{dt}V_b,$$

(3.1)

where f is the volume fraction of bainite, N is the number of nucleation sites and V_b is the average volume of the bainitic subunit. Following the propositions of Matsuda and Bhadeshia [36], the average volume of bainite subunits (V_b), [50, and 70] has been calculated as

$$V_b = 2\left(\frac{T-528}{150}\right)^3 \mu\,\text{m}^3,$$

(3.2)

Table 3.1: Chemical composition of the three steels validated for the present model. The values in the brackets indicate the references for the experimental data.

	Chemical compositions (wt %)						
Steel	C	Si	Mn	Ni	Mo	Cr	V
Steel-1 [36, 40]	0.44	1.74	0.67	1.85	0.83	0.39	0.09
Steel-2 [36]	0.39	2.05	0.00	4.08	0.00	0.00	0.00
Steel-3 [33]	0.38	1.29	1.73	-	-	-	-

T being the temperature in Kelvin at which the isothermal transformation takes place. The rate of change of the number density of nucleation sites, dN/dt, is given according to Ref. [37] as

$$\frac{dN}{dt} = \frac{kT}{h}(1-f)N_i(1+\lambda f)\exp\left(\frac{-Q^*}{kT}\right),$$ (3.3)

where k is the Boltzman constant, T is the temperature in Kelvin, h is the Planks constant, λ is the autocatalytic nucleation parameter (c.f. Table 3.2), Q^* is the activation energy and N_i is the number density of the potential nucleation sites that are *initially* present in the austenite.

In the present model the following expression of Singh *et al*. [34] was used for N_i

$$N_i = \frac{B}{\bar{L}\alpha_p},$$ (3.4)

where $\bar{L}$ is the mean linear intercept representing the austenite grain size (c.f. Table 3.2) and α_p relates the volume of a bainite subunit (u) and its thickness (u_w) as $\alpha_p = u/u_w^3$. In order to compute u_w, the aspect ratio of 0.2/10/10 and the value of $\bar{L}$ are summarized in Table 3.2. It should be noted that while Singh *et al*. [34] assumed B as a constant, in the present model,

Table 3.2: Values of model constants and parameters used for the three steels. Constants Ci have been chosen in such a way that they maximize the agreement between the transient profiles of the experimental data and the calculations.

Steel	C_1	C_2	C_3	C_4	λ	L [µm]	u_w [µm]
Steel-1	1.004×10^{30}	-100.49	-3.3384	2.7195	90	95	0.95
Steel-2	4.838×10^{23}	-80.549	-2.0117	1.8334	100	38	0.38
Steel-3	2.831×10^{26}	-83.865	-1.9399	1.9375	32	25	0.05

B is assumed to be a temperature-dependent function in the following form that is considered to dictate the initial reaction rate, i.e.,

$$B = C_1 \exp\left(C_2 \frac{T}{T_h} \right),$$ (3.5)

where C_1 and C_2 are two material constants to be determined later. The temperature T_h used for normalization represents the maximum temperature at which bainite formation takes place and has been chosen as a constant with a value of 629°C [37] for all steels. This expression for N_i is different from the one used by Van Bohemen *et al* [37]. Their expression of the temperature- and composition-dependent N_i relied on a parameter that was experimentally determined. Further, this parameter for the martensite and bainite was related via another geometrical factor, Z that was taken as a constant for all steels. Their expression of N_i did not account for the thickness or the volume of the bainite subunits. Further, the average value of the bainite subunit volume that the authors used in their expression cancels out with the rate of change of f and their model is essentially independent of the volume of bainite subunits. In the present model, the impact of the

bainite subunits' volume as well as thickness has been accounted for via the parameter α_p,

consistent with the propositions of Matsuda and Bhadeshia [36].

The activation energy Q^* of austenite to bainite transformation is calculated using the following

relation [37]

$$Q^* = Q_0 - K_1 \Delta G_m,$$ (3.6)

where ΔG_m is the driving pressure for bainite nucleation and Q_0 is a constant, expressing the

activation energy in the limit that the driving pressure becomes zero. Further, K_1 is a constant of

proportionality that takes the values 15.049 in this investigation. This has been obtained by a

linear extrapolation of the values of K_1 from the values reported by Van Bohemen *et al*. [37].

The values of Q_0 have been suggested in the range of 180-210 kJ mol^{-1} by Van Bohemen *et al*.

[37]. In this study, a value of 188 kJ mol^{-1} [37] has been used for all three steels at all

temperatures.   The   driving   pressure   for   bainite   nucleation, ΔG_m,   is   given   by

$\Delta G_m = G_n - 7.66(T_h - T)$ J mol^{-1} [37]. The universal nucleation function, G_n, that was originally

determined by Ali and Bhadeshia [71], has been calculated as $G_n = 3.637(T - 273.18) - 2540$ J

mol^{-1}[37].

Integrating Eq. (3.1) using the Equations (3.3) and (3.4), Van Bohemen's expression is

$$f = \frac{1 - \exp(-\kappa(1+\lambda)t)}{1 + \lambda \exp(-\kappa(1+\lambda)t)}.$$ (3.7)

In this work, Van Bohemen's rate parameter, κ, is replaced by the new rate parameter, *m*, where

$$m = \frac{kT}{h} \frac{B}{\bar{L} \alpha_p} \exp\left(\frac{-Q^*}{kT}\right) V_b. \tag{3.7A}$$

In Equation (3.7) f approaches 1 as t tends to infinity, indicating a 100% transformation of the austenite phase. However, as mentioned earlier, the incomplete reaction phenomenon prevents a 100% transformation of austenite to bainite [1]. To take this fact into account Equation (3.7) is multiplied by a temperature dependent scaling function $C_3 \frac{T}{T_h} + C_4$, where C_3 and C_4 are material constants. Thus, the final expression for f becomes

$$f = \frac{1 - \exp(-m(1+\lambda)t)}{1 + \lambda \exp(-m(1+\lambda)t)} \left(C_3 \frac{T}{T_h} + C_4\right). \tag{3.8}$$

Material constants: Four material constants have been used in this study. These have been obtained as follows: For each steel, at a given temperature a value of B was chosen such that the model was able to predict the initial reaction rate of the experimental data reasonably well in the graph of volume fraction f vs. time t. In choosing these tuning values of B, it was noted that for given steel the initial reaction rate must decrease with an increase in temperature [32]. Next, a plot of B versus the normalized temperature (T/T_h) showed that B decreased exponentially with temperature and follows the relation of Equation (3.5) (c.f. Figure 3.1).

As mentioned earlier, this temperature dependence is expected and in fact the constants C_1 and C_2 being different for each steel is also evidence that B is also dependent on the composition of the steel, i.e., these are material constants. The values of C_1 and C_2 for all three steels are summarized in Table 3.2. It must be stated that in tuning the values of B for each steel, a particular value of autocatalytic factor (λ) and the mean linear intercept $\bar{L}$ were assigned for each steel. These values are the ones reported in literature and summarized in Table 3.2.
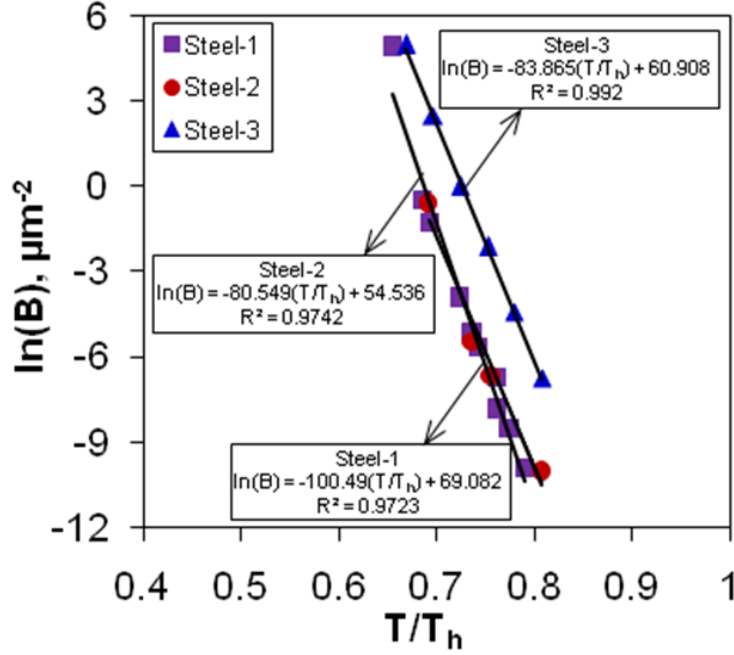
Figure 3.1: Trend of ln(B) versus the normalized temperatures.

In a similar manner, the experimentally determined maximum volume fraction, $f_{max}^{(experiment)}$, was plotted against the normalized temperature (T/T_h) for each steel at all temperatures (c.f. Figure 3.2).

As seen in this figure, $f_{max}^{(experiment)}$ follows a linear trend with the temperature, T, i.e.

$$f_{max}^{(experiment)} \approx C_3 \frac{T}{T_h} + C_4. \tag{3.9}$$

The values of the two constants, viz., C_3 and C_4, were determined from this linear trend. As in the case of C_1 and C_2, the fact that these constants are different for each steel indicates that these are also material constants and are summarized in Table 3.2.
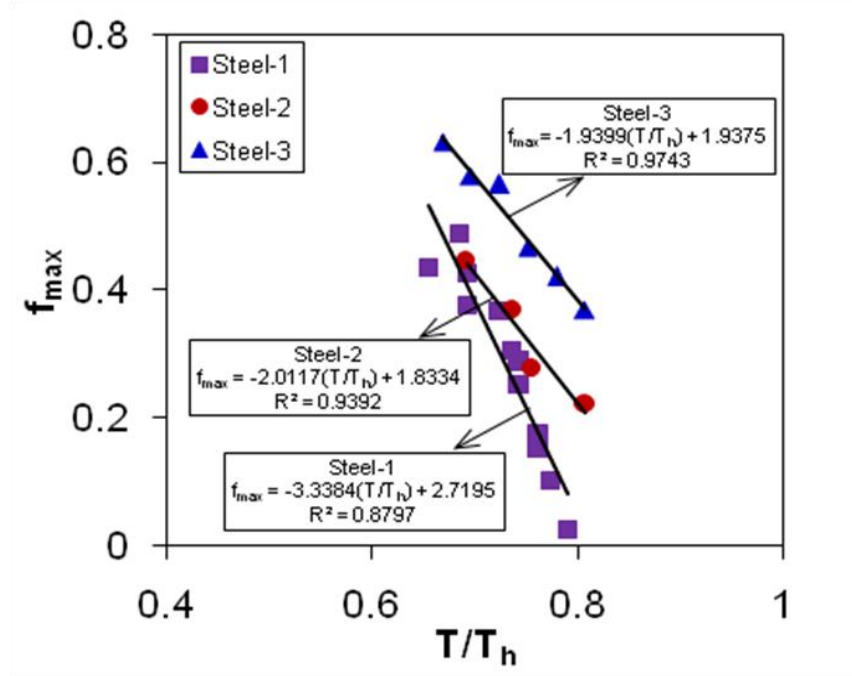
Figure 3.2: Maximum volume fraction of bainite versus the normalized temperature.

It must be noted that a higher order polynomial fit of the experimental data of $f_{max}^{(experiment)}$ in Figure 3.2 did not result in a significant improvement. Hence, the linear approximation of $f_{max}^{(experiment)}$ at a given isothermal temperature was used here.

3.2.1 Model Validation

As part of model validation, experimental data of three steels (Table 3.1) at various temperatures have been considered. In all three steels the maximum volume fraction of bainite (f_{max}) is predicted with reasonable accuracy. The accuracy is exceptionally good for Steels 2 and 3 where f_{max} is well predicted for the temperature ranges of 350°C – 455°C (Figure 3.4) and 330°C –
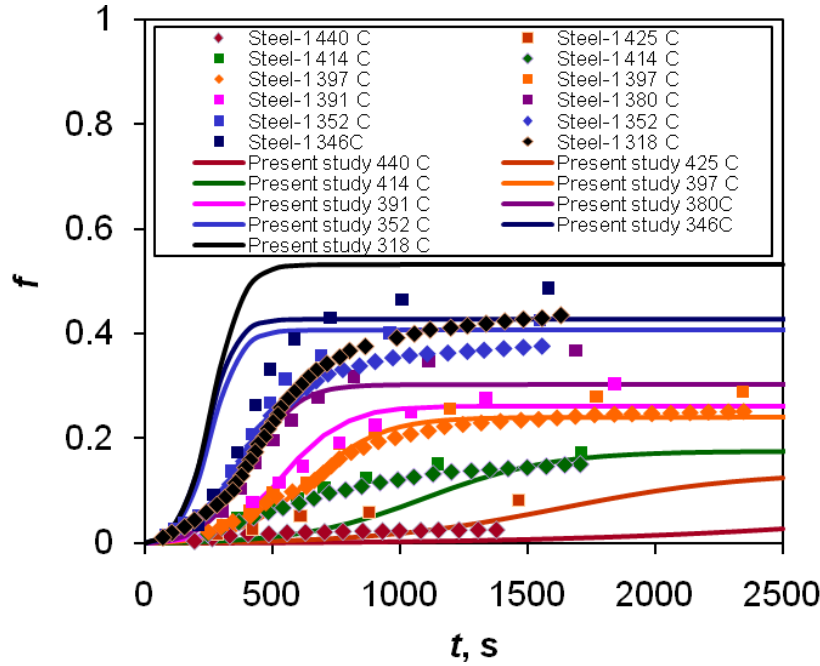
Figure 3.3: Measured (symbols) and predicted (solid lines) isothermal transformation kinetics of bainite for Steel-1. Experimental data are from Ref. [36, 40].

455°C in Steels 2 and 3, respectively (Figures 3.4 and 3.5). In Steel-1, the prediction is good only in the range 345°C $<T<$425°C (Figure 3.3).

In all three steels, the model demonstrated a mixed performance in predicting the initial reaction rate. In Steels 1 and 2, the rate of increase of *f* decreases with *T* consistent with previous findings [32].

In Steel-1 the model over- and under-predicts the initial reaction rate at lower temperatures ($T<$ 380°C) and higher temperatures (T> 400°C) respectively. For intermediate temperatures (380°C $<$ T $<$ 400°C), there is a good agreement of the initial reaction rate with the experimental data.

35
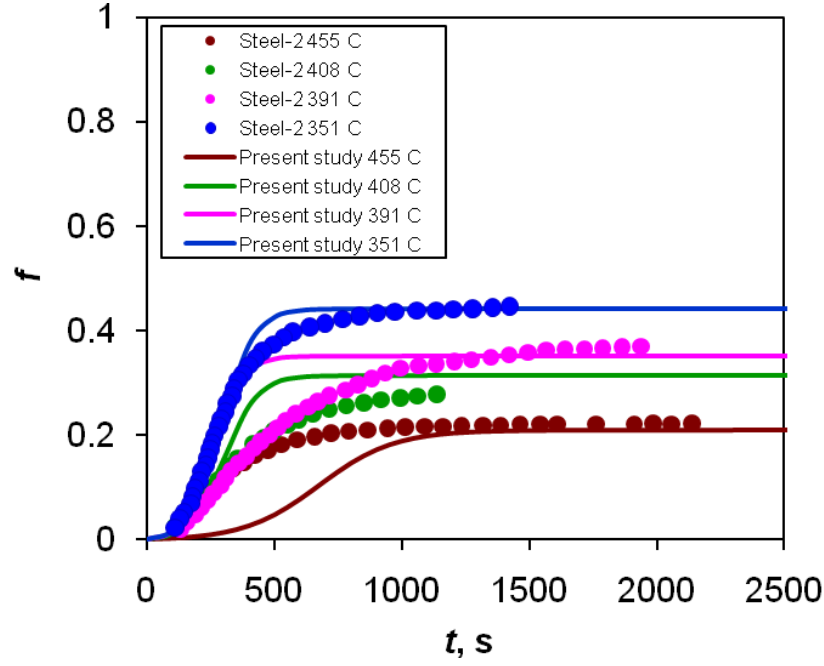
Figure 3.4: Measured (symbols) and predicted (solid lines) isothermal transformation kinetics of bainite for Steel-2. Experimental data are from Ref. [36].
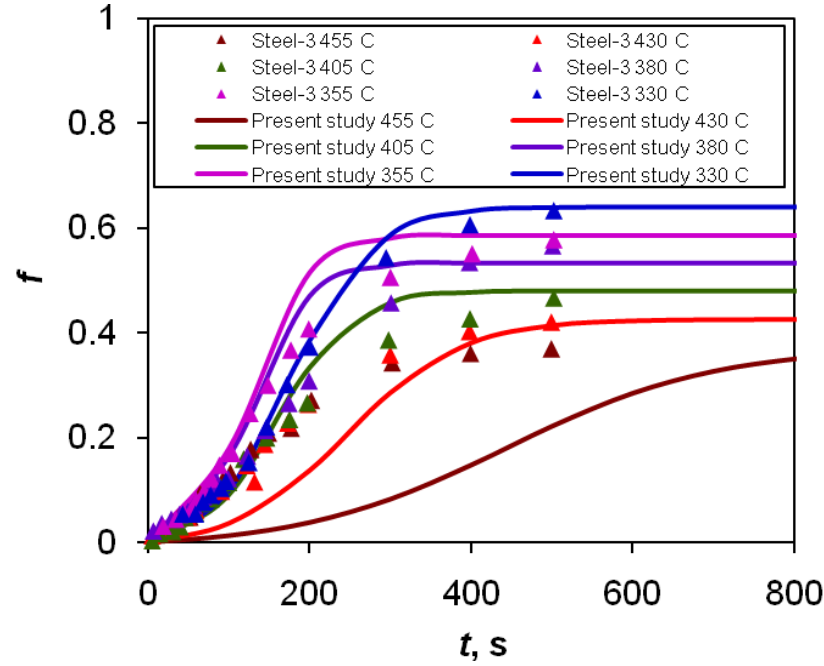
Figure 3.5: Measured (symbols) and predicted (solid lines) volume fraction of bainite for Steel-3. Experimental data are from Ref. [33].

In Steel-3 there is a good prediction of the initial reaction rate up to ~ 150 seconds for 330°C, 355°C and 405°C and an under prediction at the highest temperature of 430°C. At 330°C the model predicts the transformation kinetics very well. At 405°C and lower temperatures the model over predicts the initial reaction rate after the first 150 seconds.

This is probably an indicator that the material constants are not reflective of the high manganese content that impacts the initial reaction rate [32]. The discrepancy of the present model is similar to the computational results of a different model proposed by Chester and Bhadeshia [33] where the initial reaction rate is faster at 330°C than at 355°C.

3.2.2 Model-1: Summary

In addition to a temperature dependent expression for the initial nucleation site density, the present model also includes a temperature dependent scaling function to predict the maximum volume fraction of bainite at a given isothermal transformation temperature. Thus, unlike Van Bohemen's [37] approach, the present model incorporates the incomplete reaction phenomena. The model has been validated with respect to the experimental data of three high silicon steels at various temperatures and shows fairly good prediction of the transformation profile. The poor predictions of the initial reaction rate at certain (high) temperatures may be attributed to the fact that the model cannot take into account the contributions due to the other alloying elements.

3.3 Model-2: Background and Theoretical Framework

In the previous section, a thermodynamics-based model was presented based on the principles of displacive mechanism of bainite transformation. While the model performed fairly satisfactorily for the three low carbon steels tested, it was not very accurate at high temperatures, where the discrepancy is large for the initial kinetics (See Figures 3.3-3.5). As a result, one can expect larger errors in high carbon steels where the bainitic range of temperatures is much wider for steel due to a large gap between the B_s and M_s temperatures.

Another issue with the purely thermodynamic model is the use of the scaling function that limits the maximum volume fraction of bainite. More specifically, the nucleation rate does not tend to zero as the maximum possible transformation is reached. Thus, without the scaling function there would be a 100% transformation as is noticed in the model of Van Bohemen *et al*. [37].

Thus an improved model is proposed in this section. To this end, the primary objective is to develop a bainite transformation model that takes into account the incomplete reaction phenomenon and that is applicable for a wide variety of high-carbon as well as low-carbon steels. The following are the highlights of the modified thermostatical model presented in this chapter:

(1) Starting from the principles of the Avrami model, an improved expression for the rate of change of number density of nucleation sites (*dN/dt*) and subsequently an analytical expression for the *actual* volume fraction of bainite are derived. This is different from the models in Refs. [32, 33, 37] where the final integrated expression is for the *normalized*

volume fraction of bainite that must be multiplied by a variable corresponding to the maximum volume fraction of bainite to account for the incomplete reaction phenomenon.

(2) As before, the nucleation kinetics in this enhanced model is controlled by the activation energy, the autocatalysis effect and the number density of nucleation sites that are initially present. However, unlike Model-1, the present model is formulated in such a way as to affect the incomplete reaction phenomenon at the steady state without requiring a scaling function [72].

(3) For predicting the maximum volume fraction of bainite (f_{max}), the least-squares approach has been employed and f_{max} is proposed as a function of the isothermal transformation temperature as well as the chemical composition of the steels. For this, nine alloying elements have been considered.

(4) The number density of potential nucleation sites initially present in the austenite (N_i) has also been modeled as a function of the isothermal transformation temperature and the chemical compositions of the steels. Once again, nine alloying elements have been considered for this formulation that is developed using a least-squares approach. With these new expressions of f_{max} and N_i, the material constants presented in the section 3.2 have been eliminated. In other words, there is no need of experimental data for a prior determination of the material constants to use the model. Finally, unlike Model-1, in the present thermo-statistical model, the maximum temperature at which bainite transformation takes place is not a constant.

For the model development and validation, experimental data of twelve steels at various isothermal transformation temperatures were utilized in this study. Of these, data of six steels (three high- and three low-carbon steels) at selected isothermal transformation temperatures were used for model development (called model development data). The remaining data of these steels and the other six steels were used for the validation of the model (called testing data). Following a detailed derivation of this model, in the ensuing subsections, an exhaustive validation of this model is presented for various test criteria.

3.3.1 Model Description

In view of the fact that a 100% transformation does not take place due to the incomplete reaction phenomenon [3], in this study, a modified expression for *dN/dt* is proposed that is derived along the principles of the Avrami model [73-75] as follows: Let v^B and v^γ be the volume of bainite and austenite, respectively. Also, let v_o^γ and $v^{B,\max}$ be the initial volume of austenite and the maximum volume of bainite at equilibrium, respectively. Now, along the theory of Christian [76] and, Rees and Bhadeshia [32], the maximum, the instantaneous/actual and the normalized volume fractions of bainite can be defined as:

$$f_{\max} = \frac{v^{B,\max}}{v_o^\gamma} \ , \tag{3.10}$$

$$f = \frac{v^B}{v_o^\gamma} \ \text{and.} \tag{3.10a}$$

$$\xi = \frac{f}{f_{\max}} = \frac{v^B}{v^{B,\max}} \ ,. \tag{3.10b}$$

Now, following the Avrami model, Rees and Bhadeshia presented the differential volume fraction of bainite in the untransformed austenite in terms of the extended volume of bainite. This relation can be written in terms of the nucleation rate density in the extended volume, I, as

$$df = (1-\xi)IV_b dt, \tag{3.11}$$

Further, $IV_b dt$ represents the differential increment of the bainitic phase in the extended volume. Using the normalized volume fraction of bainite from Eq. (3.10), Eq. (3.10a) and Eq. (3.10b) in Eq. (3.11) followed by a rearrangement gives

$$f_{max} df = (f_{max} - f)IV_b dt, \tag{3.12}$$

where I in the extended volume is

$$I = \frac{kT}{h} N_i (1 + \lambda f) \exp\left(\frac{-Q^*}{RT}\right). \tag{3.13}$$

Further, the product $(f_{max}-f)I$ is the nucleation rate density in the untransformed austenite. In other words, in the untransformed austenite the new expression for the rate of change of the number density of nucleation sites is

$$\frac{dN}{dt} = I(f_{max} - f) = \frac{kT}{h} N_i (1 + \lambda f) \exp\left(\frac{-Q^*}{RT}\right)(f_{max} - f), \tag{3.14}$$

This is different from the expression in Equation (3.3) or in Refs. [37, 72]. This new expression means that when $f = f_{max}$ nucleation rate density decreases to zero ($dN/dt = 0$), i.e., there is no more nucleation, and no further transformation is expected. In other words, as transformation time progresses, the number of new nucleation events decreases and reaches a value of zero as the volume fraction of bainite (f) reaches the maximum possible value (f_{max}) for the steel.

41

By substituting the above relation in Equation (3.12) followed by an analytical integration, the final expression for the volume fraction of bainite as

$$f = \frac{f_{max} - f_{max}\exp\left(-\dfrac{\kappa}{f_{max}}(1+\lambda f_{max})t\right)}{1+\lambda f_{max}\exp\left(-\dfrac{\kappa}{f_{max}}(1+\lambda f_{max})t\right)},$$ (3.15)

where κ is

$$\kappa = \frac{kT}{h}N_i\exp\left(\frac{-Q^*}{kT}\right)V_b.$$ (3.15a)

Three important aspects of Equation (3.15) are the *activation energy*, the *number density of initial nucleation sites* and the *maximum volume fraction of bainite*. These are discussed in detail in the following paragraphs:

1)   *Activation energy (Q*)*: The activation energy $Q*$ of the austenite to bainite transformation is calculated using Equation (3.6). In this equation, for the present model, Q_0 is different for each steel and it is in the range 157kJ/mol-195kJ/mol for the investigated steels. Also, unlike Model-1, K_1 is given by the relation $K_1 = (15.049*W_C+10.057)$, where W_C is the carbon content of the steel in wt%.

Finally, the driving pressure for bainite nucleation in Equation (3.6) is calculated as

$$\Delta G_m = G_n - \Gamma(T_h - T).$$ (3.16)

In this expression, T_h is different for each steel. In fact, it has been calculated using the *MAP_STEEL_MUCG83* program of Bhadeshia [77].

The constant Γ in Equation (3.16) is $\Gamma = dG_m/dT$. Assuming a local linear approximation, it has also been deduced for each steel from the data of *MAP_STEEL_MUCG83* program [77]. The universal nucleation function, G_n, has been calculated as in Model-1.

2) *Number density of initial nucleation sites* (N_i): In a slight variation from Model-1, N_i has been modeled using the following expression [34]:

$$N_i = \frac{B}{L\alpha_p}, \ T < T_h$$
$$N_i = 0, \ T \geq T_h$$

(3.17)

The above equation ensures that N_i is zero as the transformation temperature is above the highest transformation temperature at which bainite formation takes place [78]. All the parameters in this equation are as described in Model-1.

It has been found that in Equation (3.17), B can be expressed in terms of the weighted sum of the weight fractions of the chemical composition (W_i) and the isothermal transformation temperature as

$$\ln(B) = \left(\sum_{i=1}^{9} \beta_{C_i} W_i \right) + \beta_T \frac{T}{T_h},$$

(3.18)

where β_{C_i} are weight coefficients, C_i representing the individual alloying element. The last coefficient, β_T, is the weighted contribution of the isothermal transformation temperature. It should be noted that this dependence of N_i on composition of alloying elements as well as the heat treatment temperature is also indirectly evident in a recent study by Van Bohemen *et al.* [79] where the authors proposed N_i as an exponential function of activation energy and modeled the activation energy as a regression expression of the chemical composition of the steel.

The constants, β_i in Equation (3.18) have been obtained from the experimental data of f from six different steels that are processed at various isothermal transformation temperatures, i.e., the model development data. The chemical compositions of these steels are summarized in Table 3.3 and the key parameters associated with these steels are summarized in Table 3.4.

The specific approach that has been used to determine the constants β_i is as follows: For each steel, at a given isothermal transformation temperature, values of the tuning parameters, viz., Q_0, λ and B were chosen such that the model was able to predict the initial transformation kinetics of the experimental data reasonably well in the graph of volume fraction, f, versus time, t. Knowing a specific value of B for each steel in Table 3.3 at a particular isothermal transformation temperature, a least-squares approach was then applied to determine the constants β_i that are summarized in Table 3.5.

An evaluation of the expression in Equation (3.18) with respect to the raw tuning values of B that fit the experimental data is shown Figure 3.6a. As seen in this figure, there is an excellent reproduction of the values of B using the Equation (3.18) with an R^2 value of 0.999 (to 3 decimal places). In evaluating the model with respect to other steels, this expression for B is employed and B is not a tuning parameter.

Table 3.3: Chemical composition of the six steels that were used for the development of the model. The values in the brackets indicate the references for the experimental data.

Steel	Chemical composition (wt %)								
	C	Si	Mn	Ni	Mo	Cr	V	Co	Al
Steel-1 [43]	0.98	1.46	1.89	0[a]	0.26	1.26	0.09	0 [a]	0[a]
Steel-2 [43]	0.83	1.57	1.98	0[a]	0.24	1.02	0[a]	1.54	0[a]
Steel-3 [43]	0.78	1.49	1.95	0[a]	0.24	0.97	0[a]	1.6	0.99
Steel-4 [36, 40]	0.44	1.74	0.67	1.85	0.83	0.39	0.09	0[a]	0[a]
Steel-5 [36]	0.39	2.05	0[a]	4.08	0[a]	0[a]	0[a]	0[a]	0[a]
Steel-6 [33]	0.38	1.29	1.73	0[a]	0[a]	0[a]	0[a]	0[a]	0[a]

Table 3.4: Values of model parameters used for the development of the model. The values in the brackets indicate the references for the experimental data.

Steel	T [°C]	λ	L [μm]	u_w [μm]	T_h [°C]
Steel-1 [43]	200	10	0.074	7.40E-04	545
Steel-2 [43]	200	25	0.08	8.00E-04	579
Steel-3 [43]	200	65	0.08	8.00E-04	601
Steel-4 [36, 40]	352-414	90	95	0.95	591
Steel-5 [36]	408	20	35	0.35	628
Steel-6 [33]	355-430	20	30	0.05	591

[a] The composition of these alloying elements were not given in the references and have been chosen as 0.0 for solving Equations (3.18) and (3.19).

Table 3.5: Coefficients of the least-squares estimates in Equations (3.18) and (3.19).

Eq.	C	Si	Mn	Ni	Mo	Cr	V	Co	Al	T/T_h
					β_i, i=C_1...C_9, T					
(3.18)	0	0	151.26	108.74	54.08	143.95	0	63.27	60.01	-81.22
					θ_i, i=C_1...C_9, T					
(3.19)	0	0	3.31	2.39	2.07	1.92	0	2.07	1.37	-1.84

3)   *Maximum volume fraction of bainite (f_{max})*: The following temperature and composition dependent function is used for estimating f_{max} at temperature T:

$$f_{max} = \left(\sum_{i=1}^{9} \theta_{C_i} W_i \right) + \theta_T \frac{T}{T_h},$$

(3.19)

where θ_c are weight coefficients, C_i representing the individual alloying element. θ_T is the weighted contribution of the isothermal transformation temperature. As in the case of *B*, knowing the maximum possible bainite volume fraction from the experiments, the constants θ have been determined using a least-squares approach.
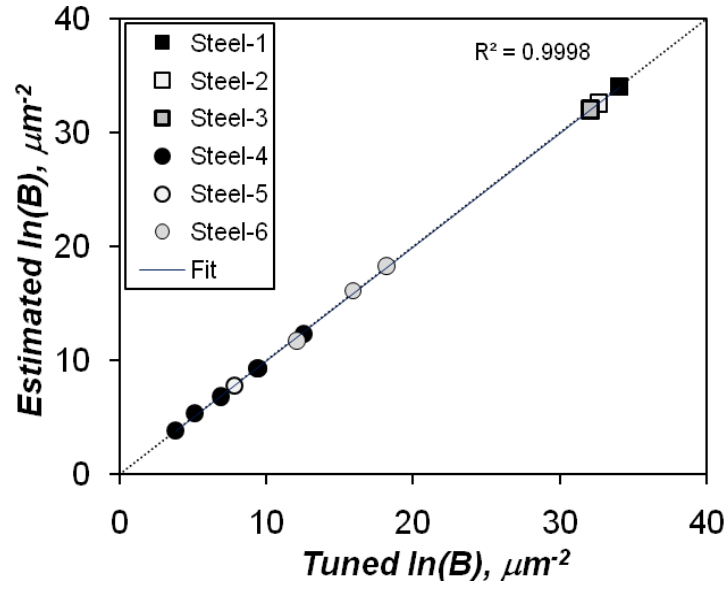
Figure 3.6a: Comparison of the tuned value of ln(B) and value obtained from Equation (3.18).
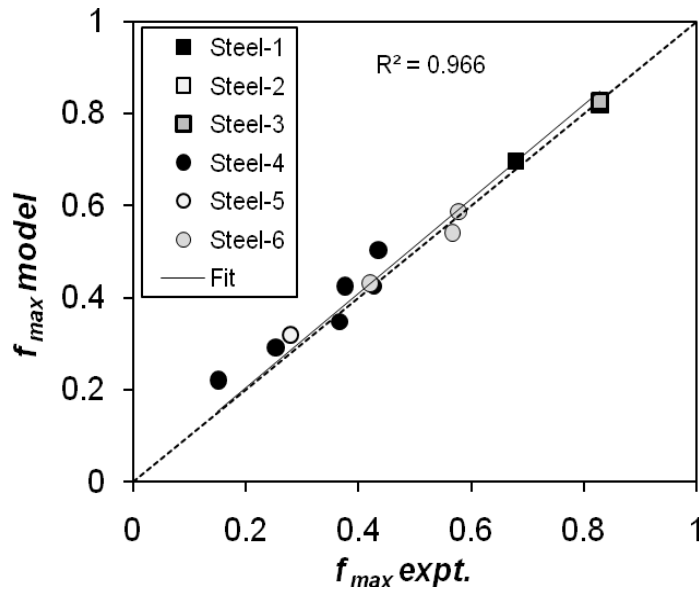
Figure 3.6b: Comparison of the experimental value of f_{max} with the predictions from Equation (3.19).

A comparison of the estimate of f_{max} via Equation (3.19) and the values f_{max} from the experiments are shown in Figure 3.6b. As seen in this figure, there is an excellent prediction of f_{max} by Equation (3.19) with an R^2 value of approximately 0.966 (to 3 decimal places). The values of θ obtained from the model development data are summarized in Table 3.5.

3.3.2 Model-2: Validation and Discussion

The validation of the model was performed with respect to the following progressively stringent criteria: (a) The model must work for the six steels that were used for the derivation of the coefficients in Eq. (3.18) and (3.19), i.e., the model development data. (b) Additionally, for these steels, the model must give good predictions at other isothermal transformation conditions whose data were not used for model development. (c) The model must also be able to capture the transformations in steels when the parameters such as austenite grain size are varied. This is because it is known that with such variations, there is a change in the bainitic kinetics and thereby the volume fraction of bainite [43]. (d) Finally, the model must work for other steels that have a carbon content that is within the range of the carbon concentration of the steels used for the development of the model.

All the steels that were used for validation of the model are summarized in Tables 3.3 and 3.6. For each steel, using one of the bainite plate dimensions from the literature, the model parameters, viz., the other two plate dimensions and the mean linear intercept were obtained as per the relations in Ref. [72]. The autocatalytic factor of each steel was a tuning parameter that was chosen to match the model predictions with the experimental data at one isothermal

Table 3.6: Chemical composition of the additional steels that were used only for model validation. The values in the brackets indicate the references for the experimental data.

Steel	Chemical composition (wt %)								
	C	Si	Mn	Ni	Mo	Cr	V	Co	Al
Steel-7 [80]	0.46	2.10	2.15	0[a]	0[a]	0[a]	0[a]	0[a]	0[a]
Steel-8 [44]	0.80	1.59	2.01	0[a]	0.24	1.00	0[a]	1.51	0[a]
Steel-9[b] [43]	0.83	1.57	1.98	0[a]	0.24	1.02	0[a]	1.54	0[a]
Steel-10[b] [43]	0.78	1.49	1.95	0[a]	0.24	0.97	0[a]	1.6	0.99
Steel-11 [45]	0.79	1.59	1.94	0.02	0.30	1.33	0.11	0[a]	0[a]
Steel-12 [40]	0.31	1.40	1.97	1.70	1.41	0.26	0[a]	1.13	1.01

transformation temperature. Subsequently, this value of λ was fixed for the other values of T. All these parameters are summarized in Table 3.7.

In the following paragraphs, the performance of the model with respect to each of the above criteria is evaluated. The last criterion being the most stringent, validation results with respect to several steels are shown for this criterion.

---

[a] The composition of these alloying elements were not given in the references and have been chosen as 0.0 for solving Equations (3.18) and (3.19).

[b] Steel-9 and Steel-10 are Steel-2 and Steel-3, respectively, but with a finer austenite grain size.

49

Table 3.7: Values of model parameters of the steels that are used for the validation of the model. Values in the brackets indicate the references for the experimental data.

Steel	T [°C]	λ	L [µm]	u_w [µm]	T_h [°C]
Steel-1 [43]	250	10	0.074	7.40E-04	545
Steel-2 [43]	250	25	0.07	8.00E-04	579
Steel-3 [43]	250	65	0.09	8.00E-04	601
Steel-4 [18,40]	346, 391, 425	90	95	9.50E-01	591
Steel-5 [36]	351, 391, 455	20	35	3.50E-01	628
Steel-6 [33]	330, 405, 455	20	30	5.00E-02	591
Steel-7 [87]	270, 290	10	7.9	7.90E-02	509
Steel-8 [44]	200, 250, 300	-^{c}	-^{c}	-^{c}	579
Steel-9 [43]	200	0.1	0.056	5.6E-4	601
	250		0.092	9.2E-4	
	300		0.122	1.22E-3	
Steel-10 [43]	200	50	0.082	8.20E-04	591
	250		0.078	7.80E-04	
	300		0.096	9.60E-04	
Steel-11 [45]	190, 250, 300	-^{c}	-^{c}	-^{c}	535
Steel-12 [40]	325, 350, 375, 400	-^{c}	-^{c}	-^{c}	565

^{c} For these steels, only f_{max} was given in the references and this was calculated directly using Equation (3.19).

This criterion is also the most important one since it establishes the validity of the model for steels other than the ones that are used for the development of the model.

3.3.2.1 Criterion (a): Evaluation of the Steels that were used for Model Development

In this first criterion it was tested to see if the values of B and f_{max} predicted by Equations (3.18) and (3.19), respectively, are accurately reproducing the experimental data that were used for the deducing the coefficients β and θ. The chemical composition and the model parameters of the steels that were studied for this criterion are summarized in Tables 3.3 and 3.4, respectively. Specifically, the data that was used in Equations (3.18) and (3.19), viz., the experimental data of Steels 1 through 3 at T=200°C and the data of the low carbon steels (Steels 4 through 6) at 350°C <T<455°C, was used.

The model prediction with the experimental data is shown in Figures 3.7a and 3.7b. As seen in these figures, using the value of B and f_{max} from Equations (3.18) and (3.19), respectively, in conjunction with the respective composition of the steel and the other model parameters, the model predictions are in close agreement with experimental data. More precisely, in the high carbon steels (see Figure 3.7a), in addition to the initial kinetics, the model predicts the maximum volume fraction of bainite in these three steels to within 3% of the experimental data. Similarly, in case of the low carbon steels, the experimental data is well predicted by the
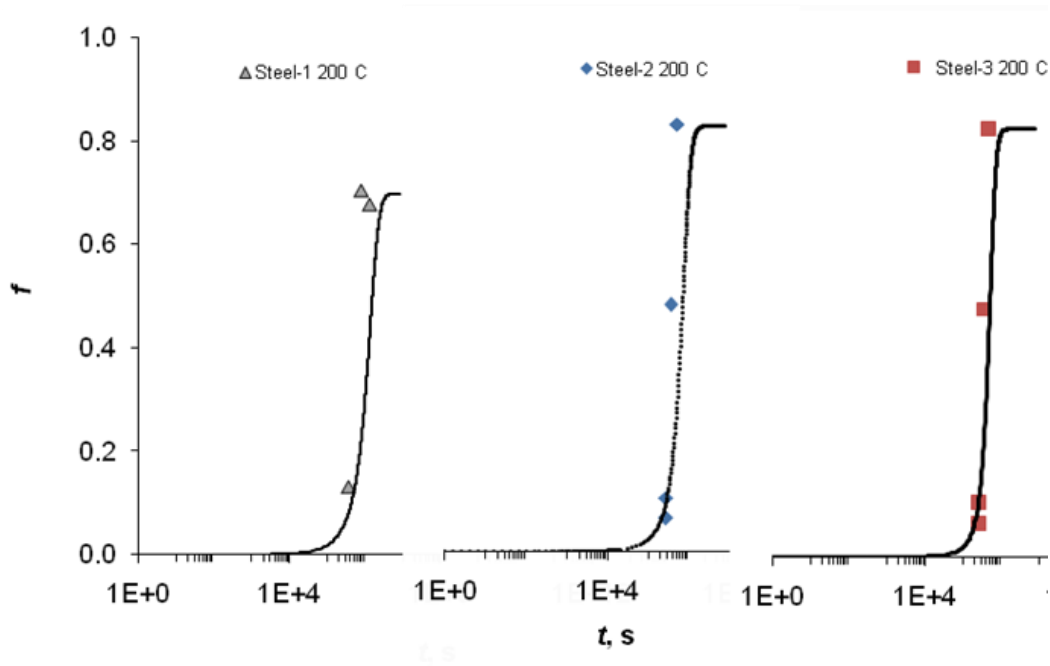
Figure 3.7a: Performance of the model for the high carbon steels, viz., Steel-1, Steel-2 and Steel-3, at T=200°C. These data were used for the development of the model. The symbols are the experimental values and the lines are the model predictions.

model over a wide range of temperature (see Figure 3.7b). In this figure, the average relative error is approximately 12%, 14.7% and 4.5% for Steel-4, Steel-5 and Steel-6, respectively. In all cases, the disagreements between the model and experimental data over the initial bainitic kinetics despite a high R^2 value of 0.999 in Figure 3.6a is due to the fact that *B* is a very sensitive parameter and slight variations in B can result in strong fluctuations in the prediction of the initial transformation kinetics.

From a closer look at Figure 3.7b, it can be seen that in case of Steel-4 and Steel-6, the effect of the chemical composition of the steel is very well captured by the model. This is justified based on the fact that at the isothermal transformation temperature of 380°C, the bainitic kinetics is

52
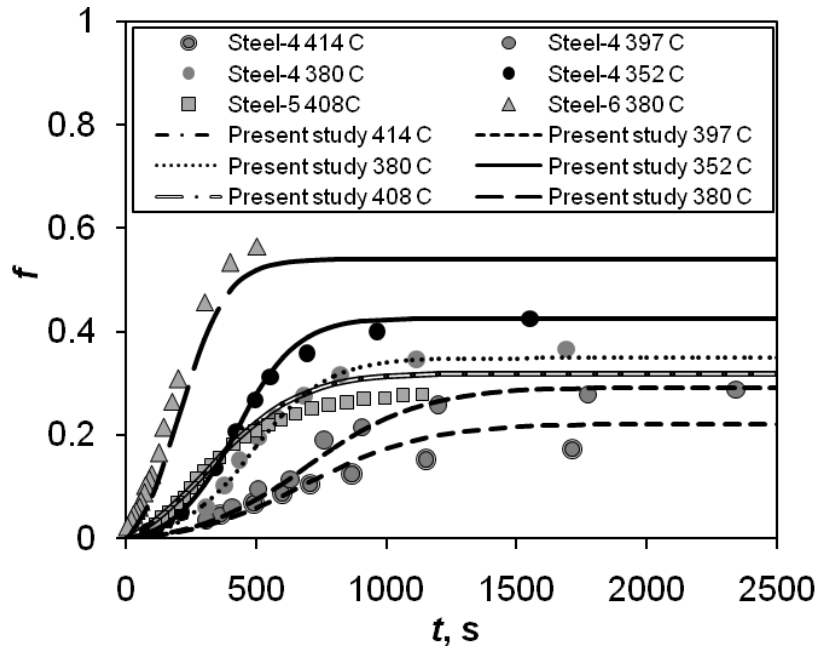
Figure 3.7b: Performance of the model for some of the data of the three low carbon steels, viz., Steel-4, Steel-5 and Steel-6, that were used for the development of the model. The symbols are the experimental values and the lines are the model predictions.

very different in these two steels, a clear indication of the fact that the chemical composition plays a key role in determining the volume fraction of bainite. This ability of the model is also seen while comparing the results of the three steels in Figure 3.7a.

3.3.2.2 Criterion (b): Model Performance at Other Isothermal Transformation Temperatures

The objective of this criterion was to ensure that the model is able to predict the bainite transformation kinetics at the other isothermal transformation temperatures for the six steels in Table 3.3. The isothermal transformation temperatures that were considered for these six steels, along with the corresponding model parameters are summarized in Table 3.7.
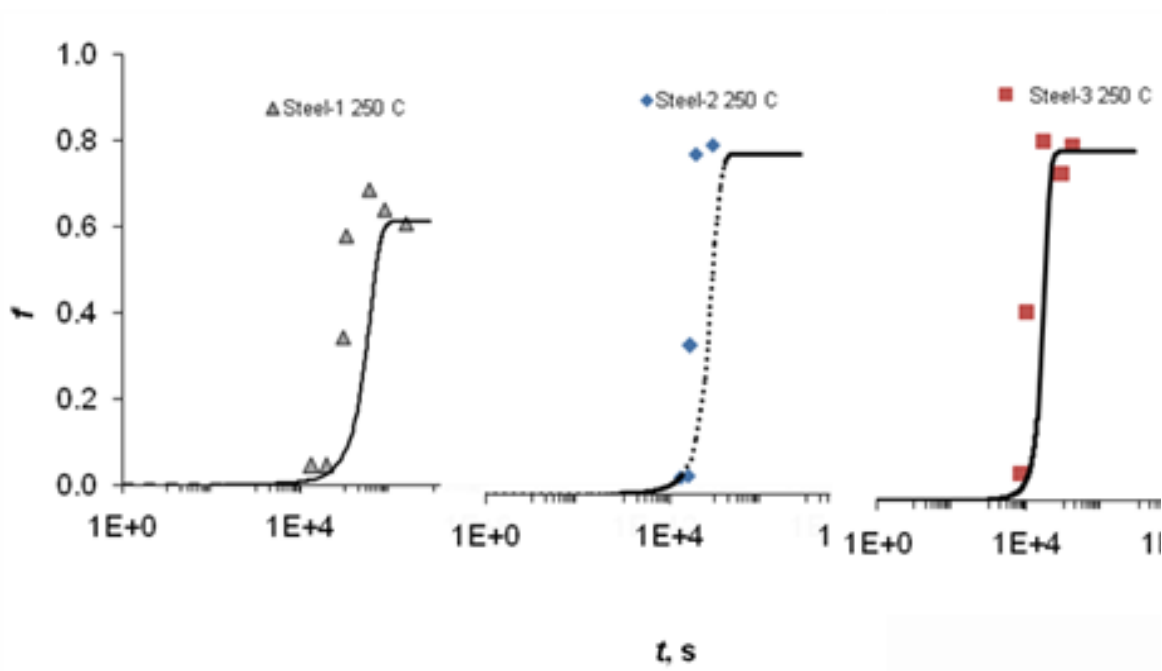
Figure 3.8a: Validation of the model for Steel-1, Steel-2 and Steel-3 at T=250°C. The symbols are the experimental data and the lines are the model predictions.

The model predictions for the three high carbon steels at T=250°C are shown in Figure 3.8a. As seen in this figure, the predictions of the initial kinetics for Steel-2 and Steel-3 are in excellent agreement with the experimental data. Again, the larger error seen in Steel-1 is due to the sensitive nature of B. In all three steels, the relative error in the maximum volume fraction of bainite is 0.7%, 2.5% and 1.6%, respectively, for the three steels.

In other words, it can be claimed that the value of f_{max} is predicted fairly accurately to within the experimental error limits in all three cases. The bainitic kinetics of the three low carbon steels is shown in Figure 3.8b. For clarity in representation, only selected temperatures for the steels are shown. From this figure the following observations can be made for the model predictions: (i) for all steels, the initial as well as the final bainite transformation kinetics is well predicted (average

54
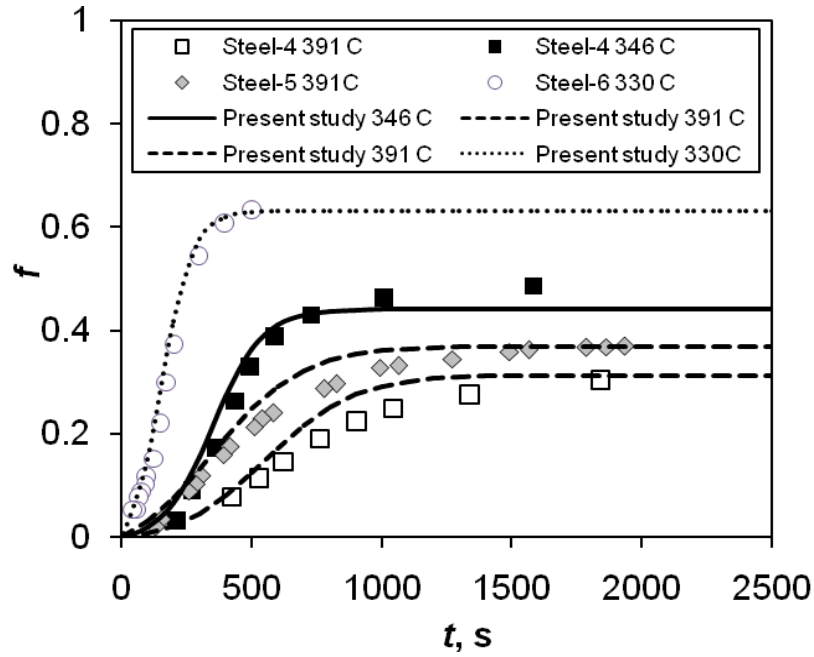
Figure 3.8b: Validation of the model for Steel-4, Steel-5 and Steel-6 at different temperatures. The symbols are the experimental data and the lines are the model predictions.

relative error of about 6%, 0.02% and 0.25% for Steel-4, Steel-5 and Steel-6, respectively). (ii) From the graph of Steel-4 and Steel-5 at T=391°C, it is clear that the model can account for the effects of the chemical composition of the steels. In fact, this is also visible from the fact that the model can be used to predict the bainitic characteristics for all the three steels in this figure. (iii) As in the high carbon steels, the model can predict f_{max} to within the limits of the experimental error.

3.3.2.3 Criterion (c): Effect of Austenite Grain Size

Garcia-Mateo *et al*. [43] have shown that with the variation in the austenite grain size, the final volume fraction of bainite also changes. An experimental evidence for two steels has been presented by the authors to validate the above claim. Since it is important for a bainite transformation model to be able to predict these changes, the model presented in this study was evaluated with respect to this criterion. For this, the bainite transformation kinetics of Steel-9 and Steel-10 were evaluated using the model. These are the same as Steel-2 and Steel-3, respectively, but with a finer austenite grain size. In the present model, the plate thickness observed by Garcia –Mateo *et al*. [43] were used to determine the mean linear intercept. Also, an autocatalytic factor that is lower than with the coarse grain steels was used to be able to match the experimental data. The choice of a smaller value of λ is explained as follows: With a fine austenite grain size (or a larger ASTM grain size number), more grain boundaries are available for bainitic nucleation. In other words, bainitic kinetics is primarily driven by grain boundary nucleation than an autocatalytic growth. In this model, a subdued effect of the autocatalytic growth is represented by a smaller value of λ. Van Bohemen *et al*. [37] have also observed such a direct relationship between the austenite grain size and the autocatalytic factor.
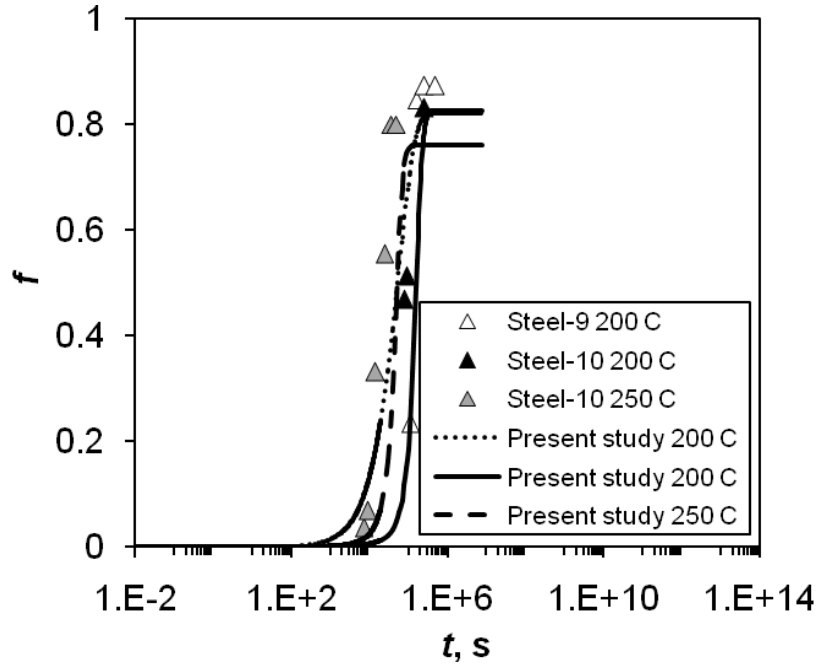
Figure 3.9: Validation of the model for Steel-9 and Steel-10. These are Steel-2 and Steel-3, respectively, with a fine austenite grain size. The symbols are the experimental data and the lines are the model predictions.

The chemical composition and model parameters of the two steels studied for this criterion are summarized in Tables 3.6 and 3.7, respectively. The performance of the model for these two steels is shown in Figure 3.9. As seen in this figure, the model is able to predict the initial kinetics as well as the final volume fraction of bainite fairly accurately. In fact, the final volume fraction of bainite is predicted to within 9% of the experimental data. Again, this is most likely within the probable experimental error.

3.3.2.4 Criterion (d): Performance with Respect to Other Steels

The model presented in this study has also been tested on other steels from the literature. Specifically, steels whose carbon content is within the range of the carbon content of the steels used in the development of the model were considered. The chemical compositions of the steels (Steel-7, Steel-8, Steel-11 and Steel-12) that are evaluated for this criterion are summarized in Table 3.6.

Among these, in the steels where only the final volume fraction of bainite has been provided in the literature, the calculated values of f_{max} and the experimental f_{max} for these steels are shown in Figure 3.10. This figure also includes a comparison of the calculated and experimental f_{max} of all the other steels that were considered in the various criteria in the previous sections. As seen in this figure, the model predictions are in excellent agreement with the experimental data.

The relative error of the experimental and model is shown in Figure 3.11. In this figure, the relative errors for almost all the steels, at various transformation temperatures, is less than 10%. There is a small set of data that has an error between 10% and 25%. Also, approximately five data points, corresponding to f_{max} values of steels heat treated at above 400°C have errors that are greater than 25%. It must be clarified that this large error is primarily due to the fact that at high values of T, the volume fraction of bainite is small. As a consequence, a small value of f implies a high sensitivity in the relative error.
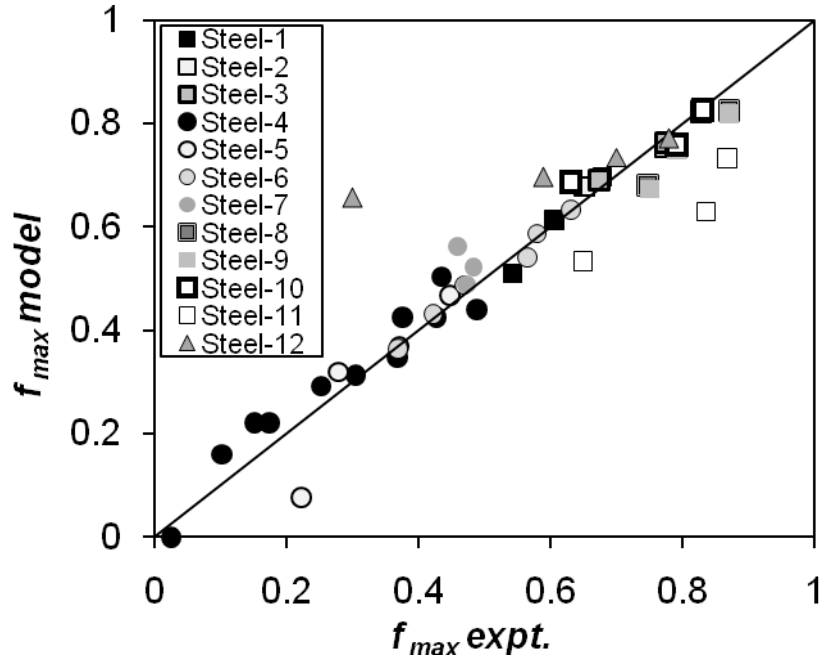
Figure 3.10: Validation of the model for twelve steels at various isothermal transformation temperatures.
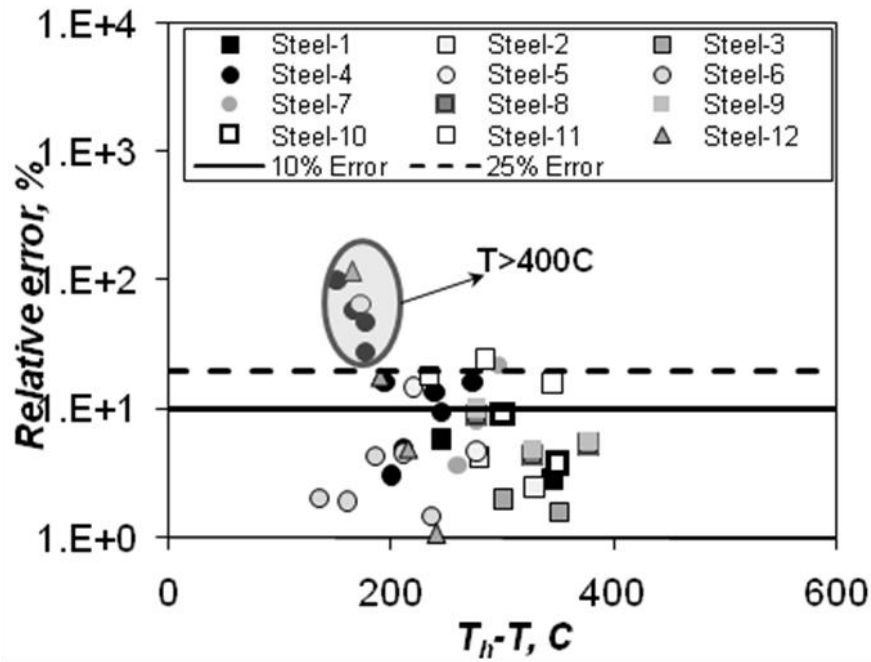
Figure 3.11: Relative error of f_{max} as a function of the isothermal transformation temperature.

Chang's [80] experimental data for complete transformation kinetics for Steel-7 has also been validated with the current model. Specifically, transformations at temperatures, viz., 270°C and 290°C, have been plotted in Figure 3.12. At both temperatures, the initial kinetics of the model is predicted to within experimental uncertainty. At 300°C (data not shown), the kinetics is marginally faster than the experimental data. However, the maximum volume fraction at this temperature is within 4% of the experimental data. At 270°C and 290°C model predicts a relative error of 8% and 22%, respectively. In all three cases, the model is able to reproduce the timescale of transformation fairly accurately.
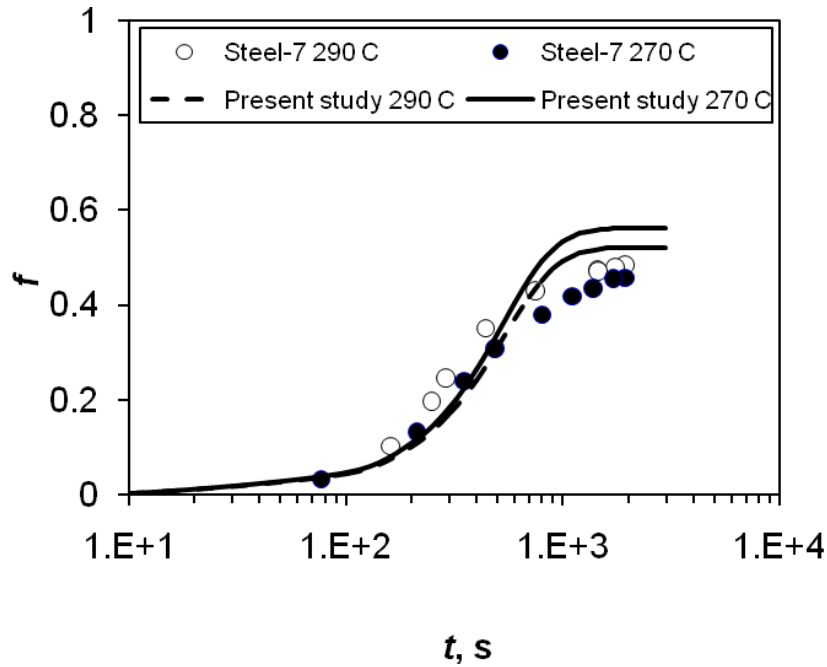
Figure 3.12: Validation of the model for Steel-7 at two isothermal transformation temperatures. The symbols are the experimental data and the lines are the model predictions.

3.3.2.5 Remarks on the Models

A comparison of the present model with the performance of Model-1 as presented in Section 3.2 is shown in Figure 3.13. To highlight the improved performance of this model, only a few selected temperatures are shown in this figure. From this figure it can be concluded that the enhanced model performs very well in predicting the initial kinetics as well as the maximum volume fraction of bainite for a range of temperatures.

In an attempt to understand the performance limits of the model, its ability to predict the maximum volume fraction in a low carbon steel (Steel-12) with a carbon content of 0.31 wt% was made. This carbon content is lower than the carbon composition of the six steels that were used to develop the model. The results are presented with triangular symbols in Figures 3.10 and 3.11. From these figures, it seems that the model can perform reasonably well for steels that are slightly outside the range of the carbon composition for which the model was developed, especially if the bainite transformation temperature is low.

At higher values of T (T>400°C) the relative errors are high. This is because in addition to the fact that the carbon content is beyond the range of the model, there is an added contribution due to the low levels of transformations that one is likely to be observed at these temperatures.
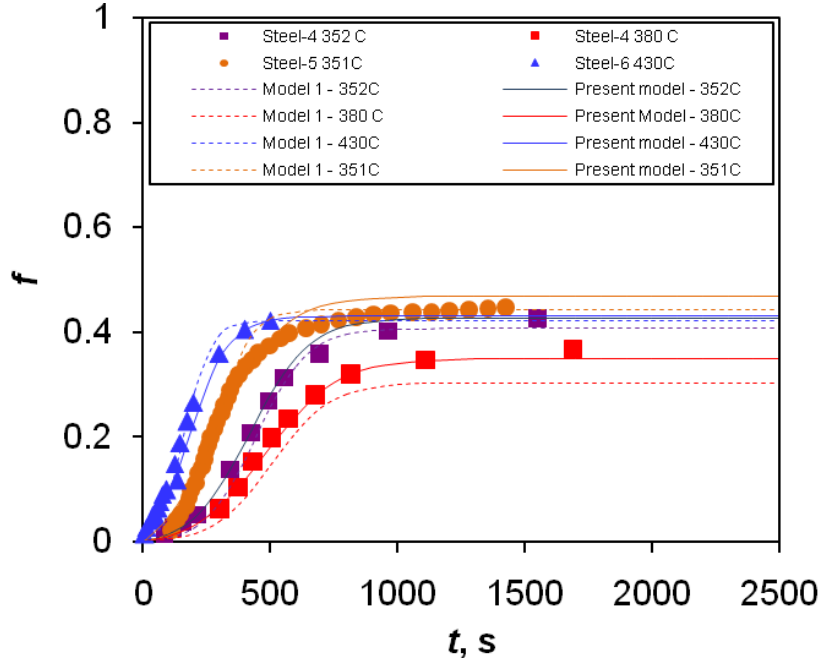
Figure 3.13: Comparison of the bainite transformation kinectics of three steels (solid symbols) predicted by the present model (solid lines) and the thermodynamic model of Section 3.2 (Model-1, dotted lines) [72].

Such small volume fractions will result in a high sensitivity in the relative errors. Nevertheless, more experimental data from other steels will have to be tested for validating this claim further.

Among the inputs to the model, one of the plate dimensions that are obtained from the experimental data is currently being used. To move the model a step further by avoiding this required experimental data at every temperature, one can probably use a correlation between one of the plate dimensions and the isothermal transformation temperature. Such a correlation for low carbon steels has been used by Chester and Bhadeshia [33].

Finally, it is important to state that the autocatalytic factor, λ, a unique value for each steel in this study, has been a free parameter that has been used for tuning the model. Specifically, as mentioned earlier, for each steel, the value of λ has been chosen to match the experimental data at one of the transformation temperatures. Subsequently, this value was fixed for all values of T. At this time it is not clear what is the true value of λ for each steel. In fact, understanding and developing a model for autocatalysis is a complete study in its own right.

3.3.3 Model-2: Summary

The modified thermostatistical model accounts for the incomplete reaction phenomenon that prevents the transformation of all the austenite into bainite. In formulating this model a new expression for the rate of change of the number density of nucleation sites (dN/dt) has been used such that dN/dt reduces to zero as f approaches the maximum possible volume fraction of bainite. Other important features of the model include temperature and composition dependent expressions for the maximum volume fraction of bainite as well as the number density of initial nucleation sites. With the implementation of such composition dependent expressions, four material dependent constants in Model-1 have been completely eliminated.

The model has been verified with respect to the experimental data of several steels over a wide range of temperatures. For validation of the model, several criteria were used including the evaluation of model for various isothermal transformation temperatures, different austenite grain size and other steels from the literature that were not used for the development of the model. For all the investigated steels, it was found that the model performs extremely well in predicting the

maximum volume fraction of bainite. The model was also able to predict the initial reaction kinetics of the bainite transformation process fairly accurately. In addition to these, preliminary tests indicate that the model might also be valid for steels whose carbon composition is marginally outside the range of the carbon content of the steels that were used in developing this model.

In conclusion, it can be stated that the objective of developing a model that is applicable to low as well as high carbon steels and that can predict the bainite transformation kinetics as well as the maximum volume fraction of bainite accurately for a range of transformation temperatures has been successfully realized.

Chapter 4

Determination of Volume Fraction of Bainite in Low Carbon Steels using Artificial Neural Networks

4.1 Introduction

Material properties such as hardness, tensile strength, fatigue, yield strength, etc., are important engineering design parameters that are a function of many parameters, viz., alloying elements, heat treatment conditions, etc [81]. However, due to the complexity in developing models for these properties, it is not easy to present them quantitatively as a function of these parameters. In these circumstances, Artificial Neural Networks (ANN) can be employed to study various problems for which quantitative evaluations are either lacking or not well formulated.

In steel related research ANN has been used extensively to understand a wide range of problems including phase transformations [82], surface texture [83-85] and mechanical properties [86-89]. For instance, Trzaska and Dobrzanski [90] applied ANN to determine the composition of steel for achieving a particular hardness. Monajati *et al*. [91] used ANN to understand the effects of the processing parameters on the mechanical properties such as yield strength, work hardening and plastic strain ratio. Corrosion studies have also been made using the ANN [92-93]. An overview of the application of neural networks to study material science problems has been presented by Mukherjee and Singh [94], and Bhadeshia *et al* [95].

In this chapter, as an alternative to the *thermodynamic* and the *thermo-statistical* models presented in Chapters 3, an ANN framework is proposed to determine the volume fraction of bainite. This is because, despite several improvements in the other two models, at several transformation temperatures, there is still an error in predicting the initial transformation kinetics or the final volume fraction of bainite, or both. The deficiencies of these models are because of insufficient or inaccurate representation of the influential parameters and the interaction between these large numbers of variables. These drawbacks can be overcome using an ANN, whose configuration can capture complex interactions of many parameters.

Specifically, ANN has been used to determine the volume fraction of bainite as a function of nine alloying elements, isothermal transformation temperature and time, and the maximum temperature at which bainite formation can take place for a given steel. Collectively these parameters represent the input variable space for the ANN. While the alloying elements are added to instill certain material properties or enhance the bainite transformation process, the isothermal transformation temperature and time directly influence the bainite transformation kinetics. Further, some alloying elements are also known to impact the bainite transformation kinetics. For instance, Co and Al enhance the transformation rate [68]. The elements such as Si, Mo, Cr and V that are ferrite stabilizers are expected to decrease the volume fraction of bainite [13]. On the other hand, elements such as Mn and Ni that are austenite stabilizers are expected to aid the bainitic transformation [13]. Thus, a combination of a wide variety of parameters determines the final volume fraction of bainite in steel.

The theory behind the ANN configuration and the performance with respect to low-carbon steels is discussed in the ensuing sections. Specifically, using the experimental data of three steels, the ANN has been developed to predict the volume fraction of bainite for a given set of input variables mentioned above. The chapter also discusses the role of the austenite and ferrite stabilizers among these alloying elements by comparing the network predictions against the established metallurgical theory.

4.2 Neural Network Theory

A brief overview of the neural network theory [96] is discussed in this section. The schematic of a general neural network is shown in Figure 4.1a. Each circular node in the figure represents a neuron. The first and the last layers of the neurons (represented by circles) are the hidden and output layers, respectively of the neural network. The hidden layer receives an input from the input layer that simply passes on the input parameters to the neurons in the hidden layer. Thus, the network shown in Figure 4.1a has n nodes (represented by the rectangles) for the n–parameter input, k hidden neurons and m neurons for the m output quantities of interest from this network. In principle, one can have more than one hidden layer in the neural network. The addition of more hidden layers, which might be needed, depending upon the problem, increases the complexity of a neural network.
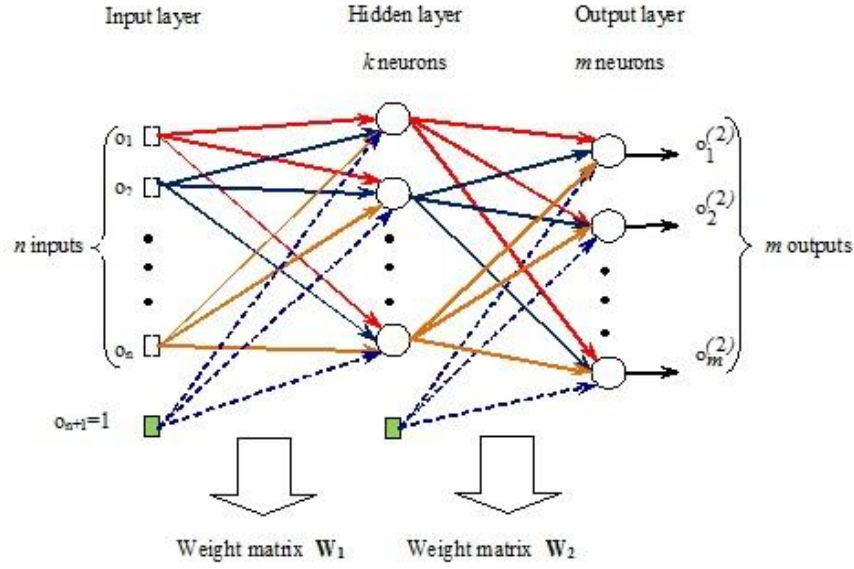
Figure 4.1a: Schematic of a neural network with one hidden layer.

Neurons in the hidden and the output layers produce output response value by processing a *weighted* set of input variables through a predetermined *activation* function, *s*. On the other hand, the input layer simply passes on the weighted input values to the neurons in the hidden layer. For the network in Figure 4.1a, the weight connecting the ith input neuron and the jth neuron in the hidden layer is represented by $w_{ij}^{(1)}$. Likewise, the weight between the hidden neuron i and the output neuron j is $w_{ij}^{(2)}$.

In the input layer, in addition to the *n* input variables, an additional input with a value equal to 1 is provided (indicated by the colored box symbol). The weight applied to this input is $w_{n+1,j}^{(1)}$ and is called the *bias* value that is included in the network to account for the variables whose impact on the output has been neglected. In matrix notation, the $(n+1) \times k$ weights can be presented between the input and the hidden layer as $\mathbf{W_1}$ with components $w_{ij}^{(1)}$ in the ith row and j^{th} column.

Similarly, a bias $w_{k+1,j}^{(2)}$ is also included for each neuron in the hidden layer. In matrix notation the weights can be written as between the hidden and the output layer as $\mathbf{W_2}$ that has the component $w_{ij}^{(2)}$ in its ith row and j^{th} column.

Finally, each neuron in the hidden and output layers produces an output response value by applying the activation function to the weighted sum of the input values. While there are several activation functions that can be found in the literature, the more commonly used ones are the *sigmoid* and *tanh* functions. In this thesis, the *sigmoid* function that is applied to each neuron is

$$s(x) = \frac{1}{1+e^{-x}}. \tag{4.1}$$

The application of this non-linear activation function translates the weighted sum of the inputs to a value between 0 and 1. Thus, the response of the jth neuron in the hidden layer is calculated as

$$o_j^{(1)} = s\left(\sum_{i=1}^{n+1} w_{ij}^{(1)} \hat{o}_i \right), \tag{4.2}$$

where $\hat{o}_i$ is the ith component of the vector $\hat{\mathbf{o}} = (o_1,\cdots,o_n,1)$ that is the extension of the n-dimensional input vector $\mathbf{o} = (o_1,\cdots,o_n)$. The schematic of the input and output of the first neuron in the hidden layer is shown in Figure 4.1b.

In matrix notation, Equation (4.2) can be written as

$$o^{(1)} = s(\hat{o}\mathbf{W}_1). \tag{4.3}$$

Likewise, the m-dimensional response of the output layer, $\mathbf{o}^{(2)}$, is

$$o^{(2)} = s(\hat{o}^{(1)}\mathbf{W}_2), \tag{4.4}$$

$$\text{where } \hat{\mathbf{o}}^{(1)} = (o_1^{(1)},\cdots,o_k^{(1)},1).$$
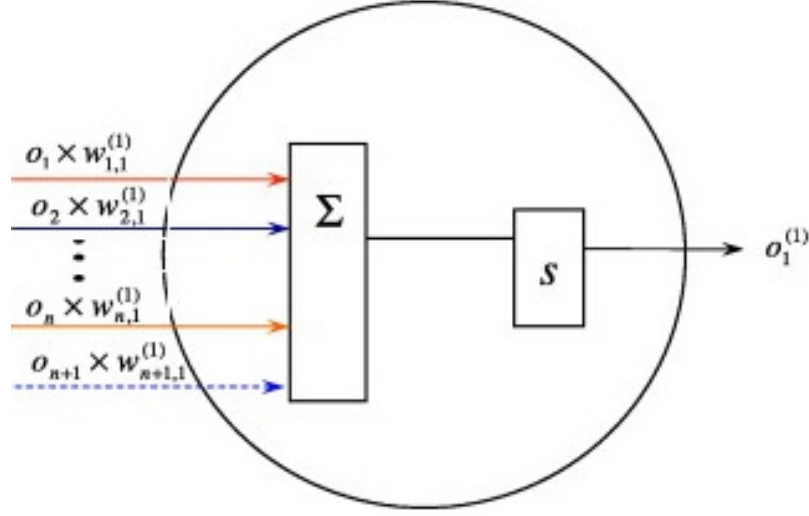
Figure 4.1b: Schematic of the input and output of the first neuron of the hidden layer.

Thus, knowing the weight matrices for the neural network and applying the input vector to the network will yield a response that corresponds to the *m*-dimensional output vector. In other words, the key to a neural network formulation is the choice of the appropriate weights for the network. This is discussed next.

4.3 Database and Training Description

The process of determination of the weights of the neural network is referred to as *training*. For this, a database of the *n*-dimensional input vectors (*n*-dimensional for the *n* input variables) along with the true *m*-dimensional output is used. The objective of the training process is to determine a set of weights of the network that minimizes the error

$$E = \sum_{i=1}^{p} e_i,$$ (4.5)

where *p* is the number of input vectors in the database and e_i is

70

$$e_i = \sum_{j=1}^{m} \frac{\left(o_j^{(2)} - t_j\right)^2}{2} \quad . \tag{4.6}$$

In the above equation, t_j is the jth component of the true m-dimensional output vector $\mathbf{t}$. For training, the *backpropagation* algorithm has been used [96]. The key steps of this algorithm are as follows:

Step 1: Starting with random initial weights, compute vectors $\mathbf{o}^{(1)}$ and $\mathbf{o}^{(2)}$ for the input vector $\mathbf{o}$. Knowing these, compute the matrices $\mathbf{D}^{(1)}$ and $\mathbf{D}^{(2)}$ as follows:

$$\mathbf{D}^{(1)} = \begin{bmatrix} o_1^{(1)}(1-o_1^{(1)}) & 0 & \cdots & 0 \\ 0 & o_2^{(1)}(1-o_2^{(1)}) & \cdots & 0 \\ \vdots & \vdots & \ddots & \vdots \\ 0 & 0 & \cdots & o_k^{(1)}(1-o_k^{(1)}) \end{bmatrix}. \tag{4.7}$$

$$\mathbf{D}^{(2)} = \begin{bmatrix} o_1^{(2)}(1-o_1^{(2)}) & 0 & \cdots & 0 \\ 0 & o_2^{(2)}(1-o_2^{(2)}) & \cdots & 0 \\ \vdots & \vdots & \ddots & \vdots \\ 0 & 0 & \cdots & o_m^{(2)}(1-o_m^{(2)}) \end{bmatrix}, \tag{4.8}$$

In this step the error vector $\mathbf{e}$ is also calculated as per Equation (4.6).

Step 2: Compute the m-dimensional vector $\delta^{(2)}$ of the backpropagated error to the output neurons as

$$\delta^{(2)} = \mathbf{D}^{(2)}\mathbf{e}. \tag{4.9}$$

Step 3: The k-dimensional backpropagated error to the hidden layer is

$$\delta^{(1)} = \mathbf{D}^{(1)}\mathbf{W}_2\delta^{(2)}. \tag{4.10}$$

Step 4: In this final step, the corrections are applied to the weight matrices as

Table 4.1: Chemical composition of the three low carbon steels investigated in this study. The values in the brackets indicate the references for the experimental data.

Steel	Chemical composition (wt %)						
	C	Si	Mn	Ni	Mo	Cr	V
Steel-1 [36, 40]	0.44	1.74	0.67	1.85	0.83	0.39	0.09
Steel-2 [36]	0.39	2.05	0	4.08	0	0	0
Steel-3 [33]	0.38	1.29	1.73	0	0	0	0

$$\begin{aligned} \mathbf{W}_2^T &= \mathbf{W}_2^T - \delta^{(2)}\hat{o}^{(1)}, \\ \mathbf{W}_1^T &= \mathbf{W}_1^T - \delta^{(1)}\hat{o} \ . \end{aligned} \qquad (4.11)$$

Step 5: These four steps are calculated for each input vector in the database and the total error of the network is determined using Equation (4.5). If this error is within a desired threshold then the network is trained. Otherwise, more sweeps through the database are conducted for a predetermined number of iterations.

In this chapter, the neural network has been trained for low carbon steels. For this, the experimental data of three low-carbon steels with different chemical compositions have been used [36, 40, and 33]. The chemical compositions of these steels are summarized in Table 4.1. The input variables of the neural network are the weight percent of the alloying elements, the highest temperature at which bainite formation takes place for the respective steel, the isothermal transformation temperature and the transformation time. The choice of these parameters as the input variables is motivated by the thermodynamic and the thermo-statistical models of Chapter 3, where it has been found that the volume fraction of bainite is governed by these parameters. These parameters along with their range are summarized in Table 4.2. The output of the neural network is just one value, i.e., the volume fraction of bainite (V_f).

Table 4.2: The parameters and their range used in the neural network.

Parameter	Range
Input	
C, wt%	0.38-0.44
Si, wt%	1.29-1.74
Mo, wt%	0–0.83
Cr, wt%	0–0.39
V, wt%	0–0.09
Ni, wt%	0–4.08
Mn, wt%	0–1.73
T_h, C	591–628
T, C	318–455
t, s	6.29–2592.38
Output	
V_f	0.0045–0.6327

The database itself has 437 vectors and was constructed as follows: For Steel-1, experimental data of the volume fraction of bainite from eleven isothermal transformation temperatures were included. For Steel-2 data from the experiments performed at four different isothermal transformation temperatures were added. Finally, for Steel-3, experimental data from six different transformation temperatures were added to the database. The neural network was trained using 35 points from this database. The training algorithm terminated if E<1e-6 or 100000 iterations were reached.

It should be noted that since the order of magnitude of the parameters such as temperatures and time are much larger than the parameters corresponding to the chemical composition of the

steels, all the input variables have been normalized between -0.5 and +0.5. Thus, normalization ensures that an alloying element in small amounts is not completely insignificant.

4.4 Choice of Number of Hidden Units

The number of neurons in the hidden layer (nH) dictates the accuracy as well as the complexity of the neural network. While too few neurons may not capture the trend of the training database accurately, too many neurons can lead to over-fitting of the training data set (see Figure 4.2). Hence, in order to get the optimal number of neurons in the hidden layer, in this study, neural networks have been generated with nH varying from 1 to 20. Further for each value of nH, 10 neural networks have been generated.

The impact of the number of neurons in the hidden layer is shown in Figure 4.3. For each nH case, the standard error of the network has been calculated as

$$\text{Std. err.} = \sqrt{\frac{\sum_{i=1}^{p} e_i}{p}} .$$ (4.12)

As seen in this figure, the standard error decreases monotonically as the number of neurons in the hidden layer increases. The average value of the standard error for the twenty values of nH is approximately 5.18×10^{-4}.
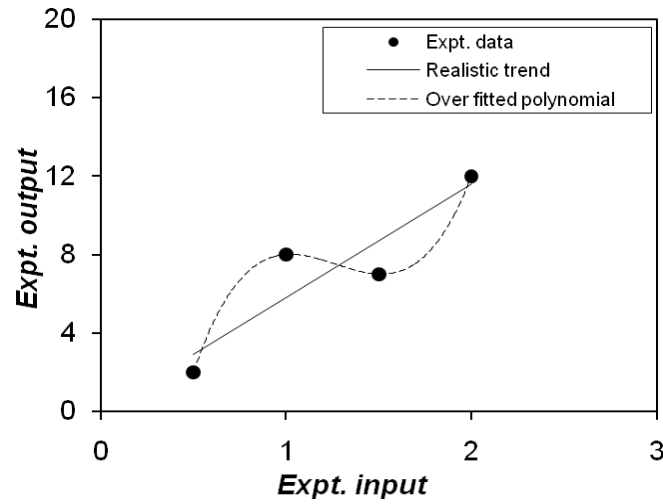
Figure 4.2: Example of overfitting of the neural network.
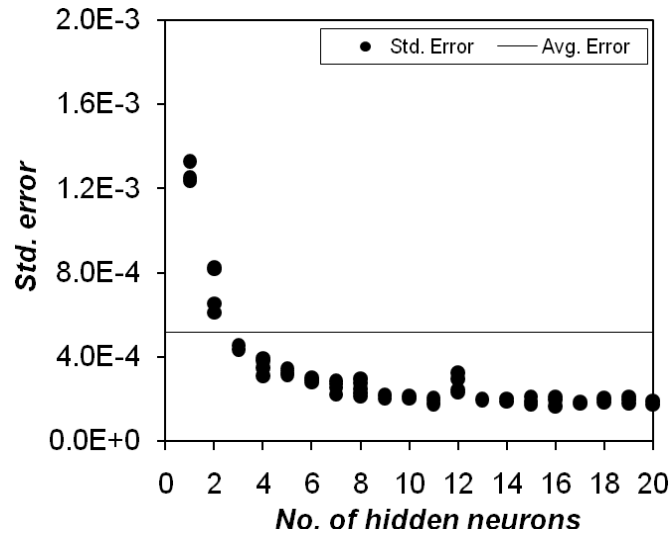
Figure 4.3: Impact of the number neurons in the hidden layer on the standard error.

Since *nH*=3 gives a standard error that is lower than this average value, it has been chosen as the minimum number of neurons needed in the hidden layer for an acceptable performance of the neural network. Thus, the rest of the chapter uses only three neurons in the hidden layer.

4.5 Multiple Trained Network

It is important to note that the backpropagation algorithm starts with a random set of initial network weights. As a result, at the completion of training, the final network weights will depend upon the choice of initial weights. To ensure that better networks that model the experimental data set more accurately are not missed out due to poor initialization, it is logical to generate several neural networks with different initial weights. While it is possible to use more systematic approaches such as the genetic algorithm to address this issue [96], in this preliminary study, a more direct approach has been pursued by designing 25 networks and calculating the volume fraction of bainite as an average of the predicted values predicted by these networks.

4.6 Analysis of Test Data

In this study, all the neural networks were trained using 35 input vectors from the database. Following the training of the neural network, all these networks were applied to the remaining 402 input combinations in the database.

The error of each of these networks for the training and the test data set is shown in Figure 4.4. As seen in this figure, all the networks give a consistent performance. As expected, the error of the networks for the training data set is lower than the error of the test data set (average values of 0.022 and 0.650, respectively). The average value of the volume fraction of bainite estimated by these 25 networks and the associated standard deviations are plotted in Figure 4.5.
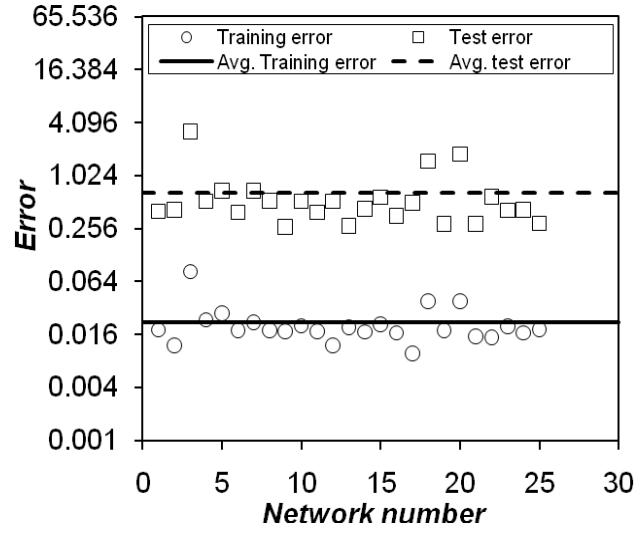
Figure 4.4: Error of the training and test data from the 25 networks as computed using Equation (4.5).
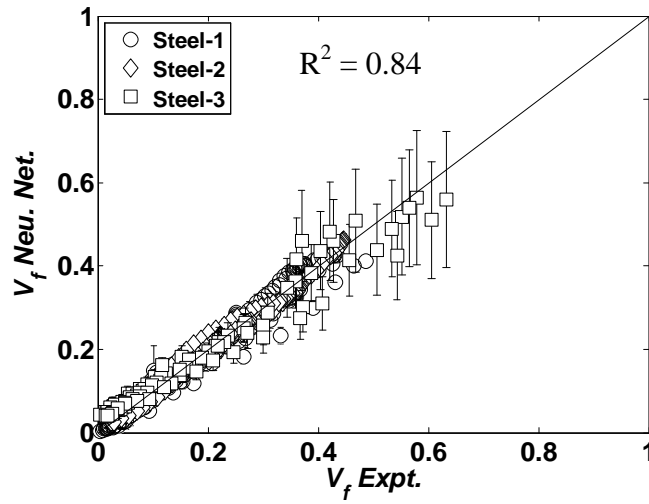
Figure 4.5: Volume fraction of bainite for the three steels as estimated by the neural network.

In this figure, the the experimental volume fraction of bainite is predicted by the neural networks with an R^2 value of 0.84. Specifically, the performance of the ANN is better for Steel-1 and

Steel-2 than for Steel-3. In Steel-3, there is a slightly larger standard deviation in comparison to the predictions of the other two steels. This is primarily due to the fact that the number of data points from this steel that were included in the training database was less than the number of data points of the other steels. Nevertheless, it can be reasonably concluded that the ANN performs quite well for these low carbon steels.

4.7 Impact of Alloying Elements

Four of the alloying elements in the current steels are ferrite stabilizers, viz., Si, Mo, Cr and V. On the other hand, Mn and Ni are austenite stabilizers. All the trained ANN was employed to study the effect of these alloying elements on the volume fraction of bainite. Specifically, for each steel, starting from its original chemical composition (baseline composition) the content of one alloying element at a time was varied at the input of each ANN, keeping the amount of the other alloying elements at the baseline value.

Further, for each steel, this analysis was done for three different isothermal transformation times, viz., 0.5h, 1h and 2h. The choice of these times was based on the fact that the transformation in all these steels was completed within 2h. For all three steels the lowest transformation temperatures from the database were chosen, i.e., 318°C, 351°C and 330°C for Steel-1, Steel-2 and Steel-3, respectively. The impact of each alloying element on the volume fraction of bainite in the steels is discussed next.

Silicon: The addition of Si decreases the volume fraction of bainite in all three steels (see Figures 4.6-4.8). While there is a polynomial behavior in the graphs of Steel-1 and Steel-2, there is a nearly linear relationship between the volume fraction of bainite and the percentage of Si in Steel-3. Further, in Steel-2 (see Figure 4.7) there are indications of a saturation value of Si, beyond which there is no impact of Si. The inverse relation between the Si content and V_f is in agreement with the observations of Suzuki *et al.* [97].

In all three steels, it was found that this decreasing trend was more pronounced as the transformation time increased. More precisely, for a short transformation time the impact of Si content was negligible. However, as the transformation time increased there was a steeper decline in V_f with an increase in Si (see Figures 4.9-4.11).
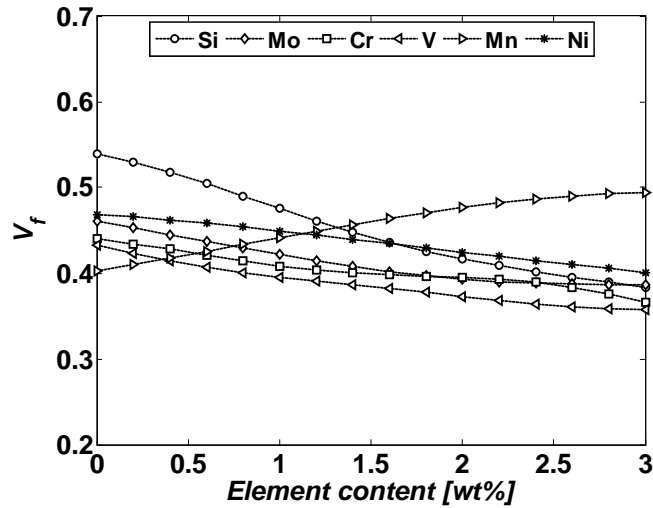
Figure 4.6: Effect of alloying elements on the volume fraction of bainite in Steel-1 at an isothermal transformation temperature of 318°C and for a transformation time of 2h.

79
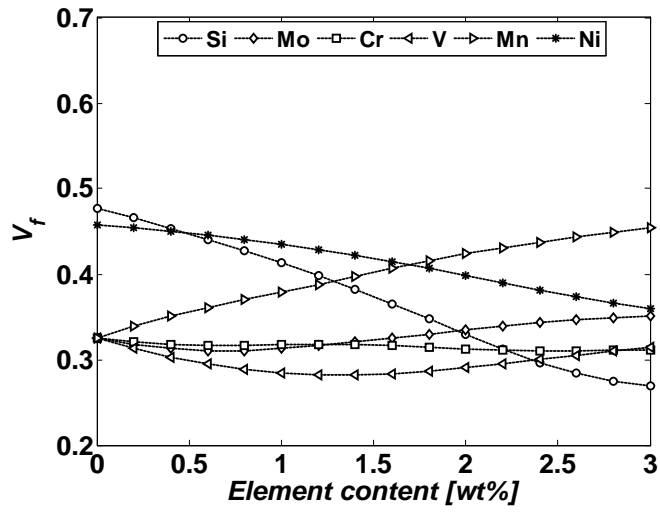
Figure 4.7: Effect of alloying elements on the volume fraction of bainite in Steel-2 at an isothermal transformation temperature of 351°C and for a transformation time of 2h.
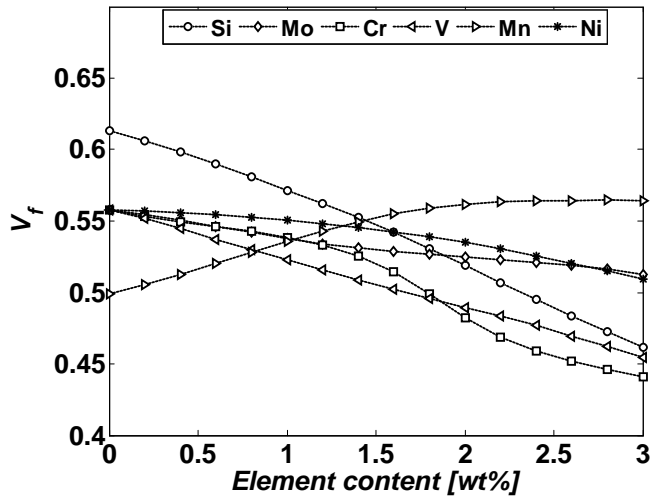
Figure 4.8: Effect of alloying elements on the volume fraction of bainite in Steel-3 at an isothermal transformation temperature of 330°C and for a transformation time of 2h.
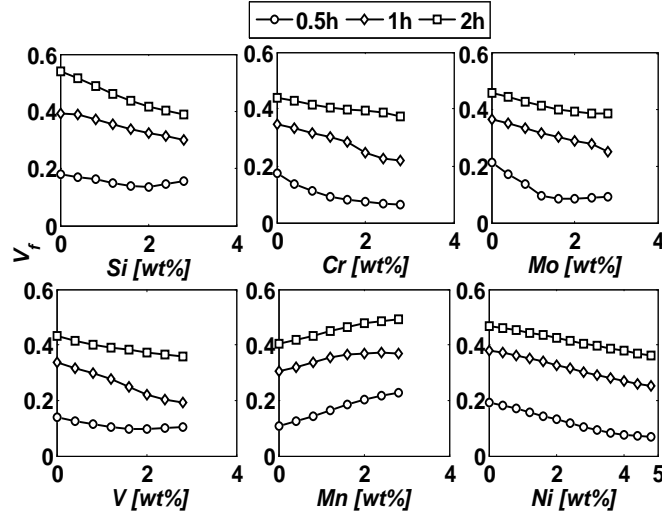
Figure 4.9: Effect of the alloying element content on the volume fraction of bainite in Steel-1 for three different transformation times, at an isothermal transformation temperature of 318 ℃.

Chromium: Suzuki *et al*. [97] have recently shown that Cr tends to retard bainitic transformation. The neural networks of this study have been able to capture this inverse relationship accurately. More precisely, as shown in Figure 4.6, there is a slow and almost linear decrease in the volume fraction of bainite as the Cr content increases in Steel-1. Interestingly, Cr has a very negligible effect in Steel-2 (see Figure 4.7). In Steel-3, following a slow initial decrease until its percentage reaches 1.5 wt%, a further increase in Cr content results in a relatively faster decline in V_f (see Figure 4.8).

For all three steels, when the isothermal transformation time is 0.5h, it was found that as Cr content increases, V_f tends to decrease asymptotically to a steady state value. When the transformation time is increased to 1h, this decrease happens at a slower pace. At an isothermal transformation time of 2h, the decrease in V_f with an increase in the percentage of Cr is very
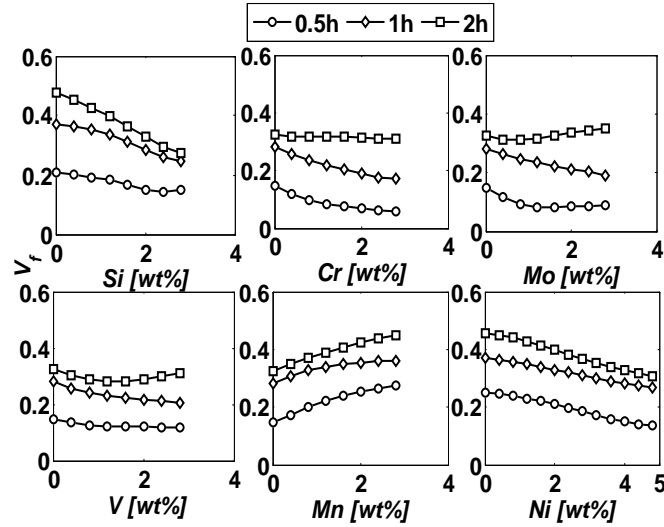
Figure 4.10: Effect of the alloying element content on the volume fraction of bainite in Steel-2 for three different transformation times, at an isothermal transformation temperature of 351 °C.

small. The impact of Cr content on V_f for the three isothermal transformation times is shown in Figures 4.9-4.11 for the three steels.

Molybdenum: In Steel-1 and Steel-3, V_f decreases nearly linearly with Mo, but at a very small rate (see Figures 4.6 and 4.8). In Steel-2, after an initial decline until the Mo content is approximately 1wt%, there is a marginal increase in the volume fraction of bainite with a further increase in the percentage of Mo (see Figure 4.7). The overall behavior of a decrease in V_f with an increase in Mo content is similar to the observations of Yakubovsky *et al.* [98].

As in Cr, for the very short transformation time of 0.5h, there is an asymptotic reduction in the volume fraction of bainite as the Mo in Steel-1 increases (see Figures 4.9-4.11). However, for the longer transformation time of 1h, the rate of decrease of V_f is sufficiently small. Thus, for the
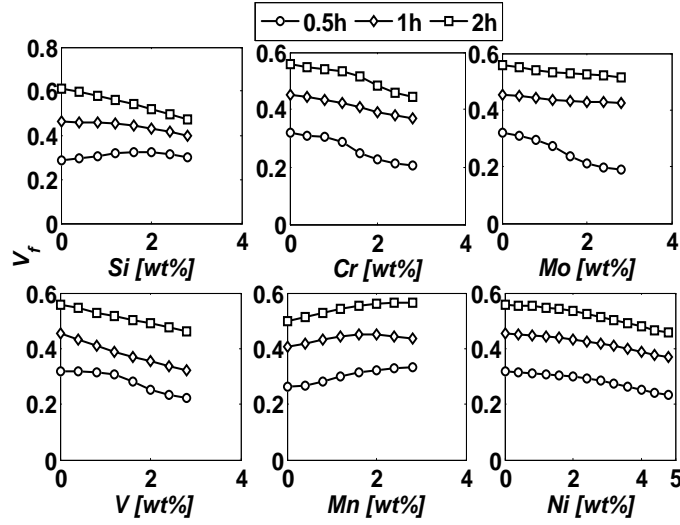
Figure 4.11 Effect of the alloying element content on the volume fraction of bainite in Steel-3 for three different transformation times, at an isothermal transformation temperature of 330℃.

range of Mo content investigated the asymptotic behavior seen when the transformation time of 0.5h, was not observed. This low rate of decrease of V_f is also seen when the transformation time is increased to 2h in Steel-1 and Steel-3. In Steel-2, there is a small initial decrease followed by marginal increase in the volume fraction of bainite. Nevertheless, the variation in V_f is very small as in the other two steels. These trends were also seen for the other two steels.

Vanadium: As seen in Figures 4.6 and 4.8, an increase in the V content results in a nearly linear decrease in the volume fraction of bainite in Steel-1 and Steel-3. In Steel-2, after an initial decline with increasing V, a V content greater than 1.5wt% results in a marginal increase in the V_f (see Figure 4.7). For the three transformation times investigated in this study, the impact of V on V_f is similar to the impact of Cr on V_f (see Figures 4.9-4.11).

Overall, in the Figures 4.9-4.11 it is seen that the neural network predicts that the effects of Cr, Mo and V on the volume fraction of bainite are nearly the same. From their investigations, Hillert *et al*. [99] also reached a similar conclusion

Manganese: As seen in Figures 4.6-4.8, unlike the ferrite stabilizing elements, Mn has a positive impact on the volume fraction of bainite. Specifically, as the percentage of Mn increases, there is an increase in V_f in all three steels.

More precisely, V_f follows a logarithmic profile with respect to the content of Mn. Also in all three steels, this increase in V_f is seen for all three isothermal transformation times. This increasing trend is shown for the three steels in Figures 4.9-4.11. Radovic *et al*. [100] investigated the effect of Mn in low carbon steels and found that Mn aids the formation of bainitic structures in the low carbon steels. It must be noted that addition of Mn usually shifts the TTT-curves to the right [3], requiring longer transformation times for a complete transformation. For the steels investigated in this part of the study, the ANN uses a transformation time of 2h, much longer than the transformation time needed for a completion of bainite formation in these steels.

Nickel: Unlike the expected trend of a positive relationship between Ni and V_f, in all three steels, an increase in Ni results in a gradual decrease in V_f (see Figure 4.6-4.8). Further, for all three steels, this inverse trend was observed at all three transformation times (see Figures 4.9-4.11). The inability of the network to accurately capture the effect of this alloying element may be attributed to: (a) the sparse number of data (35) for training the large range of Ni in the database,

(it must be recalled that Ni has the largest percentage range in the database,) and (b) the scatter in the experimental data.

4.8 Summary

In this chapter, artificial neural network has been proposed as an alternative method to determine the volume fraction of bainite in low carbon steels. Among the several influential parameters, the six alloying elements in the steels, isothermal transformation temperature and time, and the maximum transformation temperature at which bainite formation takes place have been given as the input to the neural network. The network itself had one hidden layer with three neurons and one neuron in the output layer that predicted the volume fraction of bainite.

For training the network the backpropagation algorithm was used. The database needed for the training and testing of the neural network was created from the experimental data of three low carbon steels from the literature. Following an analysis of the number of neurons needed in the hidden layer, three neurons were used in this layer to accurately capture the trends. Further, for this study, 25 networks were trained and the results were presented as the average value obtained from these networks. It was found that the neural networks were able to predict the value of V_f with an average total error of about 0.2% for each data point in the database.

The impact of the individual alloying elements on the volume fraction of bainite was also studied. Except for Ni, the relation between the volume fraction of bainite and the percentage of the other alloying elements was correctly predicted by the ANN. Specifically, as per the

metallurgical theory, it was found that as the content of the austenite/ferrite stabilizers increased, the volume fraction of bainite increased/decreased. Thus, it can be concluded that well trained ANN can be used to determine V_f as a function of several influential parameters and is a good alternative to the physical models in the literature.

Chapter 5

Development and Experimental Validation of a Neural Network Model for Prediction and Analysis of the Strength of Bainitic Steels

5.1 Introduction

Theoretical approaches to determine the volume fraction of bainite in an isothermally heat treated steel were presented in Chapters 3 and4. In this chapter, efforts have been made to develop a theoretical method to predict a material property of the heat treated steel, viz., hardness. More specifically, as a primary objective, in this chapter, an ANN approach has been presented to study the hardness of isothermally heat treated high-carbon bainitic steels containing as many as nine alloying elements. Given that the strength of the material depends upon several contributing factors such as heat treatment conditions, alloying elements etc., that contribute to the hardness of the material in a very complex manner, developing physical models are quite challenging. Under these circumstances, employing ANN to develop a model for the hardness of materials is pertinent. The applicability of ANN to such complex problems is already discussed in the previous chapter.

As briefly mentioned in Chapter 2, the focus on high carbon steels is guided by the fact that for industrial applications such as rails and automobiles, as well as structural applications [42], steels must have a combination of properties such as high strength and ductility, which usually involve

a tradeoff. Such properties may be achieved through an appropriate combination of chemical composition coupled with proper heat treatment procedures that will enable us to design steel with lower bainitic microstructures in the nanometer range. Unlike the low carbon steels that are more likely to form a coarse upper bainitic steel, the high carbon steels are well suited for obtaining fine bainitic microstructures at low transformation temperatures since a high carbon content in steel widens the gap between the bainite start (B_s) and martensite start (M_s) temperatures [42]. This much wider bainitic range of temperature facilitates the tempering heat treatment near the M_s temperature that leads to extremely fine bainitic microstructure. Further, the addition of suitable alloying elements to these high carbon steels can control the thermodynamics of the transformation process to obtain a large volume fraction of bainite that will lead to steels with high strength, toughness as well as improved ductility properties. Thus, the neural network model proposed for the high carbon steels will therefore be applicable to study the experimental steels considered in the following chapters.

The model presented in the subsequent sections takes into account the effect of as many as nine alloying elements as well as heat treatment conditions, viz., austenitization temperature (T_{aus}), isothermal transformation time (t_{iso}) and isothermal transformation temperature (T_{iso}), in predicting the hardness of the material. As mentioned in the previous chapter, in view of certain degree of randomness involved in the development of an ANN, 35 neural networks have been generated and as before our reference to the output of the neural network model (NN-model) implies an average of the output values predicted by these 35 neural networks. In this chapter, to develop the NN-model, experimental data from 15 high carbon steels that have a variety of chemical compositions have been used from the literature (see Table 5.1, first 15 steels).

Table 5.1: Chemical composition of the 24 carbon steels that have been used for the development and testing of the NN-model. The austenization data are taken from Refs. [42, 43, 45, 101, 102].

Steels	C	Si	Ni	Mn	Mo	Cr	V	Co	Al
1	0.98	0.08	0	1.84	0	0	0	0	0
2	0.58	0.89	0.06	0.81	0.02	1.27	0.11	0	0
3	0.91	0.23	1.35	0.65	0	0.6	0	0	0
4	0.89	0.19	4	0.39	0	1.58	0	0	0
5	0.6	0.3	2.75	0.6	0.5	1.25	0.12	0	0
6	0.76	0.25	0	0.61	0.006	0.017	0	0	0.0065
7	0.75	0.27	0	0.61	0.1	0.004	0	0	0.0065
8[a]	0.98	1.46	0	1.89	0.26	1.26	0.09	0	0
9	0.76	0.25	0	0.82	0.16	0.6	0	0	0.0065
10	0.76	0.27	0	0.6	0.3	0.58	0	0	0.0065
11	0.79	0	0	0.76	0	0	0	0	0
12	0.89	0	0	0.29	0	0	0	0	0
13	0.98	1.46	0	1.89	0.26	1.26	0.09	0	0
14	0.79	1.59	0.02	1.94	0.3	1.33	0.11	0	0
15	0.8	1.84	0	2.18	0.3	1.04	0	1.31	0.85
16	0.73	1.62	0.12	0.73	0	0.1	0.01	0	0
17	0.97	0.26	0.05	0.27	0.01	0.77	0	0	0
18	0.75	0.25	1.35	0.7	0.3	0.75	0.15	0	0
19	0.95	0.24	1.79	0.58	0.25	0	0	0	0
20	0.95	0.22	3.27	0.6	0.13	1.23	0	0	0
21	0.83	1.57	0	1.98	0.24	1.02	0	1.54	0
22	0.78	1.49	0	1.95	0.24	0.97	0	1.6	0.99
23	0.69	1.92	0	1.38	0.24	1.39	0	0.14	0.75
24	0.79	2.48	0	2.06	0.27	1.49	0.158	0	0

Following the successful formulation, the NN-model has been validated on experimental hardness data from 8 other steels that were not used for the development of the model. These are the Steels 16-23 in Table 5.1. The NN-model has also been compared with three recent

[a] This steel had P=0.002 and this element has been neglected in the present study.

correlations presented by Zou [103] to justify its development and need.

5.2 Artificial Neural Networks Model

The schematic of a two layer artificial neural network is similar to the neural network for the volume fraction of bainite in Chapter 4. The neurons in the first layer receive the user defined, i.e., the chemical composition and heat treatment parameters, whereas the inputs to the neurons in the subsequent layers are the outputs from the neurons in the previous stages. The output of the neuron in the last stage is the desired material property, a quantitative estimate of which is being sought (hardness in this case).

5.2.1 Network Topology

For the present model, a two layer neural network has been used. One neuron has been used in the second layer (output layer) the output of which corresponds to the hardness value of the steel for the particular heat treatment condition. As in the previous chapter, the number of neurons (nH) in the first layer has been finalized after a more systematic study. More precisely, in order to get the optimal number of neurons, several networks have been generated with nH varying from 1 to 20. Further for each value of nH, ten neural networks have been generated. It was found that beyond $nH=5$, an increase in nH did not produce a reasonable improvement in the mean square error of the neural network. In other words, five neurons in the hidden layer are sufficient for an accurate performance of the network. The actual generation of the networks, including the database preparation and the network training, is discussed below.

5.2.2 Database and Training Description

The network database consists of hardness values of 23 standard steels with several heat treatment conditions. The database has been compiled from the Atlas [101] for the steels summarized in Table 5.1. In all, 220 hardness values have been used in the database. The 24th steel in Table 5.1 is a new research steel whose data has been included in the database to ensure that the NN-model's range includes the high value of Si (2.58wt %) in this steel, thereby making it applicable to the experimental steels of this thesis. In Table 5.2, the range of the individual alloying element, heat treatment conditions and the hardness values are given to present an overview of the range of the parameters in the database. To ensure that the actual numerical

Table 5.2: The parameters and their range used in the neural network.

Parameter	Range
Input	
C, wt%	0.58-0.98
Si, wt%	0-2.48
Ni, wt%	0-3.27
Mn, wt%	0.29-2.18
Mo, wt%	0-0.27
Cr, wt%	0-1.49
V, wt%	0-0.15
Co, wt%	0-1.6
Al, wt%	0-1.02
T_{aus}, C	845-1000
T_{iso}, C	200-500
t_{iso}, s	$12-5.88 \times 10^{6}$
Output	
HV	314.75-764.84

value or the range of any particular parameter does not overshadow the influence of other parameters on the hardness model, each parameter including the hardness values was standardized and normalized. In other words, every input parameter and the target hardness value had a mean of zero and a range of [-1, 1].

For network training, i.e., determination of the optimal set of network weights, the *Levenberg-Marquardt backpropagation* (LMBP) algorithm described in the previous chapter has been employed. For training 175 data points from the database were used. These correspond to the experimental data of the first 15 steels and the two experimental data of Steel-24 listed in Table 5.1. The training was done until one of the following termination criteria was met:

(i) The number of iterations reached 100,000.

(ii) The mean square error of the network was less than 0.001.

(iii) The gradient of the search direction in the LMBP algorithm was less than 1×10^{-9}.

5.2.3 Validation of Neural Network

The performance of the network was tested by applying the remaining 47 points of the database that was not used in the training of the algorithm. These correspond to the experimental data of the Steels 16-23 listed in Table 5.1. 35 neural networks that meet the error tolerance criterion were generated, and the hardness value of steel that is processed via a particular heat treatment condition is the average value predicted by these networks.

The average prediction of the networks for the training and the test data along with the standard deviations is shown in Figures 5.1a and 5.1b, respectively. As seen in these figures, the neural network estimates the experimental data of the literature with an R^2 value of 0.8 and 0.69, respectively.

It is important to note that the size of the database is an order of magnitude smaller than what is usually preferred in the design and development of a neural network. Yet, the NN-model is able to predict the hardness values of a wide range of steels. This is an indicator of the fact that there is an inherent correlation between the hardness of the steel and the material composition/heat treatment conditions.
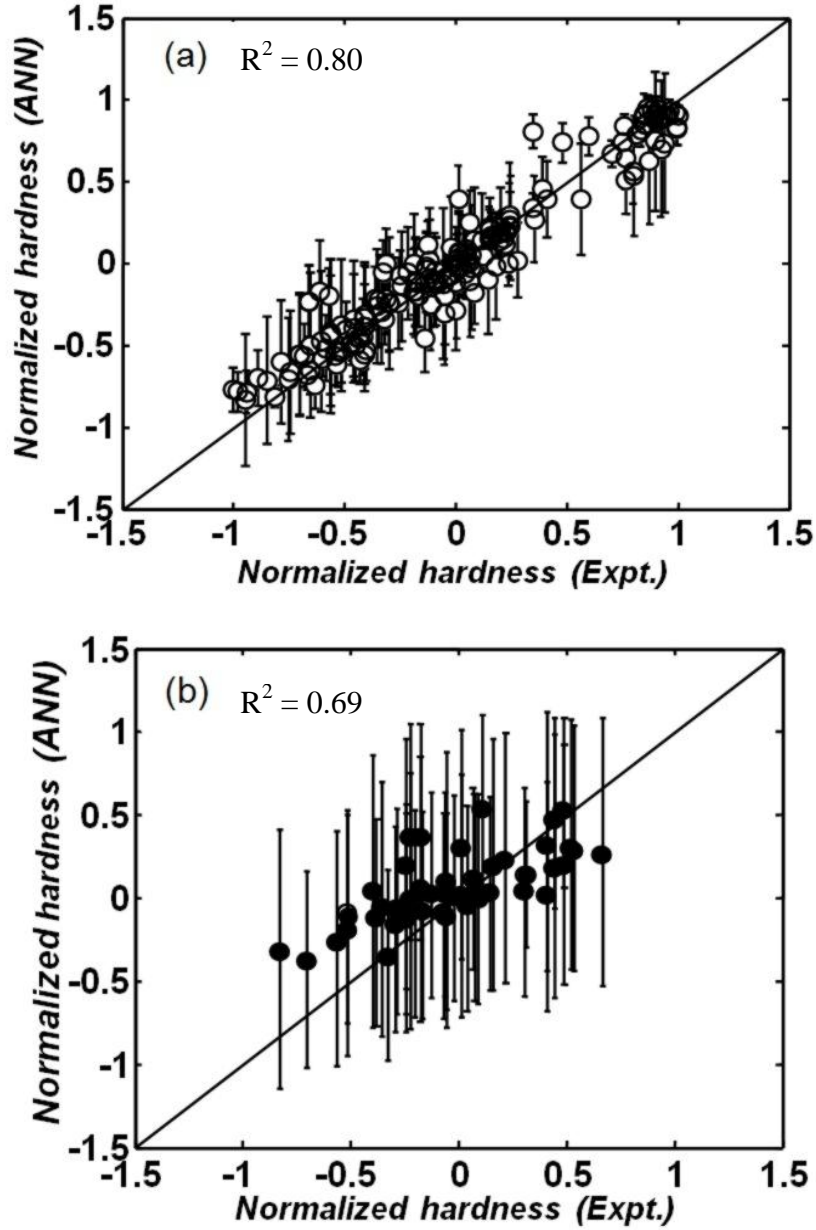
Figure 5.1: Comparison of the hardness of the bainitic steels in the database as estimated by the neural network and from the experimental values in the literature. (a) The neural network is trained using 15 standard steels from the literature and one steel of this thesis. (b) The validation is presented for 8 other steels that were not used for the development of the model.

Nevertheless, as discussed below, to quell further arguments against the size of the database, the NN-model has also been applied to the 24 experimental data points from the five newly designed steels that the model has not seen before.

5.3 Comparison with Other Correlations in Literature

In order to establish the neural network model as a valuable utility tool from the industrial point of view it is important to compare its performance with other models in the literature. For this, the performance of the present model has been made with respect to three recent correlations from the literature. These correlations were proposed taking into consideration the effect of the alloying elements and the heat treatment conditions of the steels, and are discussed next.

Zou [103] proposed the hardness, $H^{(1)}$ of the steel based on the tempering temperature (T) and the carbon content (W_C) as

$$H^{(1)} = 70.3 - 0.082T + 8.85W_C, \tag{5.1}$$

where W_C is in weight percent. The author arrived at the above expression following a regression analysis of the hardness of 18 steels that had carbon content in the range of 0.4wt% to 1.2wt%. Subsequent to this, the author also proposed an improved correlation after considering a much larger number of steels as

$$H^{(2)} = 75.5 - 0.094T + 6.66W_C, \tag{5.2}$$

Zou [103] also found that using the equivalent carbon content instead of the weight percentage of carbon yielded good results and accordingly suggested a correlation for the Rockwell hardness as
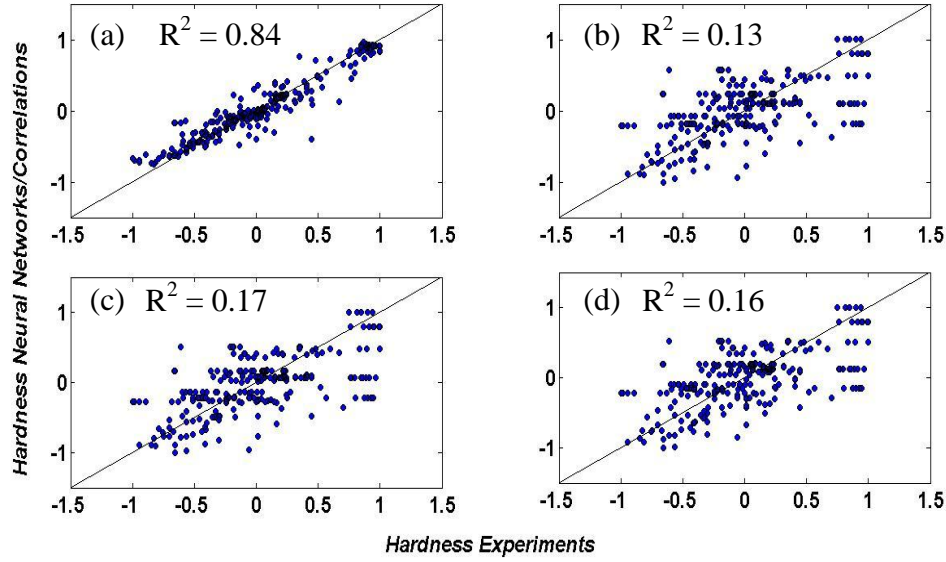
Figure 5.2: Hardness of bainitic steels of the database as estimated by (a) neural network model (b) Correlation A (Eq. (5.1)), (c) Correlation B (Eq. (5.2)) and (d) Correlation C (Eq. (5.3)), plotted againt the corresponding experimental values from the literature.

$$H^{(3)} = 75.5 - 0.094T + 6.66 \left(W_C + \frac{W_{Mn}}{6} + \frac{W_{Cr} + W_{Mo} + W_V}{5} + \frac{W_{Ni} + W_{Cu}}{15} \right),$$ (5.3)

In Figure 5.2a-5.2d, the results from the application of the NN-model and the above correlations to the steels from the present database have been shown. The R^2 values in the four approaches are 0.84, 0.13, 0.17 and 0.16, respectively.

5.4 Significance Analysis

In view of the numerous parameters that have been used as input to the neural network to model the hardness value of steel, it is important to first justify the choice of these parameters by considering their impact on the modeled property (hardness in this case). For this, a significance analysis has been made where the impact of each input parameter on the predicted hardness of all the steels in Table 5.1 is determined quantitatively.

To obtain the significance value of a parameter, the sensitivity of hardness values to the input parameters is quantitatively evaluated. For this the hardness ($H^{(1)}$) of the steels in the database is determined by setting the corresponding weights in the input layer to zero. More precisely, for the kth parameter, w_{ik} is set equal to zero where $i=1, 2, ...n$, n being the number of neurons to which this input parameter is fed. It must be recalled that in the present investigation $n=5$. This value is compared with the hardness values (H) obtained without setting the corresponding weight to zero. The significance value of the parameter is then

$$s = \frac{1}{l}\sum_{i=1}^{l}\left(\frac{h_i - h_i^{'}}{h_i}\right) \times 100, \tag{5.4}$$

where h and h' are the elements of the vectors H and $H^{(1)}$, respectively. l is the size of the database that is evaluated, 221 in this case. The sensitivity of the twelve parameters of this study is summarized in Figure 5.3.

As seen in this figure, almost all the parameters have an important influence on the hardness of the material. In other words, the choice of the parameters is completely justified. It must also be
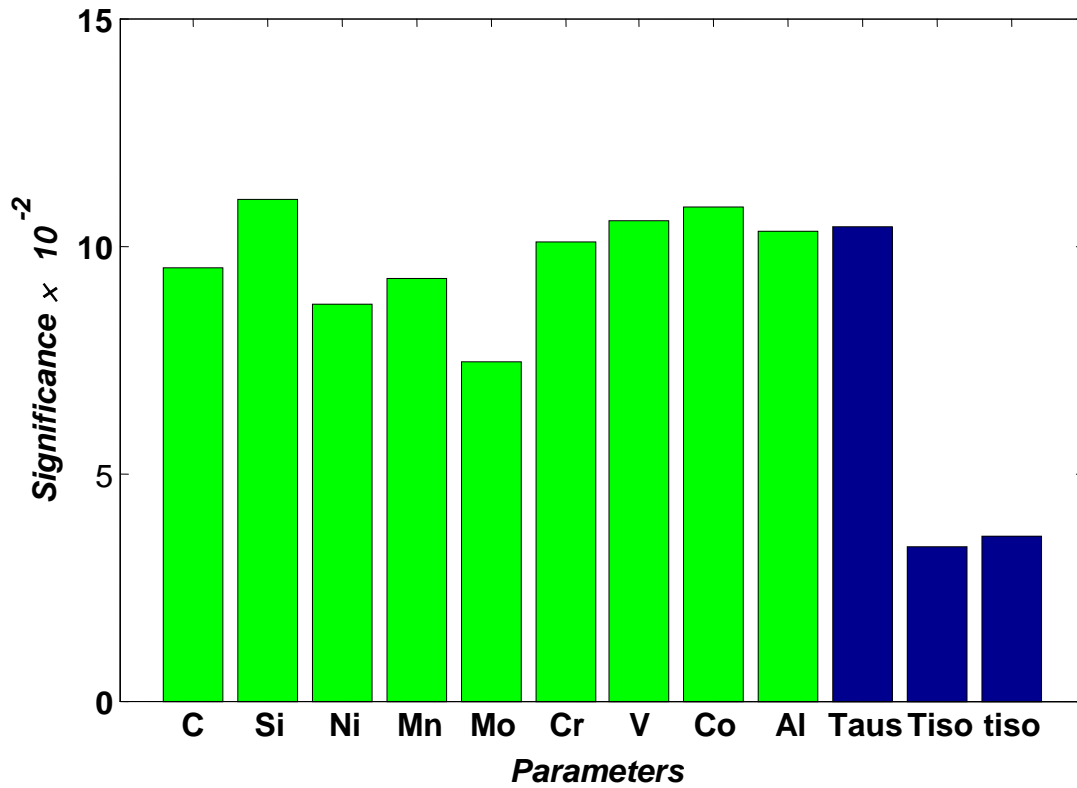
Figure 5.3: Significance of each variable of the chemical composition, heat treatment for the hardness model, the inputs listed in Table 5.1.

pointed out that the relatively high significance of all the parameters and the inherent cross-correlation is further evidence of the complexities of modeling the hardness of the material as a function of these parameters.

5.5 Summary

In this chapter, an artificial neural network approach has been presented to predict the hardness of bainitic steels with a carbon content in the range of 0.5<C<1.0 wt%.

Thirty five networks were developed using approximately 175 experimental hardness data from 16 different steels (15 standard steels selected from the literature and one experimental steel of the present thesis). The average value of the hardness predicted by these networks gives an estimate of the hardness of the steel of given composition and heat treatment conditions. The performance of this strategy was tested on 47 experimental hardness data from eight other standard steels that were not used for the model development. The hardness of the steels was well predicted by the artificial neural networks for these data points, thereby establishing the predictive abilities of the present neural network model. Additionally, a comparison of the hardness predictions from the neural network models with the ones from three recent correlations proposed by Zou [103] clearly showed the superior performance of the present approach. This makes the proposed neurocomputing method a valuable and reliable tool in the design and development of bainitic steels in industry.

In summary, given the objective of developing a computational tool that can predict the mechanical property, hardness in particular, of the isothermally heat treated steels more accurately, that is applicable for a wider variety of steels and that can be employed in an industrial environment, the neural network approach presented in this chapter meets these requirements satisfactorily. The model will be applied to study the hardness of the bainitic steels of this thesis in Chapter 7.

Chapter 6

Materials and Experimental Procedures

6.1 Introduction

The focus of this chapter is to provide details about the materials, experiments and procedures used in this research. Specifically, details are presented for the equipment and methods that are used for the initial characterization of the materials, heat treatment of the materials and finally the post-transformation analysis for the final characterization of the heat treated samples.

Initial characterization of the material involves the following:

1. Dilatometry, that is used to determine the M_s temperature to ensure that the isothermal heat treatment is conducted above this temperature. It also provides the range of temperatures in which austenitization takes place. Finally, the dilatometry results can also be used to calculate the coefficient of thermal expansion that is needed to determine the carbon content of austenite.

2. Differential scanning calorimetry (DSC) that is used to determine the range of temperatures in which austenite and bainite phases can be obtained.

The final material characterization involves the following:

1. Scanning electron microscopy (SEM) analysis that is employed to observe and understand the microstructure morphologies and verify bainitic transformation.

2. X-ray diffraction (XRD), that is used to identify phase transformation and obtain the lattice parameters for calculating the volume fraction of retained austenite.

3. Mechanical testing including the hardness and compression tests to characterize the strength and the deformation ability.

In the ensuing sections, the equipment and experimental method are presented in detail for each of the aforementioned steps.

6.2 Steel Design

Three experimental steels have been chosen for the present thesis. All steels had high carbon content. As mentioned in Chapter 1, this allows for a wide range of bainitic transformation temperatures by increasing the temperature range between the B_s and M_s temperatures. Additionally, the design of the steels was based on shifting the T_o curve to greater austenite carbon content at any transformation temperature by adjusting the substitutional solute content. Such a shift will increase the volume fraction of bainite and minimize the blocky austenite in the microstructure. The addition of alloying elements also aid in accelerating the rate of transformation thereby minimizing the amount of heat treatment time needed for the maximum possible phase transformation.

6.2.1 Raw Material Preparation

All three steels were prepared by CANMET-MTL as a 200 kg vacuum melted heat and cast as 4 ingots in an argon atmosphere. Slabs were then cut from the ingots and soaked at 1200°C. After

Table 6.1 Chemical composition of the high carbon steels selected in the present study (in wt %).

Alloy	C	Si	Mn	Mo	Cr	V	Co	Al
Steel-1	0.88	1,63	2.15	0.25	1,25	0.144	-	-
Steel-2	0.78	1.74	2.15	0.24	0.89		1.48	1.02
Steel-3	0.82	2.45	2.1	0.27	1.5	0.096		

soaking, the slabs were rolled with recrystallization occurring between the temperatures of 1180-1030°C. Next, the slabs were finish rolled in the no-recrystallization zone with a finishing temperature of 870-810°C for a total accumulated true strain of 1.0. The total number of rolling passes in both rough and finish steps was 15, resulting in a final plate thickness of 0.5 in and 0.25 in . After finish rolling, accelerated cooling at 50°C/s occurred between 790-200°C. Below 200°C the plate was air-cooled to room temperature. A thermocouple inserted at mid-thickness was used to monitor plate temperature during rolling and cooling. The chemical composition of the steels in wt% is summarized in Table 6.1.

6.3 Initial Material Characterization

Initial material characterization was done to determine the M_s temperature, the range of temperatures in which austenitization and bainitic transformation takes place. This initial characterization has been done via dilatometry and DSC, and is discussed below.

6.3.1 Dilatometry

A Bähr 805 dilatometer was used to study the length change (dilatation) of the specimen during a heat treatment. The monitoring of the dilatation is a commonly used method to study phase transformations in steels. The cylindrical massive specimens for dilatometry experiments were prepared with a size of 10 mm in length and 5 mm in diameter. A specimen is placed in the dilatometer between two quartz rods with a thermocouple spot-welded in the middle of specimen in order to control the temperature. In the dilatometer the specimen is heated by induction. Sufficiently high cooling rates (up to 85°C/s) are obtained by helium gas quenching. A description of the phase transformations investigated in the present work is presented in next chapter.

The test conditions used are:-

1. Heating to 900°C @ 5°C/s, 30min holding, heating to 1100°C @ 5°C/s, cooling to RT (power OFF), to determine the austenitization temperature.
2. Heating to 900°C @ 5°C/s, 30min holding, cooling to 250°C/s@ 10°C/s, cooling to RT (power OFF), to verify completion of transformation (see Appendix A, Figure A6).

The dilatometry was done atCanmet MATERIALS, Hamilton, Ontario, Canada.

6.3.2 Differential Scanning Calorimetry

A differential scanning calorimetric thermal analyzer (NETZSCH, STA 409 PC, and Burlington, MA) was used to determine the phase transformation temperatures with heating and cooling rates

of 1°C/min. These investigations revealed the phase transformation temperatures for the powders of the present steels, in terms of, A_s (austenite start), A_f (austenite finish), and A_p (austenite peak). The DSC tests were conducted at W. M. Keck Biomedical Materials Research Lab, School of Mechanical and Materials Engineering Washington State University, Pullman, Washington, USA.

6.4 Heat Treatment

The as received plates of the three steels were cut into strips with the dimensions of 15.1×1.3 mm. Finally, the strips were cut into small cubic specimens of length 6 mm and grinding marks were made on the samples to avoid mixing of the samples. These samples were then homogenized at 1200°C for 48 h in a furnace with a continuous Argon flow and were then left in the furnace to cool down to room temperature over a period of 24 h, resulting in a fully pearlitic microstructure. The homogenization of the samples was done at CANMET-MTL, Hamilton, Ontario, Canada.

The subsequent heat treatment, viz., austenitization and isothermal transformation was done in the lab. The furnaces for the austenitization (high temperature furnace) and isothermal heat treatment (low temperature furnace) are shown in Figure 6.1a. Heat treatment in both furnaces was done in a batch processing mode. Specifically, each batch consisted of three samples placed in a stainless steel mesh shown in Figure 6.1b. For heat treatment in both furnaces, the mesh crucibles containing the samples were placed as shown in the schematic in Figure 6.2.
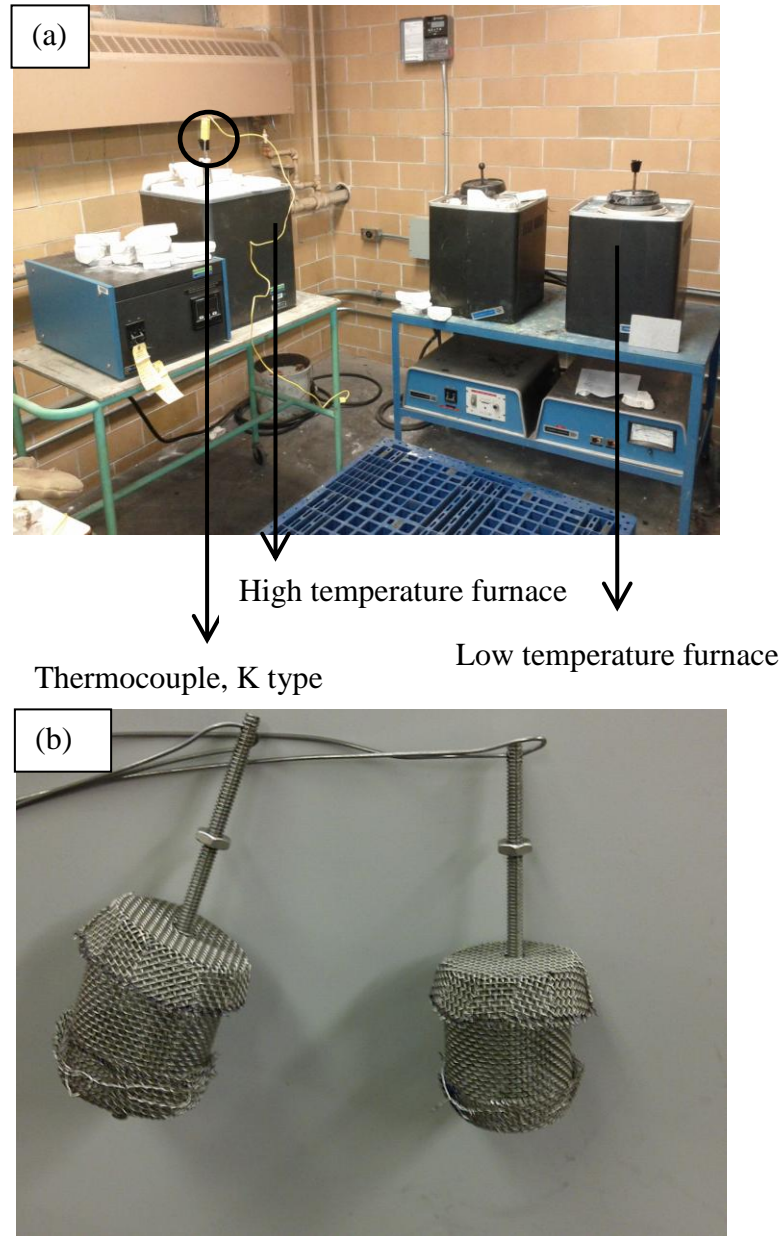
Figure 6.1: (a) Salt bath furnace used during the heat treatment experiments. (b) The mesh crucibles that were used for batch heat treatment of the steel specimens.

Austenitization as well as isothermal heat treatment of the homogenized samples was done in salt bath furnaces. This is because a salt bath technology offers several advantages:
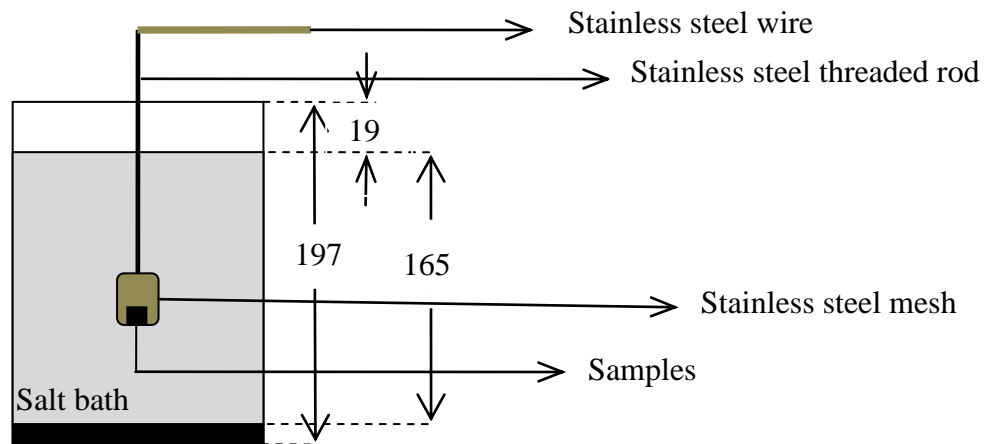
Figure 6.2: Schematic of the sample positioning in the salt bath furnace during the heat treatment experiments. Dimensions are in mm.

1. When parts are immersed in the molten salt, heat is transferred by direct contact to the surface. Since the parts are immersed in the salt bath, air cannot contact the specimen thereby avoiding scaling, oxidation and decarburisation.

2. Heat transfer into components is very rapid, much faster than with radiation or convection methods.

3. Salt bath provides a uniform rate of heat transfer and are therefore suitable for samples with complex geometries and diverse cross-sections.

4. It provides flexibility in the process with various quenching methods (i.e., oil, water, polymer, or into another salt bath).

5. The salts themselves are not expensive and the furnaces employing them compares favorably with other types of furnaces.

In this thesis, austenitization was carried out in an ISO-HEAT 871 salt bath furnace. Subsequently, the samples were transformed in ISO-THERM 142 salt bath furnace which was kept at the chosen bainite transformation temperature. The details of the heat treatment conditions along with the results are presented in the next chapter.

6.5 Final Material Characterization

Following heat treatment, the first objective is to ensure the formation of bainitic phase. This was done via SEM in which the microstructure images of the heat treated samples were compared with the reference images in the literature. SEM was preferred because its resolution is much higher than an optical microscope (OM). This is due to the fact that in SEM, the electrons accelerated to 10,000 keV have a wavelength of 0.12 Angstrom, while the visible light in OM has a wavelength from 4000 to 7000 Angstroms. The sample preparation and the equipment used for this are discussed next

6.5.1 SEM Sample Preparation

Following heat treatment, the samples were ground on 120 grit silicon carbide paper to remove nicks. Next, the samples were mounted using Bakelite powder into Buehler Simpliment 2000 automatic mounting press and hot mounting was used to prepare the moulds for microscopy. The temperature and pressure used for hot mounting were 150°C and 4200 psi respectively and water was used for cooling. The molded samples were ground again on silicon carbide paper of 120 grit followed by 320 grit, 600 grit and 1200 grit, in that order. For polishing the samples, Leco

VP-160 automatic polishing machine was used. The polishing was done using 8"diameter Leco polishing cloth by using diamond paste of 6 μm followed by 3 μm and 1 μm with diamond extender. The polished samples were etched using a solution of 2% Nital and picric acid (equal weight ratios) in order to enhance the clarity of the microstructure.

6.5.2 SEM Equipment

For the SEM analysis, the polished and etched samples were examined using a high performance JSM-6380LV scanning electron microscope with an embedded energy dispersive X-ray spectroscopy (EDS) system which allows for seamless observations and has a high resolution of 3.0 nm. The customizable graphical user interface (GUI) allows the instrument to be intuitively operated, and Smile Shot ^{TM} software ensures optimium operation settings. Standard automated features include auto focus, auto stigmator, auto gun (satuation, bias and alignment), automatic contrast and brightness. Depending upon the requirement, the three equipped detectors, viz., the secondary electron detector, backscattered detector and energy dispersive X-ray detector, were employed.

The SEM images were analyzed via a Discrete Fourier Transform based method to determine the average bainitic plate thickness in the heat treated steel. The details of this method are summarized in Appendix B. The method is fast and accurate, and it is verified that the results from this method are comparable to the Stereological method that is commonly used in studying microstructures.

6.5.3 X-ray Diffraction

Following the SEM analysis, a secondary verification of the phase formation was done via XRD analysis. For this, a multi-functional PANalytical X'Pert PRO X-ray diffractometer was used to identify the formation of phases in the heat-treated samples. X-ray diffraction (XRD) was performed using CuK_{α} radiation (wavelength $\lambda=0.15406$ nm) at 45 kV and 40 mA. The diffraction angle (2θ) at which the X-rays hit the sample varied from 40° to 100° with a step size of 0.04° and 2 s in each step. In addition to the verification of the phase formation, XRD analysis also provided the lattice parameters that are needed for the calculation of the volume fraction of retained austenite

6.6 Material Properties

6.6.1 Hardness Tests

The next step following the SEM and XRD analysis is to quantify the material strength. For this, Vickers microhardness tests were performed on the unetched samples using computerized Buehler Micromet-5100 microhardness testing machine that is coupled to a hyper terminal for computerized recording of the hardness data. The micro-hardness values were obtained by applying a load of 500 g and a dwell time duration of 15 s on the samples. For each sample, 15 measurements were made as described in Figure 6.3. The hardness of the material is taken as the average of these values. Prior to measuring the hardness of the samples, the hardness tester was calibrated using the reference block to verify the accuracy of the hardness values.
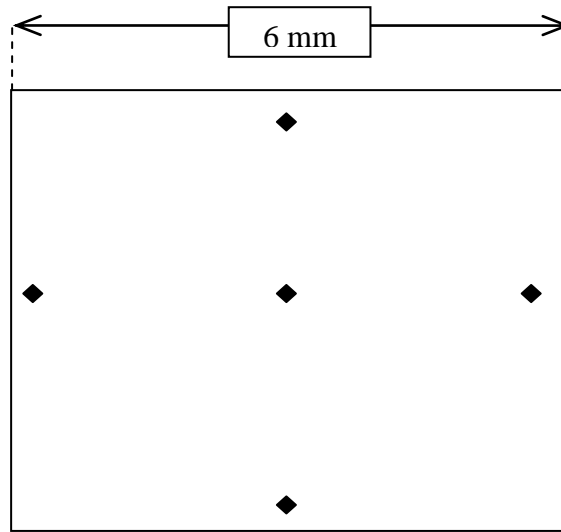
Figure 6.3: Position of indentations for the hardness measurements. The points close to the border are at a distance of 0.25mm from the edge of the sample.

Hardness tests were also performed on Bakelite mounted samples, using a load of 30 kg. For these tests, the hardness measurements were made at the five points shown in Figure 6.3. For micro-hardness measurements, two additional indentations were made at a distance of 0.5 mm from these positions. While these additional indentations were along the edge of the sample for the outer indentations, at the center, the two additional indentations were made along the horizontal direction. All the values presented were an average of these values taken on the same specimen. All the indentations were adequately spaced to avoid any potential effect of strain fields caused by adjacent indentations.

6.6.2 Compression Tests

The samples for compression tests were prepared according to the ASTM E 9M [104] standard. All samples were machined and prepared along the rolling direction, using the center lathe machine turned down to cylindrical samples. A schematic of the samples is shown in Figure 6.4 and the test schematic is shown in Figure 6.5. In order to avoid the damage to the compression plates, two additional steel plates were used to sandwich the specimen between the compression plates. These steel plates were martensitic and their high hardness, larger than the hardness of the bainitic steels of this thesis, prevented damage to the compression plates.

The tests were performed at room temperature using a computerized United testing machine. Three different strain rates were selected for the present study, viz., 1×10^{-2} s^{-1}, 1×10^{-3} s^{-1} and 1×10^{-4} s^{-1}. At least two samples were tested at each strain rate. The 0.2% offset yield strength and engineering stress-strain curves were recorded and these data were used to determine compressive strength of the material.
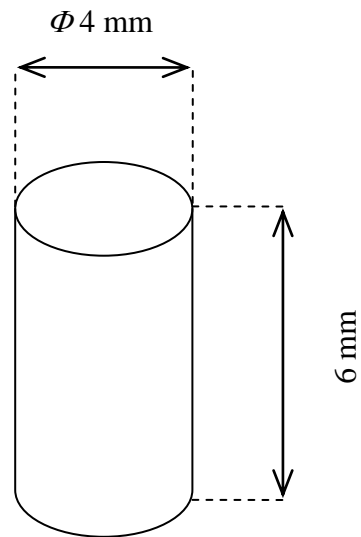
Figure 6.4: Specimen dimension for the compression test, prepared according to ASTM E 9M standards [104].
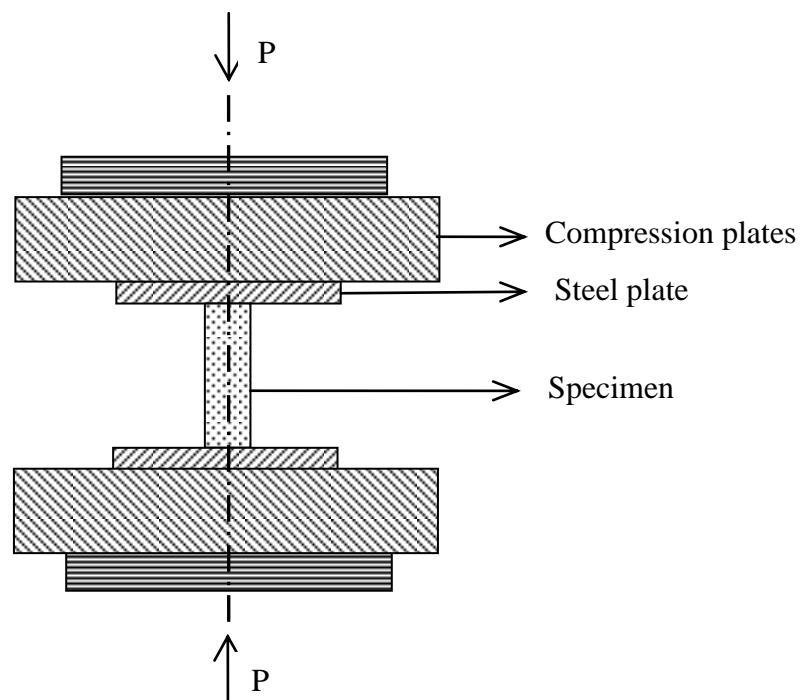
Figure 6.5: Schematic of the compression test.

In the following chapter, the results from the experiments discussed in the previous sections are presented in detail. Also, the experimental data from the steels are used to evaluate some of the models from the previous chapters.

Chapter 7

Experimental Results and Discussion

In this chapter, the results of the various analyses and test methods described in the previous chapter for the three experimental high carbon steels (see Table 6.1), are presented in detail. This chapter also includes a discussion on the models described in Chapters 3 and 5 as applied to these steels.

7.1 Determination of the Bainite Transformation Temperature

The dilatometry and DSC analysis was done to determine the appropriate isothermal temperatures to be used for the heat treatments.

7.1.1 Dilatometry

The first heating treatment condition, viz., heating to 900°C at 5°C/s, 30 min holding, heating to 1100°C at 5°C/s, furnace cooling to room temperature via power-off, described in Chapter 6, is used to determine the M_s temperature for the three steels. The change in length of sample as a function of temperature for this heat treatment condition is shown in Figure 7.1. The M_s temperatures of the three steels, below which martensite will be formed, are indicated by the arrows in Figure 7.1 and are summarized in Table 7.1. This M_s temperature indicates that the isothermal heat treatment temperature for achieving bainitic structures must be above this temperature.

(a)

(b)

(c)
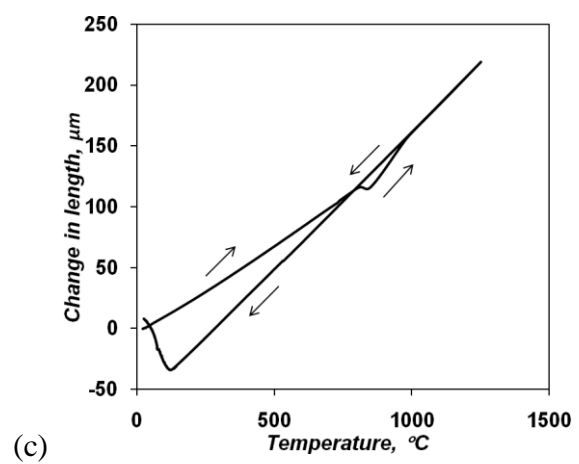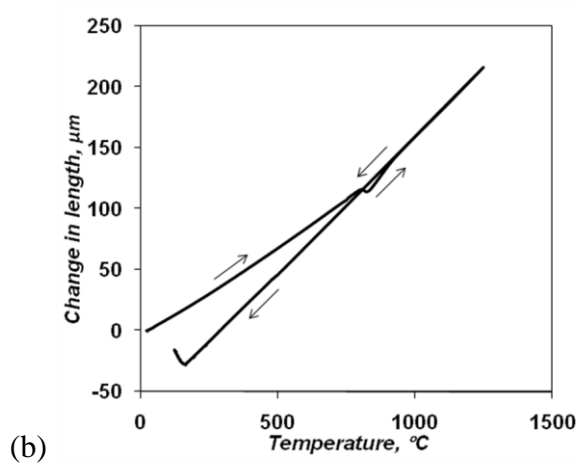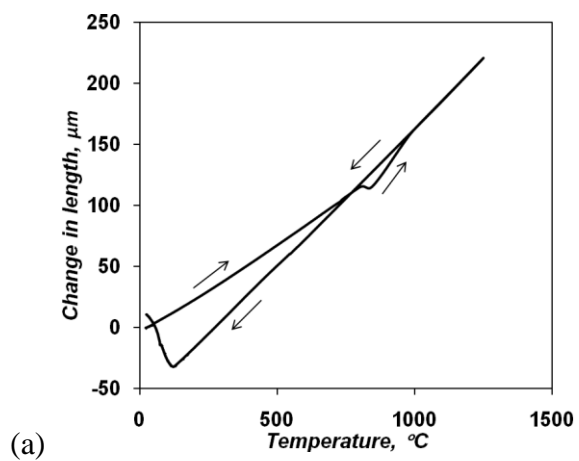
Figure 7.1: Dilatometry curves of the three steels of this study.

115

Table 7.1: The M_s and B_s temperatures of the three experimental steels.

ID	M_s, °C	B_s, °C
Steel-1	140	309
Steel-2	164	358
Steel-3	125	302

Hence, in the heat treatment experiments, the temperatures were maintained above this temperature.

7.1.2 Differential Scanning Calorimetry Analysis

DSC was done to determine the austenitization temperature (as seen in Table 7.2 and Figure 7.2). This is essential because, to obtain bainitic phase from an initial austenite phase, an initial heat treatment of the steel at a sufficiently high temperature (austenitization temperature) to obtain the austenite phase is necessary.

In this study, for each steel, DSC was done up to two temperatures, viz., 1250°C and 1350°C. The DSC curves corresponding to both final temperatures for the three steels are shown in Figures 7.2 (a)-(c). In all these figures, a ferrite phase is present in the material to the left of the peak start temperature summarized in Table 7.2.

Table 7.2: DSC results of the three steels indicating the start and end of ferrite to austenite phase transformation.

ID	Conditions	Peak (°C)		
		Start	Max	End
Steel-1	(1250°C)	760	773	819
	(1350°C)	753	774	825
Steel-2	(1250°C)	775	791	837
	(1350°C)	768	792	830
Steel-3	(1250°C)	779	802	847
	(1350°C)	782	800	837

As the temperature increases above this temperature, a gradual transformation of ferrite phase into austenite phase takes place. This continues and a fully austenite phase is present beyond the peak end temperature indicated in Table 7.2. The temperatures corresponding to the start and completion of the phase transformation are indicated by the vertical dotted/solid lines for 1250°C/1350°C on Figure 7.2a-c.
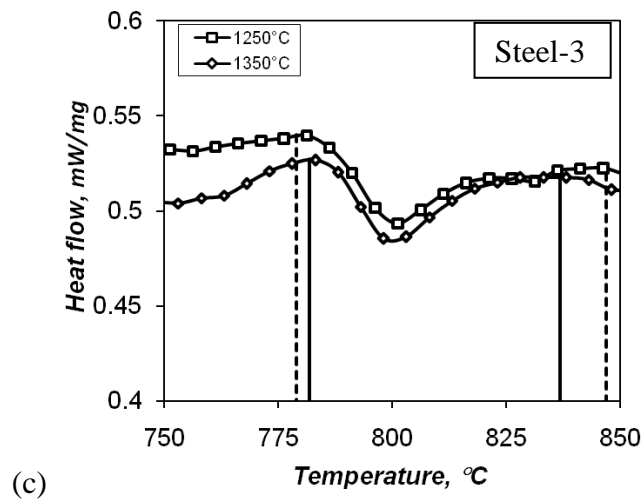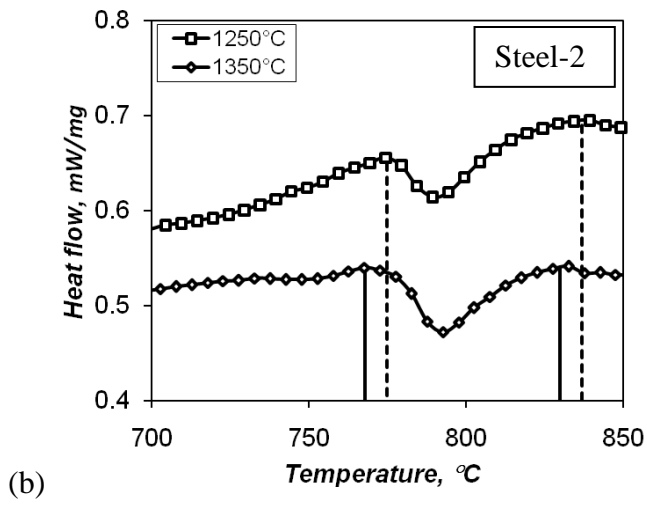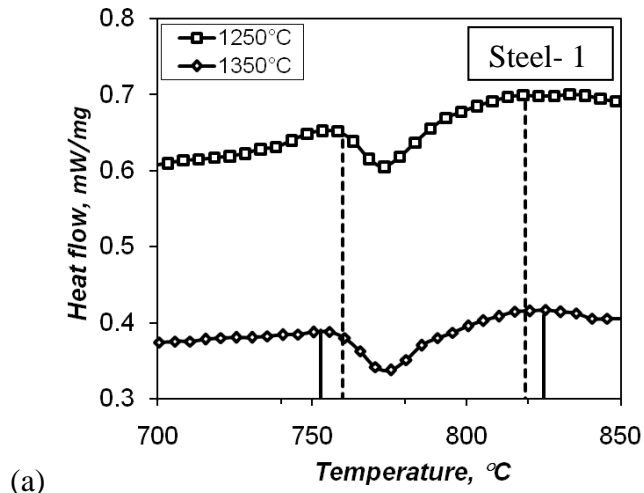
Figure 7.2: DSC curves of the three steels of this study.

From the DSC analysis, it is clear that by approximately 850°C, the austenitization is complete for all steels studied. Based on this result, T_{aus} in the present study has been set to 900°C for all the steels for 30 min. A higher temperature is not used because a further increase in austenitization temperature would result in coarser austenite grain sizes.

7.2 Heat Treatment

A typical cycle of the heat treatment for achieving nano-bainitic structures is shown in Figure 7.3, with details described in Chapter 6. Before choosing various combinations of heat treatment conditions, it is also important to know the upper limit on the isothermal transformation temperature (B_s), to avoid the formation of pearlite structure. B_s temperature can be estimated using two correlations reported in the literature. Two such equations are proposed by Stevens *et al.* (Equation (7.1)) [105] and Van Bohemen *et al.* (Equation (7.2)) [79], which are given below:

$$B_s = 830\text{-}270{\times}C\text{-}90{\times}Mn\text{-}37{\times}Ni\text{-}70{\times}Cr\text{-}83{\times}Mo, \tag{7.1}$$

$$B_S = 835\text{-}198{\times}C\text{-}91{\times}Mn\text{-}15{\times}Si\text{-}73{\times}Cr\text{-}36{\times}Ni\text{-}87{\times}Mo, \tag{7.2}$$

where the B_s temperature is in °C and the alloying elements are in wt.%. The average values of the B_s temperatures estimated via these equations were used as the upper limit for the isothermal temperatures. Along with the M_s temperatures, these values are also summarized in Table 7.1.
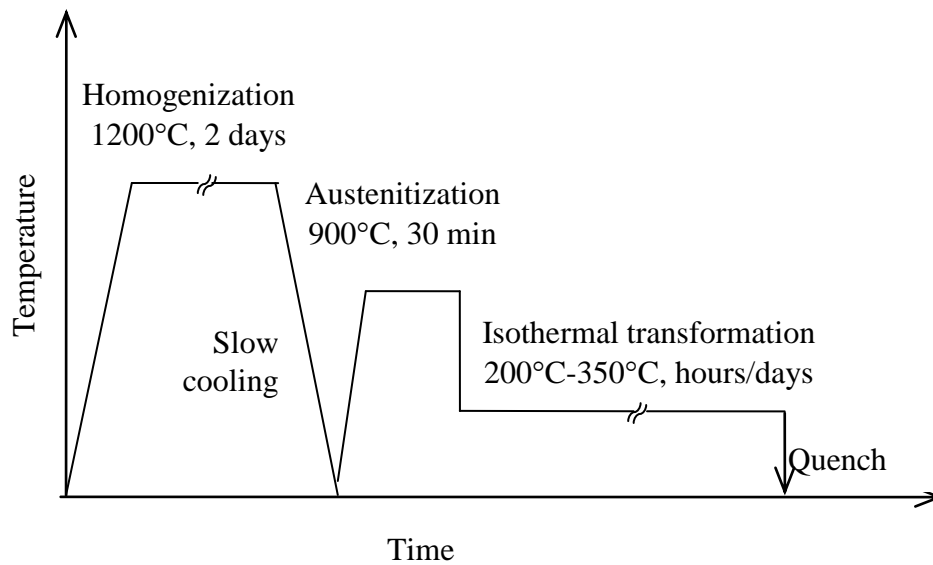
Figure 7.3: Heat treatment parameters applied to the three steels.

In this study, two heat treatment parameters, namely, the isothermal heat treatment temperature and the isothermal heat treatment time were investigated. Specifically, for each steel three isothermal transformation temperatures, namely, 200°C, 250°C and 300°C, were chosen. At these three temperatures, heat treatments for different isothermal transformation times were selected. Specifically, isothermal heat treatment times of 5h, 24h, 48h, 96h and 144h were used. Apart from these, samples from all three steels were also heat treated at an isothermal transformation temperature of 350°C for duration of 96h. This was done to confirm the theoretically calculated B_s temperature. After the heat treatment at the above isothermal temperature-time combinations, all the samples were water quenched to room temperature. A discussion about the experimental verification of the B_s temperatures of the three steels is given in Appendix A.

7.3 Characterization of Heat Treated Steels

Following the heat treatment of the samples, material characterization was pursued to verify the formation of bainitic microstructures, determine the microstructure characteristics (bainite plate thickness in nanometer range in particular) and the volume fraction of the bainitic phase. These were done using the SEM and XRD analysis, the results of which are discussed below in detail.

7.3.1 Microstructural Analysis

Typical microstructures of the three steels are shown in Figure 7.4 for the isothermal transformation temperature of 250°C. The trends are similar for isothermal transformation temperature at 200°C and 300°C. Specifically, in all cases, as the isothermal time increases, the volume fraction of bainite increases. A comparison with the microstructure reported in the literature [42, 45, 47] verifies that these are bainitic microstructures.

Next, the average plate thickness in the bainitic microstructures was determined using the DFT method described in Appendix B. For the DFT analysis of each microstructure image, in addition to bainitic sheaves at the center of the image, sheaves from four other locations in the image were also taken. Specifically, these four images were along the two orthogonal lines passing through the center of the microstructure, half way between the center and the edge of the image. The average bainitic plate thicknesses for the three steels at 200°C, 250°C and 300°C are summarized in Table 7.3 and graphically described in Figure 7.5. As seen in this figure, a general trend in each steel is that as the temperature increases, the plate thickness increases.

121

(a) Steel 1, 24 h

(b) Steel-1, 96 h

(c) Steel-2, 24 h

(d) Steel-2, 96 h

(e) Steel-3, 24 h

(f) Steel-3, 96 h
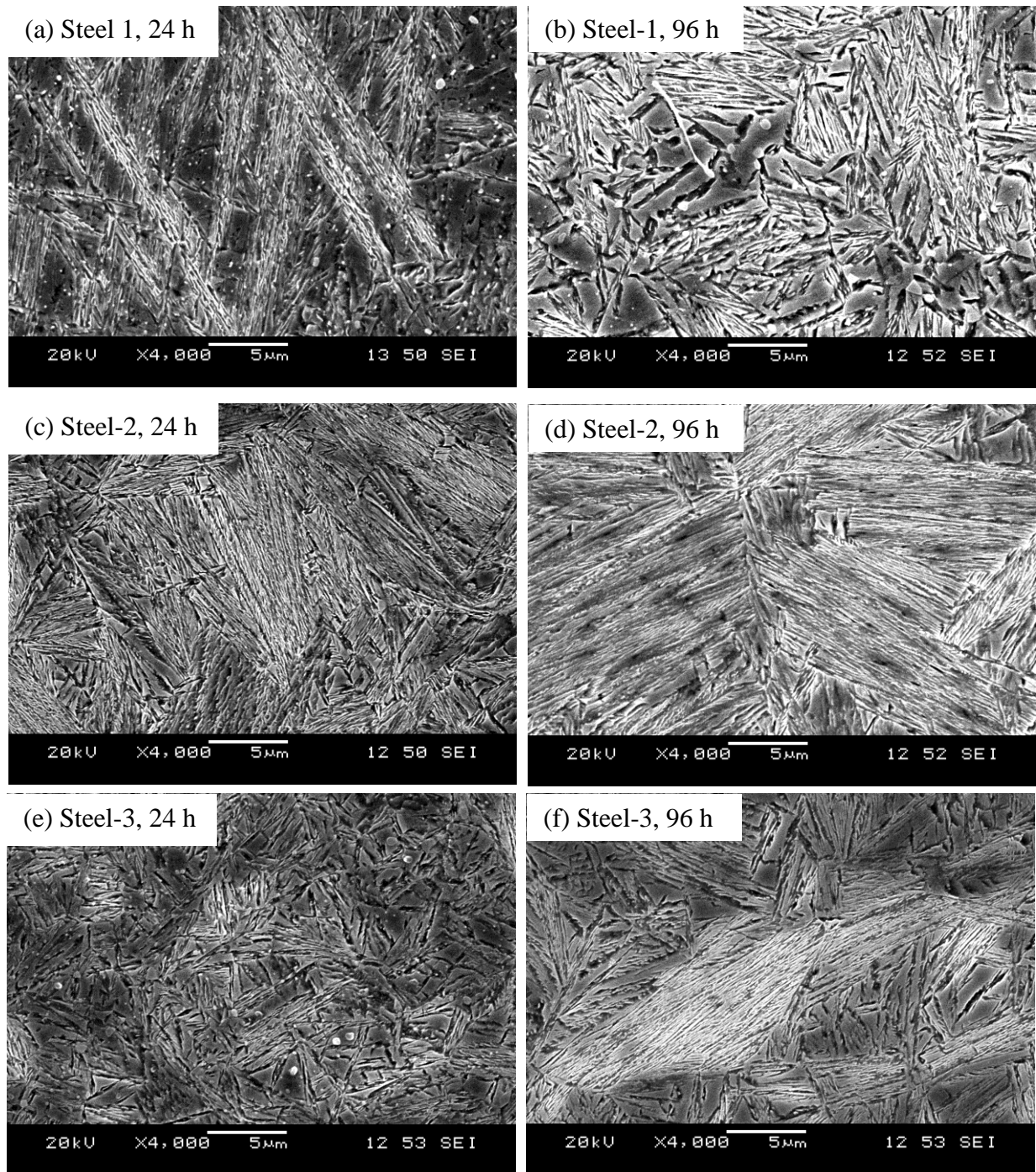
Figure 7.4: SEM images of the three steels isothermally heat treated at 250°C.

122

Table 7.3: Average bainite plate thickness (nm) at the three isothermal temperatures for the three steels measured by DFT method. For comparison, values from the Stereological methods are reported.

Isothermal temperature	DFT method			Stereological method		
	Steel-1	Steel-2	Steel-3	Steel-1	Steel-2	Steel-3
200°C	50±2.5	57±3.6	35±2.1	51±4.1	55±2.6	38±5.7
250°C	67±1.8	44±1.3	47±2.6	70±3.2	48±4.1	48±6.3
300°C	151±4	170±5.2	200±7.1	158±4.2	178±3.7	212±4.2
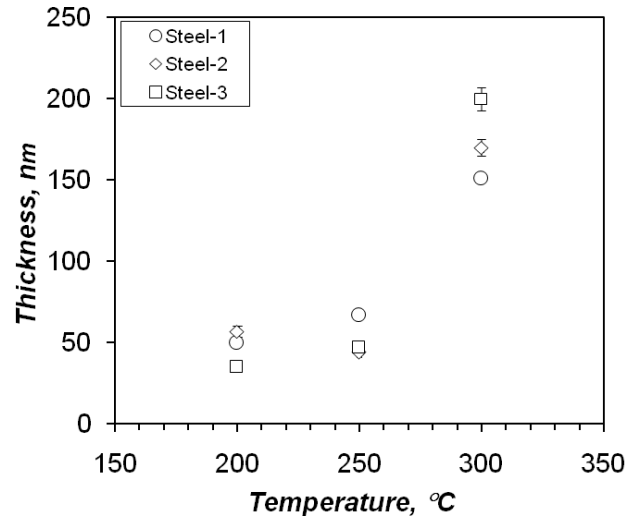
Figure 7.5: Average plate thickness of the three steels as a function of the isothermal transformation temperature for a hold time of 96h.

This trend is in agreement with the findings of Garcia-Mateo *et al.* [43] and is attributed to the fact that, as the isothermal transformation temperature increases, the upper bainite regime is approached, where thicker bainitic plates are formed.

It must be noted that the plate thickness from the DFT method is comparable to the standard stereological method used popularly in materials science. A comparison of the values from the two methods for the present steels is also summarized in Table 7.3. In view of the fact that the plate thickness of the steels are in the nanometer range, these steels can be termed nanobainitic steels.

7.3.2 XRD Results

Typical XRD results for the three nanobainitic steels are presented in Figure 7.6. In this figure, the austenite and bainite peaks are identified to indicate the formation of bainite. In these XRD spectra, the presence of austenite peaks implies that the material contains untransformed or retained austenite. The volume fraction of the retained austenite (V_γ) is proportional to the area under the austenite peaks.

In this study, the volume fraction of specimens heat treated at 200°C and 250°C has been determined for the verification of the thermo-statistical model presented in Chapter 3. These specimens were chosen because they were the ones with negligible amounts of cementite. In such samples, disregarding the volume fraction of cementite, the volume fraction of bainite (V_α) could be calculated as,
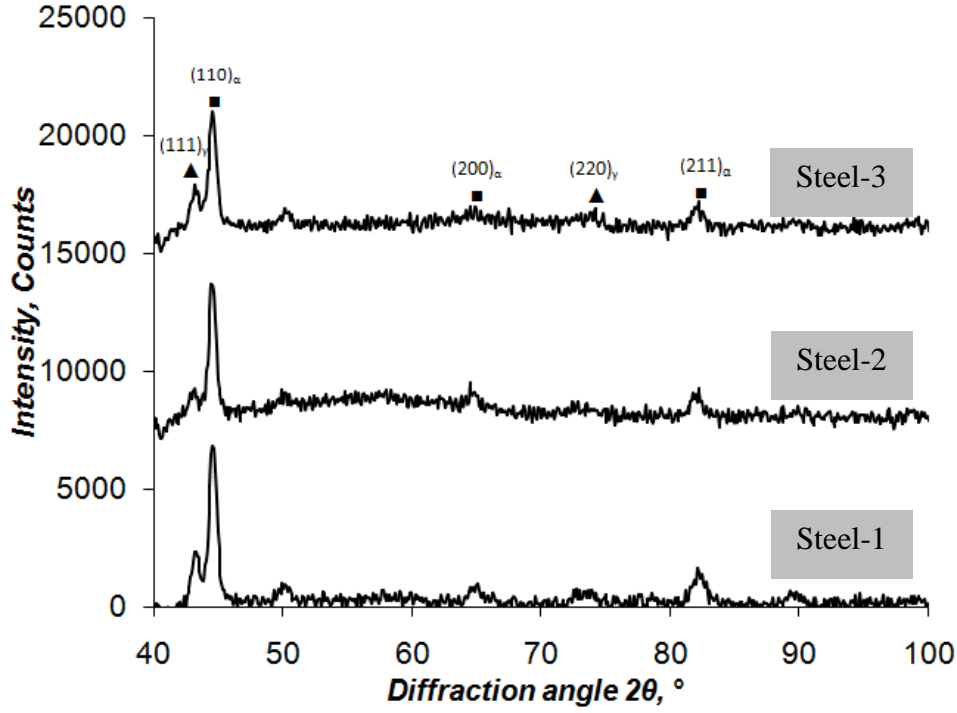
Figure 7.6: XRD scan results for the samples of the three steels heat treated at 250 °C for 96h.

$$V_\alpha = 1 - V_\gamma \tag{7.3}$$

The volume fraction of retained austenite has been determined using XRD via the relation,

$$V\gamma = \frac{\left(\dfrac{1}{n_\gamma}\right) \displaystyle\sum_1^{n_\gamma} \left(\dfrac{I_\gamma^{hkl}}{R_\gamma^{hkl}}\right)}{\left(\dfrac{1}{n_\alpha}\right) \displaystyle\sum_1^{n_\alpha} \left(\dfrac{I_\alpha^{hkl}}{R_\alpha^{hkl}}\right) + \left(\dfrac{1}{n_\gamma}\right) \displaystyle\sum_1^{n_\gamma} \left(\dfrac{I_\gamma^{hkl}}{R_\gamma^{hkl}}\right)}, \tag{7.4}$$

where the subscripts γ and α represent the austenite and ferrite phase, respectively. *I* represents the integrated intensity of the peak and *R* is given as

$$R = \frac{\left(/F/^2 \, p\mathrm{LP}e^{-2M}\right)}{v^2}, \tag{7.5}$$

125

Where $/F/^2$ is the structure factor times its complex conjugate, p is the multiplicity factor, LP is the Lorentz polarization factor, e^{-2M} is the temperature factor and v is the volume of the unit cell. The calculation of these parameters has been done using the standard procedure described in Refs. [106, 107].

The volume fraction of retained austenite as a function of time, calculated using the above procedure, is summarized in Table 7.4 for two temperatures, 200°C and 250°C. At both temperatures, the volume fraction of retained austenite decreases as the isothermal transformation time increases. This is expected since as time progresses, austenite gets transformed to bainite. At both temperatures, a logarithmic profile is followed in which the volume fraction of bainite increases rapidly initially, but as the volume fraction increases, the rate of increase decreases. Eventually, a steady state is reached indicating that the maximum volume fraction has been attained. It must be noted that a 100% transformation (volume fraction of bainite equal to 1.0) is not achieved in any steel due to the incomplete reaction phenomenon [1].

In all three steels, the maximum volume fraction of bainite is lower at 250°C than at 200°C. This is consistent with the generally observed inverse relationship between the volume fraction of bainite and the isothermal transformation temperature [1, 42-44], and is attributed to the fact that at higher isothermal transformation temperature, the critical value of the carbon content of austenite that will inhibit further isothermal transformation is lower than the critical carbon content at lower isothermal transformation temperature (see T_o concept in Sec. 2.3 of Chapter 2).

Table 7.4: Volume fraction of retained austenite and the volume fraction of bainite in the three steels, determined using the XRD analysis.

Temp., °C	Time, h	Steel-1		Steel-2		Steel-3	
		V_γ	V_α	V_γ	V_α	V_γ	V_α
200	5	0.59	-[a]	0.12	-[a]	0.26	-[a]
200	48	0.25	-[a]	0.14	0.86	0.21	-[a]
200	96	0.16	0.84	0.12	0.88	0.11	0.89
200	144	0.16	0.84	0.11	0.89	0.12	0.88
250	5	0.51	-[a]	0.24	0.76	0.28	-[a]
250	48	0.29	0.71	0.08	0.92	0.36	0.64
250	96	0.27	0.73	0.13	0.87	0.26	0.74
250	144	0.21	0.79	0.05	0.95	0.11	0.88

[a] In these specimens, the microstructure contains other phases like carbides and blocky martensite, besides bainite.

7.4 Validation of the Thermo-Statistical Model

A major objective of the present study is to adequately validate the numerical models with respect to new experimental data. The thermo-statistical model proposed in Chapter 3 has already been validated with respect to a number of experimental data reported in the literature. In this section, the proposed model has been further tested for its ability to predict the volume fraction of bainite in the three experimental steels in the previous section.

The model predictions along with these experimental data are compared in Figure 7.7. As seen in these figures, there is an excellent agreement between the present model and the experimental data. More specifically, the model is able to predict both the initial kinetics as well as the final
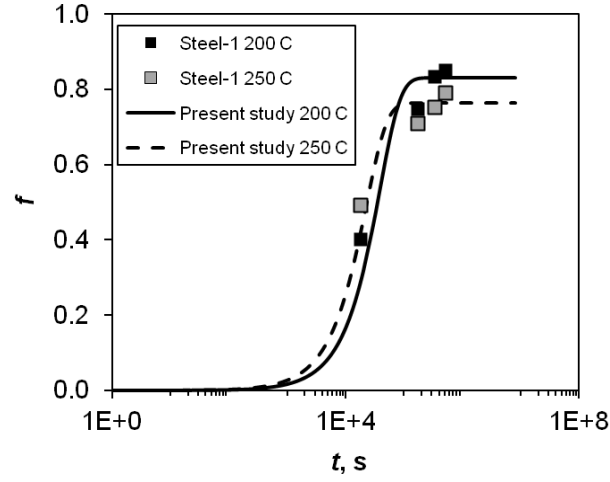
(a)
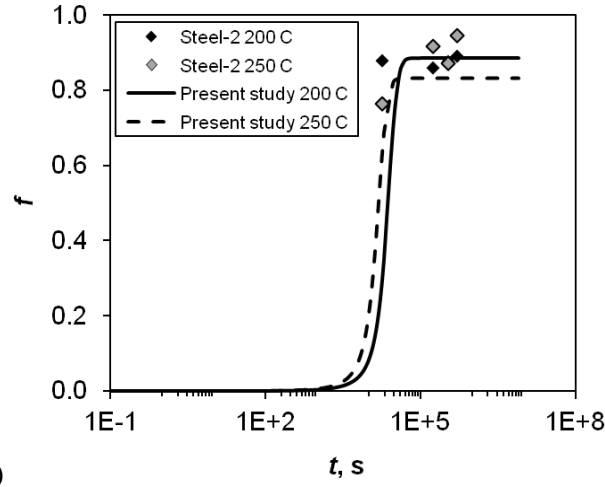
(b)
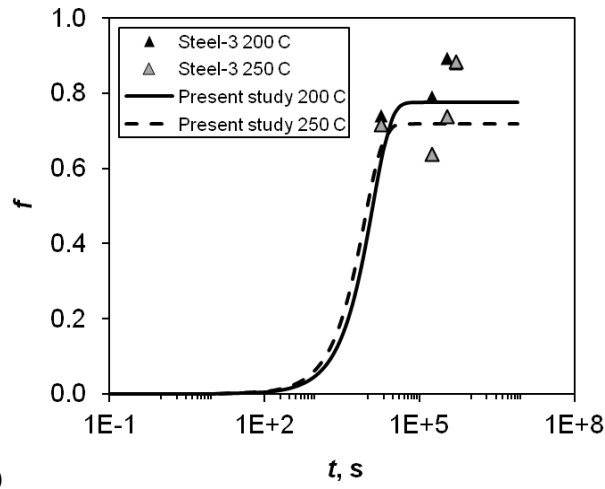
(c)

Figure 7.7: Volume fraction predicted by the thermo-statistical model of Chapter 3.

128

volume fraction of bainite fairly accurately. In fact, the relative error between model predictions and the experimental data for the maximum volume fraction of bainite is within 3%. A slightly larger error is observed for the second steel at 250°C where this error creeps to about 4.5%. The least accurate behavior of the model is for the third steel at an isothermal transformation temperature of 200°C, where the error is approximately 12%.

7.5 Mechanical Testing

In this section, the mechanical properties of the experimental steels obtained from the hardness and compression tests are presented in detail.

7.5.1 Effect of Microstructure on the Hardness

Hardness testing is a quick method of characterizing the overall effect of tempering and provides valuable information of overall change in strength. Following the SEM and XRD analysis, Vickers hardness measurements were made on the samples and data was collected as outlined in Chapter 6. The hardness values shown in Table 7.5 are the average of five readings on each steel sample.

As seen in this table, the hardness values are over 700 HV in several cases. This indicates the formation of martensite.

Table 7.5: Hardness data for three steels in different heat treatment conditions.

Steel	T_{iso}, °C	t_{iso}, h	HV30
1	200	5	720[a]
		24	693[a]
		48	721[a]
		96	641
	250	5	724[a]
		24	533
		48	481
		96	496
		144	546
	300	96	429
	350	-	760-790
2	200	5	789[a]
		24	735[a]
		48	588
		96	631
	250	5	585
		24	603
		48	561
		96	550
		144	575
	300	96	475
	350	5	546
		24	482
		48	413
		96	640
3	200	5	767[a]
		24	754[a]
		48	709[a]
		96	571
	250	5	759[a]
		24	557
		48	501
		96	505
		144	559
	300	96	480
	350	-	830-849

[a]In these steels, some amount of retained austenite gets converted to martensite and are not used for the validation of the hardness model presented in Chapter 5.
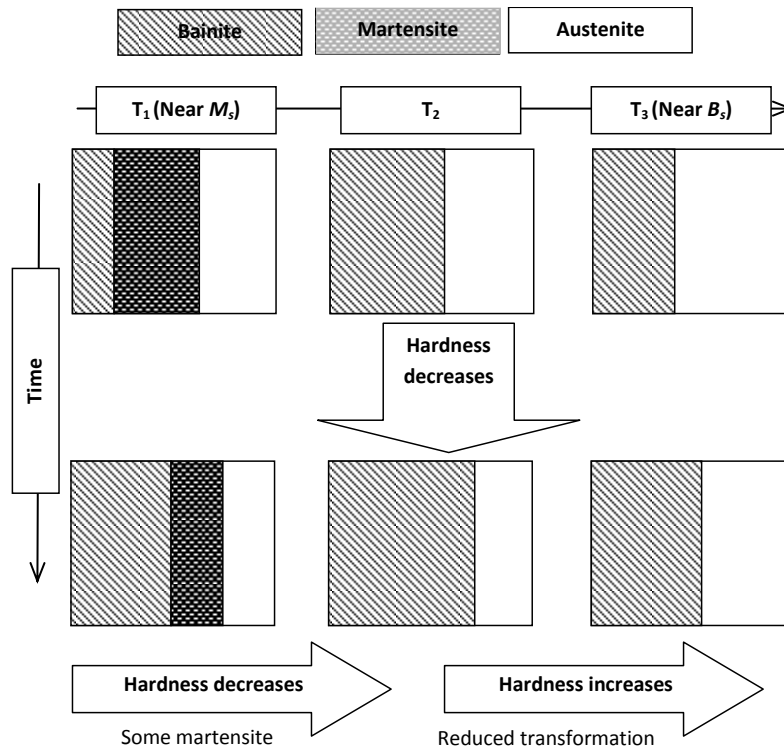
Figure 7.8: Schematic of the hardness trends of (a) Steel-1, Steel-3, and (b) Steel-2.

The high hardness values are obtained in (1) the isothermal heat treatment at 200ºC which is close to M_s, and (2) Steel-2 and Steel-3 at short isothermal transformation times where bainitic transformation is small and some fraction of the retained austenite gets converted to martensite. The hardness trends in the three steels are schematically shown in Figure 7.8. In all steels, at any given temperature, hardness decreases with time due to the increasing volume fraction of bainite.

On the other hand, for a given isothermal heat treatment time, hardness has a quadratic behavior with the isothermal transformation temperature. This can be explained as follows: At temperatures close to the M_s temperature, there is some amount of martensite in the material. This results in a very high hardness in the steel. As the temperature increases, the volume
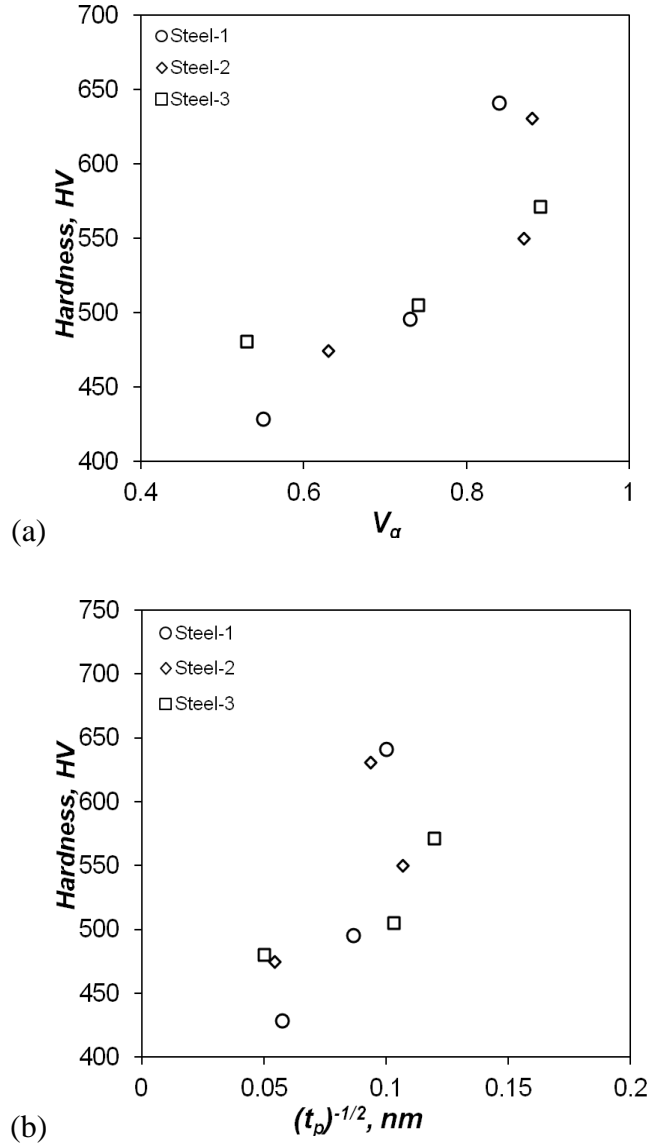
Figure 7.9: Effect of (a) volume fraction of bainite and (b) the plate thickness on the hardness of the three experimental steels.

fraction of bainite decreases (Figure 7.9a) and the thickness of the bainitic plates also increases (Figure 7.9b). Since, the major strengthening effect is due to the fine plate size, hardness of the material decreases. This happens until a certain optimal temperature is reached. Beyond this, as the temperature increases up to B_s, the volume fraction of bainite is very small due to the

incomplete reaction phenomenon. As a consequence of this incomplete reaction phenomenon, the microstructure of the material has chunks of blocky austenite. These blocks are unstable and transform into high carbon martensite under the influence of stress, making the material harder [108]. This observation is also in agreement with the experimental findings of Lee *et al* [108] and Liu *et al* [109].

In the present steels, there was practically no transformation in Steel-1 and Steel-3 at 350°C. This is not surprising since this temperature is higher than the B_s temperature (see Table 7.1) of these steels that was theoretically determined to be in the neighborhood of 320°C. Hence, in these steels, the hardness is very high at this temperature. On the other hand, Steel-2 has a theoretical B_s of approximately 370°C. In this steel there was adequate transformation, as reflected in the hardness values that are in bainitic range in Table 7.5.

7.5.2 Hardness Prediction Using the NN-Model

The NN model developed in this thesis has been applied to the experimental hardness values of these newly designed steels. Since the model is applicable only for bainitic steels, hardness values in the martensitic range (HV>700 in Table 7.5) were ignored. The average value of the normalized hardness values predicted by the networks and the experimentally determined hardness values are presented in Figure 7.10. It should be noted that these experimental data points were not included in the database for the training of the network. As seen from this figure, the neural networks are able to predict the hardness values with an R^2 value of 0.78.
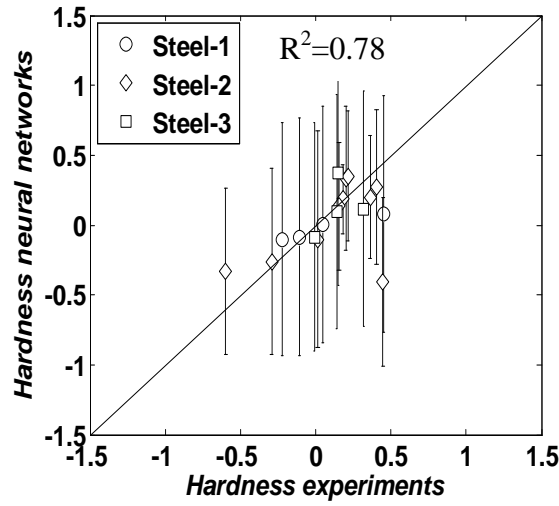
Figure 7.10: Comparison of the hardness of the three bainitic steels of the present study predicted by the NN-model and the heat treatment experiments.

7.5.3 Effect of Alloying Elements and Heat Treatment Conditions

In this section, the use of ANN to analyze the effects of the parameters on the hardness of the materials is presented. In particular, the influence of the alloying elements and the heat treatment conditions on the hardness is discussed. In addition to these, the ANN model is also used to understand the combined impact of two parameters on the hardness of the heat treated steels.

7.5.3.1 Effect of Individual Parameter

For the parameter analysis the following has been done: Starting from the baseline composition of this steel given in Table 6.1 and the heat treatment conditions as T_{aus}=900°C, t_{iso}=48h and T_{iso}=250°C, one input parameter at a time was varied.

The effect of the heat treatment conditions and the weight percentage of key alloying elements (Co and Al) on the hardness of the steel have been summarized in Figure 7.11. The following observations can be made:

1. Heat treatment conditions: As seen in Figure 7.11a, with an increase in the austenitization temperature, the hardness of the material decreases. This is due to the fact that with an increase in the austenitization temperature, the grain size becomes coarser [110], i.e., the number of grain boundaries and thereby the number density of nucleation sites decrease. As a result of this, bainitic transformation is such that the plate thickness increases. The hardness of the steel was also inversely related to the isothermal transformation temperatures (See Figure 7.11b). This trend is attributed to the fact that with an increase in the isothermal transformation temperature one approaches the regime of upper bainite that is softer than the lower bainite obtained at lower values of T_{iso}.

Finally, with respect to the isothermal transformation time, it was observed that following an initial steep decline in the hardness, it reaches an asymptotic value for a long transformation time (see Figure 7.11c). This trend can be explained as follows: For the steel considered here, the typical time needed for a bainitic reaction to complete is estimated to be in the range of 55h-60h for an isothermal transformation temperature of 250ºC. Until this time, the volume fraction of bainite increases with time and the material softens. However, further increase in time does not produce any change in volume fraction and hence there is no change in the hardness. This estimate of 55h-60h has been made after observing the data of Garcia-Mateo *et al*. [43] who studied similar steel containing Co and Al.
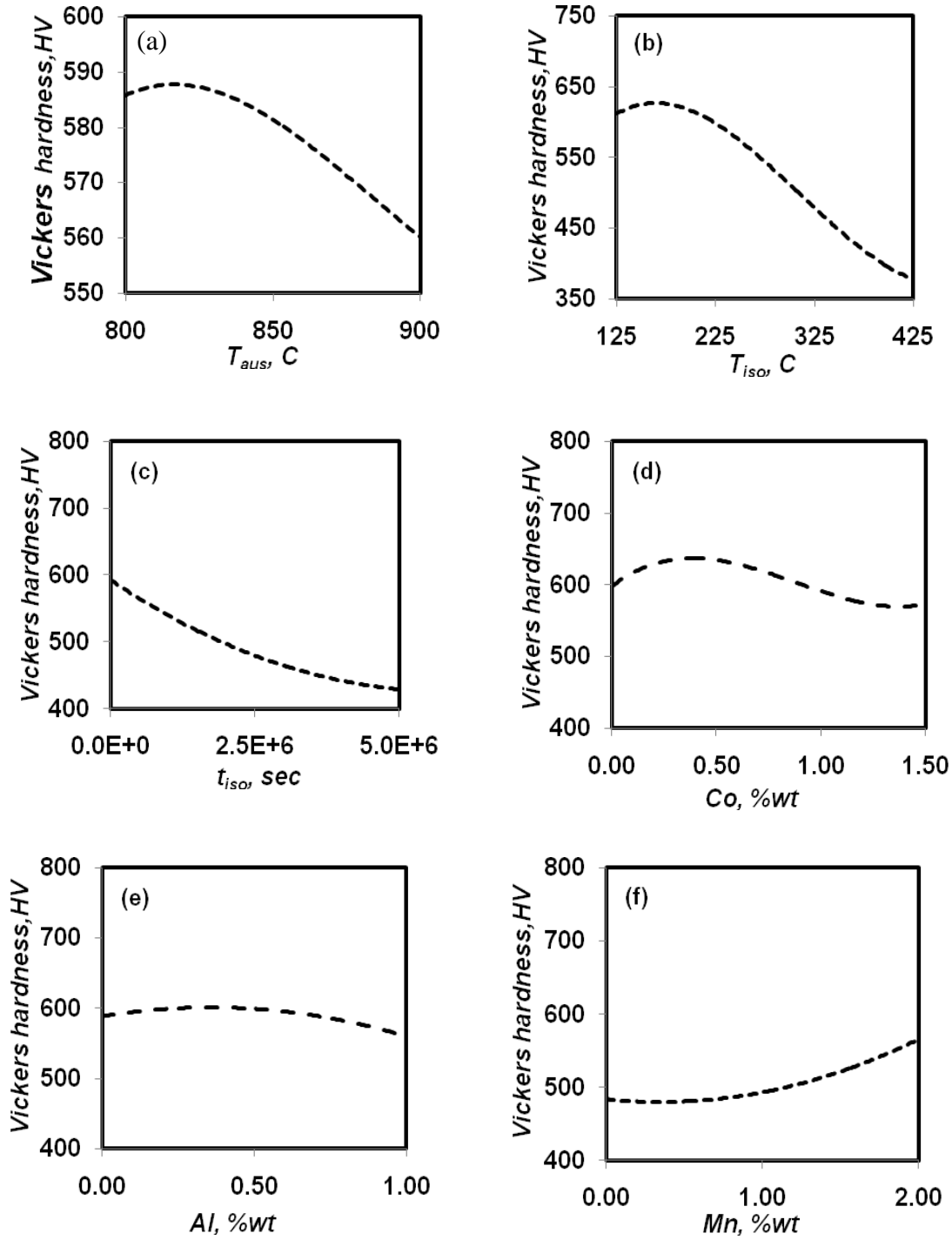
Figure 7.11: Effect of (a) T_{aus} (b) T_{iso} (c) t_{iso} (d) compositoin of Co, (e) composition of Al and (f) composition of Mn on the hardness of Steel-2.

Also, in the present experiments, the hardness of Steel-2 steel varied less than 2% between t_{iso}=48h and t_{iso}=96h. A marginally higher time is estimated because unlike the steel of Garcia-Mateo *et al*. [43] Steel-2 has a higher amount of Mn. Knowing that Mn will retard the bainitic reaction [13], the present steel must take a longer time to reach steady state.

2. *Effect of the key alloying elements*: With respect to the key alloying elements, viz., Co and Al, it was found that the addition of Co as well as Al results in a decline in the hardness of the steels (see Figures 7.11d and 7.11e). This is because both alloying elements enhance the bainitic reaction rate. Put differently, given the heat treatment conditions, more of these alloying elements means a higher volume fraction. This in turn results in a softer material with a better combination of ductility and strength, in comparison with martensitic steels.

It was noted that Mn is an important alloying element in this steel. Manganese in small quantities increases the hardness only gradually. However, beyond 1.5 wt%, addition of Mn increases the hardness of the material rapidly (see Figure 7.11f). This is because Mn retards bainitic transformation. At very high quantities of Mn, this suppression results in a large amount of untransformed austenite that gets converted to martensite upon quenching. As a consequence, the material hardness begins to increase rapidly as the content of Mn increases.

7.5.3.2 Multi-Parameter Analysis

In addition to the effect of the individual alloying elements, it is also useful to understand how the simultaneous variations of multiple parameters influence the material hardness. This is

necessary since almost always these parameters are not independent of each other and in fact act simultaneously on the final outcome, either in reinforcing or weakening each other's impact. In what follows, the use of the NN-model for developing contour maps for hardness as a function of two parameters that are simultaneously varied in the Co-Al steel is shown (Figures 7.12- 7.14)

The effect of the simultaneous variation of Co and Al on the hardness of the material is shown in Figure 7.12. The compositions of the other alloying elements are the ones summarized in Table 6.1 for Steel-2. The heat treatment parameters are T_{iso}=250°C, t_{iso}=24h. As seen from this map, if one expects a hardness that is greater than a given value, say, 580HV, then it could be obtained at several combinations of wt% of Co and Al. Noting that Co is expensive, it seems that small amount of Co (0.25-0.5 wt%) and 0.1 wt% of Al can yield this desired hardness. Alternatively, even smaller amounts of Co and large amount of Al (approximately 1wt %) can result in this hardness range as well. In other words, Al, being an accelerator alloy, can be used to replace the Co content in the steel.

Now, for any such choice, the isothermal heat treatment times can be optimized by considering the T_{iso}-Co and T_{iso}-Al contour maps where it is seen that by using a temperature of about 250°C and the lower values of Co/Al, it is possible to achieve reasonably higher hardness values, as shown in Figures 7.13 and 7.14.
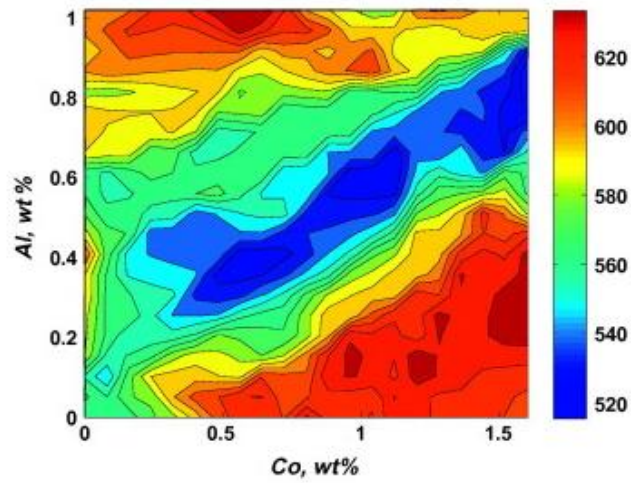
Figure 7.12 Influence of the composition of Co and Al on the Vickers hardness of Steel-2 estimated from the NN-model.
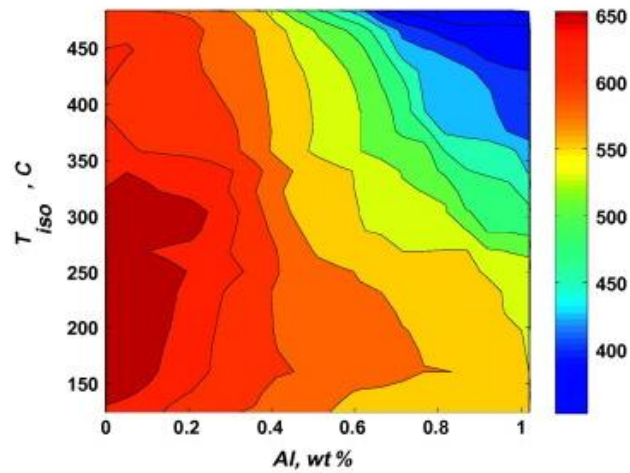
Figure 7.13: Influence of the composition of Al and the isothermal transformation temperature on the Vickers hardness of Steel-2 estimated from the NN-model.
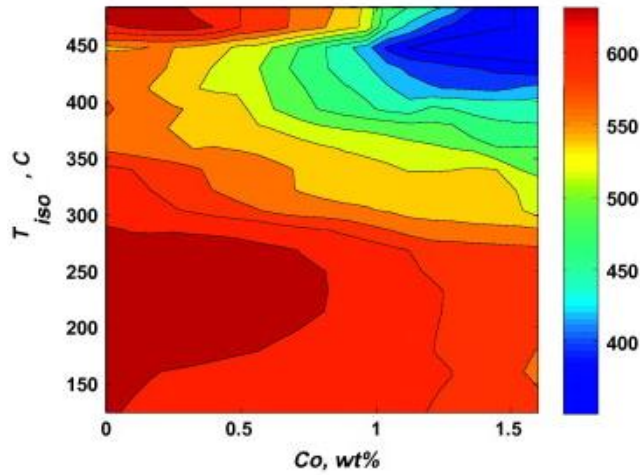
Figure 7.14: Influence of the composition of Co and the isothermal transformation temperature on the Vickers hardness of Steel-2 estimated from the NN-model.

Similarly, one can also study the heat treatment contour maps to determine the optimal heat treatment conditions for a desired hardness. A higher level of sophistication would include using such contour maps in conjunction with more advanced search methodology such as the genetic algorithm to determine the optimal chemical composition and heat treatment conditions for designing steel with desired hardness [111].

The current ability of the network is limited to predicting the hardness. The enhancement of the network to simultaneously predict other mechanical properties is a logical extension. For instance, correlations exist between hardness and tensile strength. So, one option is to predict the hardness using the neural network model and apply the predicted hardness values in such correlations to estimate the strength of the material. This is pursued further in the following section describing the results of the compression tests.

7.5.6 Compression Tests

The compression tests were performed on all three experimental steels to study the effect of strain rate, isothermal transformation temperature and isothermal time on the yield point. The experimental conditions and the corresponding results are presented below.

7.5.6.1 Effect of Strain Rate

Compression tests were performed at three strain rates, viz., 10^{-1} s^{-1}, 10^{-2} s^{-1} and 10^{-3} s^{-1} on all three steels heat treated at isothermal temperatures of 200°C and 250°C for an isothermal time of 96h.

Typical stress-strain graphs of the three steels heat treated at 250°C for 96h are shown in Figure 7.15. As seen in this figure, there is no noticeable influence of strain rate on the yield stress of any of the steels. Hence, a single strain rate of 10^{-3} s^{-1} for the remaining tests will be discussed below.

(a)

(b)

(c)
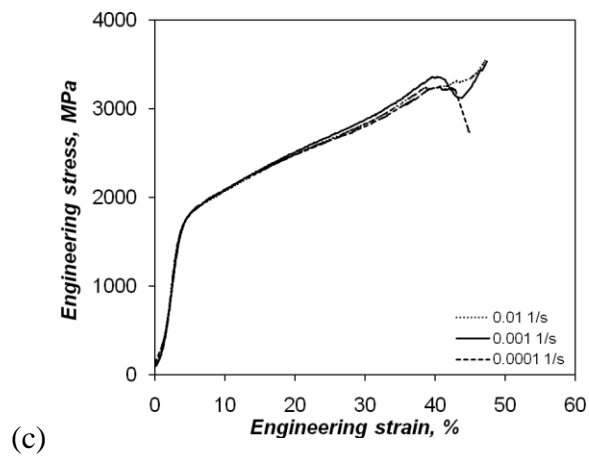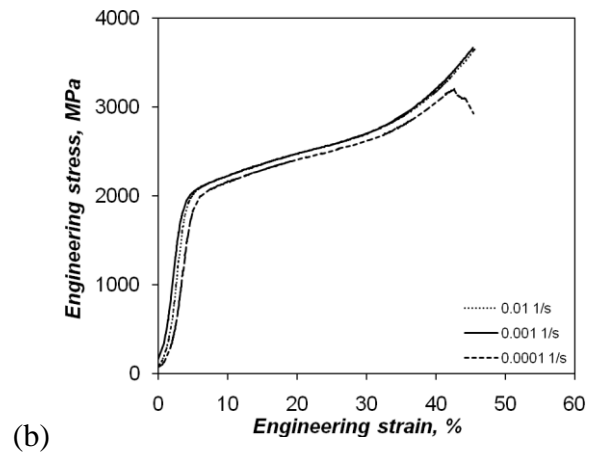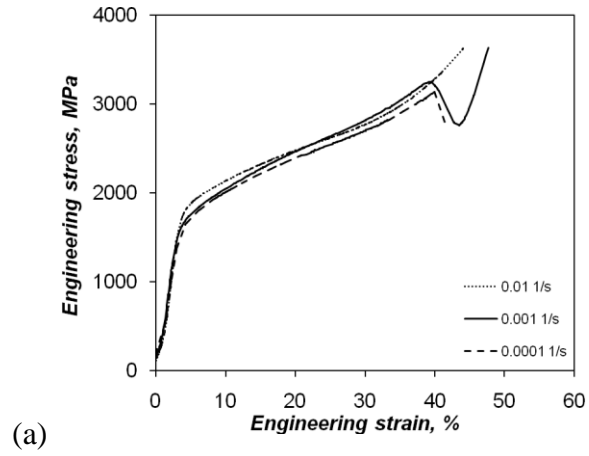
Figure 7.15: Compression stress-strain curves for (a) Steel-1, (b) Steel-2 and (c) Steel-3

at different strain rates, heat treated at 250°C for 96h.

7.5.6.2 Effect of Temperature

To understand the effect of temperature on the yield stress, additional compression tests were performed on samples of all three steels for an isothermal transformation temperature of 300°C for 96h. The value of yield stresses at different temperatures is summarized in Table 7.6.

In Steel-1 and Steel-3, there is a decrease in the yield strength with temperature. This trend can be explained as follows: At 200°C, the temperature being close to M_s temperature, there is martensite formation at this temperature, indicated by the arrows in Figure 7.16. This results in high yield strength. As temperature increases to 250°C, there is a decrease in the transformation (see Table 7.4). However, the plate thickness also increases with increasing isothermal temperature. Since the plate thickness has a major strengthening effect, the yield strength at this temperature decreases. At 300°C which is close to the B_s temperature, there is less bainitic transformation. At this temperature, there is a large amount of blocky austenite that eventually converts to blocky martensite on the application of small stresses (see Figure 7.16). However, the plate thickness is the largest at this temperature and consequently the yield strength at this temperature is the lowest. A similar explanation can be given for the effect o the temperature on the yield strength of Steel-3.

Table 7.6: Experimental values of σ_y and the values of yield strength predicted using

Equation (8.6) with the experimental data of hardness ($\sigma_y^{(calc)}$) and the neural

network values of hardness ($\sigma_y^{(nn)}$).

Steel	Temp., °C	n	$\sigma^{(expt)}$, MPa	$\sigma^{(calc)}$, MPa	$\sigma^{(NN)}$, MPa
1	200	0.399	1790±49	1339	1166
1	250	0.100	1498±9	1526	1602
1	300	0.391	1148±58	1108	1273
2	200	0.079	2151±15	1936	1843
2	250	0.002	1750±8	1832	1898
2	300	0.058	1421±1	1533	1588
3	200	0.308	1658±6	1397	1371
3	250	0.081	1522±25	1574	1623
3	300	0.374	1079±33	1251	1229

In Steel-2 due to the presence of a higher amount of Co-Al, there is an accelerated transformation and a large amount of bainite volume fraction is obtained at all three temperatures. Unlike the other two steels, this large transformation is visibly evident in Figure 7.16. However, the strength is different at the three temperatures. As discussed before, at 200°C some martensite is expected to form during the heat treatment since it is close to the M_s temperature. This results in high yield strength in this case. As the heat treatment temperature increases, the thickness of the bainitic plates increase exponentially (see Figure 7.5).
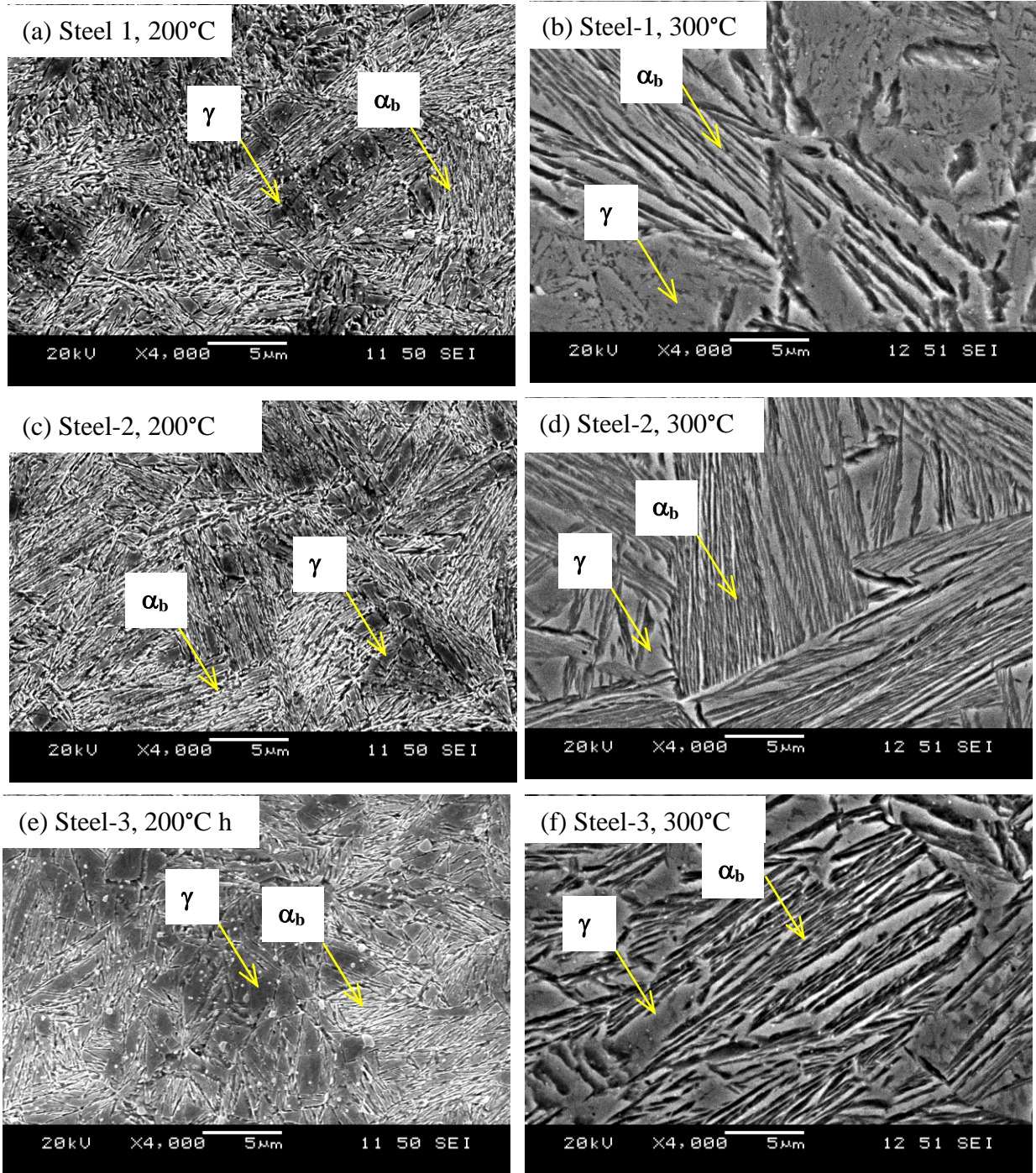
Figure 7.16: SEM images of the three steels isothermally heat treated for 96h.

As a consequence, the material becomes somewhat softer as is evident in the hardness values in Table 7.5 and this reflects in the lower yield strength in these cases.

For a better understanding, the values in Table 7.6 are plotted in Figure 7.17. As verified in this figure, in all three steels, as the temperature increases the compressive yield strength of the material decreases. This is because as the isothermal transformation temperature increases the bainite plate thickness increases (Table 7.3 and Figure 7.5) for all three steels. Specifically, close to the M_s temperature, the plate thickness is in the nanometer range. However, as isothermal heat treatment temperature increases and approaches B_s, the plate thickness is in the submicrometer range. This variation in plate thickness of the steel results in a decrease in the hardness as well as the yield strength of the material.
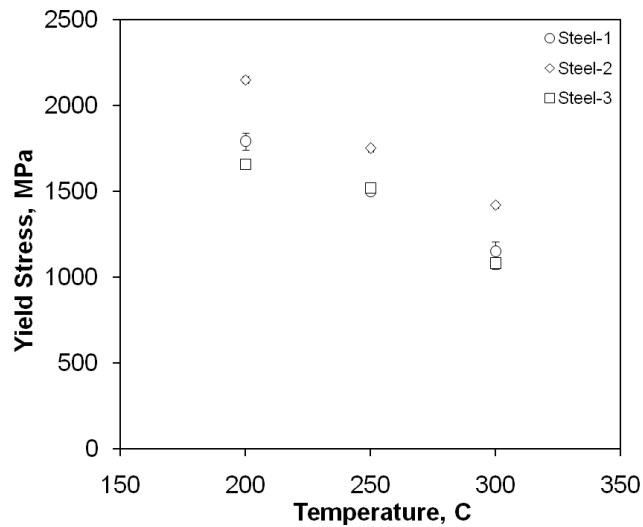
Figure 7.17 Compressive yield stress as a function of temperature for the three steels.

146

Another observation in this figure is that at any particular temperature, the strength of Steel-2 is greater than the strength of the other two steels. This is because of the Co content of this steel that considerably contributes to the strength of the material [68]. It should be noted that the other steels do not contain Co.

7.5.6.3 Effect of Time

In this final criterion, the effect of the isothermal heat treatment time on the yield strength of the material is considered. Again, typical stress-strain curves for the specimens of the three steels heat treated at 250°C for two different times, viz., 24h and 96h, are shown in Figure 7.18.

All three steels exhibit a higher shortening characteristic as the transformation time increases. This is attributed to the increasing volume fraction of bainite. In Steel-1, there is a marginal increase in compressive yield strength, σ_y, from 1439 MPa to 1498 MPa when the isothermal heat treatment time increases from 24h to 96h. This is consistent with the findings of Curtze *et al*. [113] and is attributed to the fact that the transformation is not complete at 24h, and an increase in bainitic volume fraction increases σ_y of the material. On the other hand, in the other two steels, σ_y decreases with the isothermal heat treatment time.

More precisely, in Steel-2, the yield strength decreases by about 7% from 1877 MPa to 1751 MPa On the other hand, in Steel-3, the yield strength decreases from 1671 MPa to 1522 MPa (approxiately 9%). This is because in these steels, a prolonged isothermal transformation time
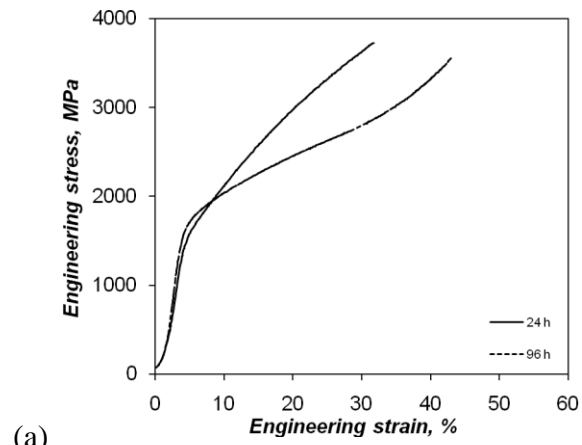
(a)
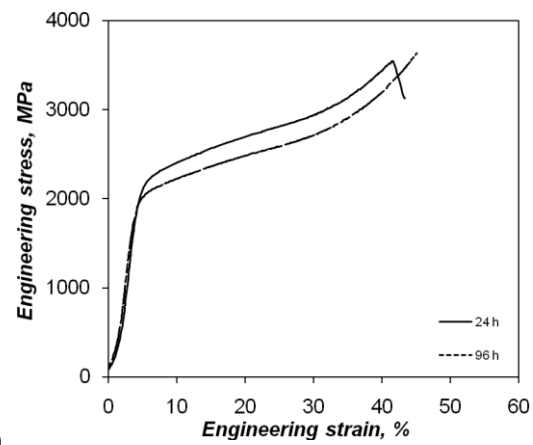
(b)
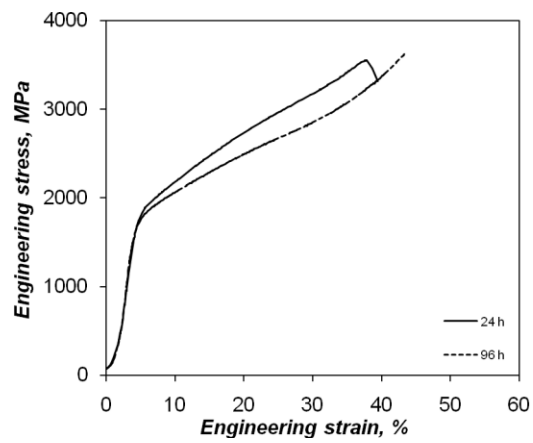
(c)

Figure 7.18: Stress-strain curves for different tempering times for (a) Steel-1, (b) Steel-2 and (c) Steel-3 at 250°C.

148

results in the precipitation of low temperature carbides. Again, this is in agreement with the findings of Curtze *et al.* [113].

A comparison between the three steels shows that after a short transformation time of 24h, Steel-1 undergoes relatively less compressive strain due to the low volume of bainitic phase (See Figure 7.19a). On the other hand, the deformation in Steel-2 is much larger than that of other two steels, and its σ_y is also the highest. Finally, Steel-3 can be slightly more deformed than Steel-1 because of its larger bainitic phase fraction, but less deformed than Steel-2. After 96h of isothermal transformation, all three steels exhibit almost similar deformability, but with varying values of σ_y (See Figure 7.19b). Clearly, with constraints on the heat treatment time, for a good combination of strength and deformation ability, Steel-2 would be preferred.

7.5.7 Compression Strength Modeling

The primary objective of the compression tests was to obtain new experimental data on the yield strength of the material and examine the current correlation in the literature to predict the yield strength.

(a)

(b)
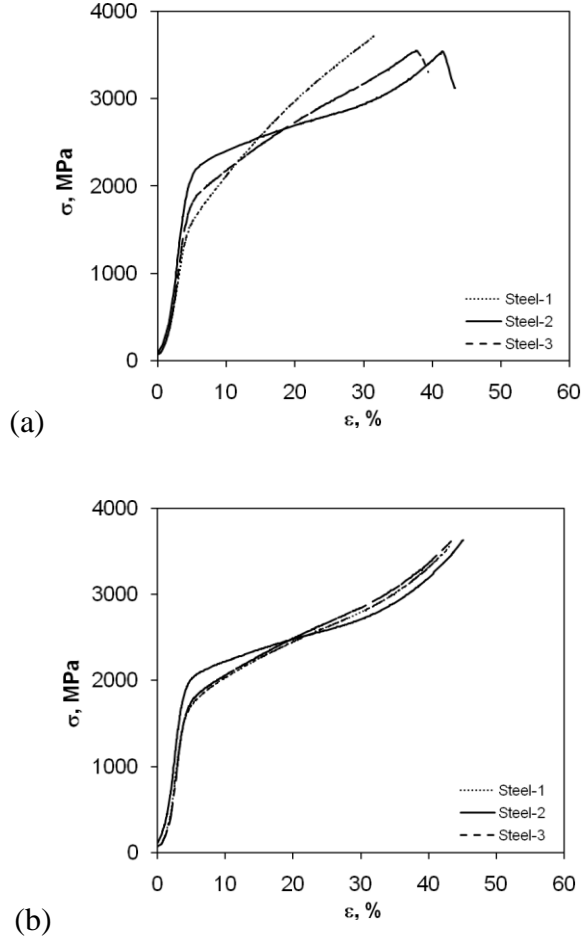
Figure 7.19: Engineering stress-strain curves of the three steels heat treated at 250 °C for (a) 24h and (b) 96h, at a strain rate of 0.001 s^{-1}.

Three equations usually used in the literature are [114, 115]

$$\sigma_y = \frac{HV}{3},$$ (7.6)

$$\sigma_y = \frac{HV}{3}(0.1)^n,$$ (7.7)

150
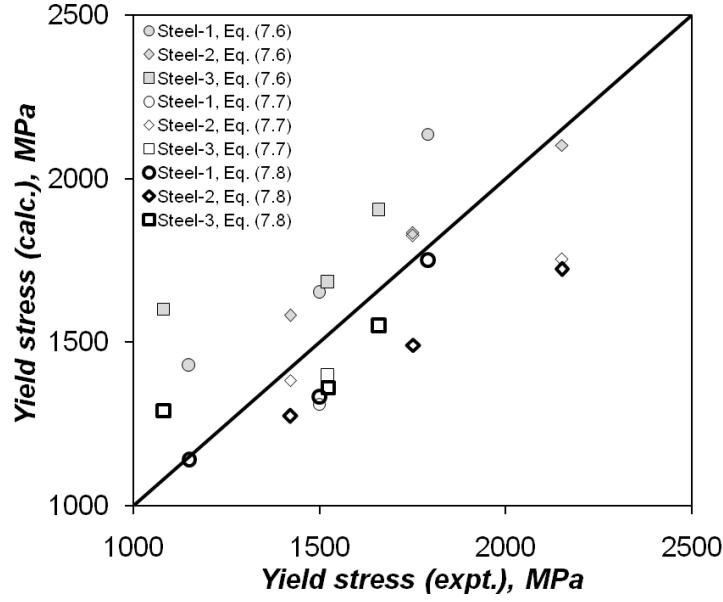
Figure 7.20: Comparison of the compressive yield strength calculated from Equations (7.6)-(7.8) with the experimental σ_y values for three Steels heat treated at 200°C, 250°C and 300°C for 96h

$$\sigma_y = -90.7 + 2.876 * HV. \tag{7.8}$$

where σ_y is the compressive yield stress, HV is the Vickers hardness and n is the strain hardening exponent that can be obtained from a log-log plot of the true stress - true strain graph. Application of these correlations to predict the yield strength is shown in Figure 7.20. Although these equations exhibit a reasonably good agreement with the experimental σ_y, they have a maximum relative error of 24%, 40% and 14%, respectively. Put differently, it can be said that Equation (7.8) is able to predict the yield strength more reliably than the other two correlations.

7.6 Summary

In summary, in this chapter, three experimental steels have been isothermally heat treated for various combinations of tempering time with temperature. The heat treated samples have been subsequently analyzed for the volume fraction of bainite and the bainitic plate thickness. Compression tests have also been performed. These data are used for the validation of the theoretical models developed in this thesis.

The following observations were made with regards to the experiments on these steels:

1. The transformation is fast in Steel-2 that contains Co and Al (the accelerating elements). These elements enable to reduce the transformation time significantly.

2. At isothermal heat treatment temperatures of 200°C and 250°C, that are close to the M_s temperature of the three steels, the bainitic plates in the microstructure are very fine (in the range of nanometers). Also, at these temperatures the bainitic volume fraction is significant. In particular, transformation at 250°C, that is fairly close but not critically neighboring the M_s temperature, is notably good for Steel-2 in which bainitic transformation were observed in a short transformation time of 5h. Additionally, the transformation at this temperature is good for other steels when the isothermal transformation time is prolonged (96h).

3. The mechanical testing of the three steels indicates a good combination of compressive strength (1100 MPa-2150 MPa), deformation ability and hardness (480 HV-600 HV) when there is adequate bainitic fraction in these steels. In particular, these properties are superior for Steel-2.

4. Three correlations from the literature that link the hardness values with the yield strength values were employed to examine the current experimental data. It was found that the best correlation has a relative error of 14%.

Chapter 8

Conclusions and Future Work

8.1 Conclusions

In this thesis, several models have been developed to understand the transformation kinetics and mechanical properties like strength and deformability of bainitic steels. Specifically, three new models have been proposed to predict the volume fraction of bainite for a given steel composition and isothermal heat treatment condition. A model is also presented for predicting the hardness of the steels. Further, this model, in conjunction with the proposed empirical equation linking hardness to yield strength, is able to predict the yield strength of the materials.

In addition to an extensive validation of the models with respect to the experimental data from the literature, the models have also been validated with respect to the experimental data from three new experimental steels that have been heat treated at various isothermal temperature-isothermal time combinations.

(1) The first model for low carbon steels (Chapter 3) is a thermodynamic model that is based on the expressions for the bainitic transformation kinetics. This model is validated with respect to the low carbon steels and requires material constants that have to be determined from experiments.

(2) A modified model is the thermo-statistical model (Chapter 3). The model incorporates a revised formulation for the number density of nucleation sites, and it does not require any *scaling functions* to account for the incomplete reaction phenomenon. This model also takes into account the chemical composition and the isothermal heat treatment conditions. Unlike the first model, it avoids the use of material constants by including linear regression expressions for the number density of initial nucleation sites and the theoretical maximum volume fraction of bainite. The model is valid for high as well as low carbon steels.

(3) A neural network model has also been developed to determine the volume fraction of bainite in isothermally heat treated bainitic steels. The model is able to predict the volume fraction of bainite for a given set of inputs consisting of the alloying element content and the heat treatment conditions. The model has been constructed from a large set of experimental data from the literature and has been validated with respect to several additional data from the literature.

(4) A different neural network model has been constructed, proposed and validated for the hardness of the material (Chapter 5). Furthermore, the ability of the model to make meaningful theoretical investigations has also been demonstrated by applying it to make a parametric study. The predictions of the neural network model were consistent with the expected outcome.

On the experimental side, several heat treatment experiments were conducted on three new experimental nanobainitic steels. Bainitic transformation in these experiments was verified via SEM and XRD analysis. The following were the conclusions of the analysis of the experimental results:

(5) Heat treatment of the steels resulted in microstructures with plate thickness in the nanometer range, confirming the formation of nanobainite. In the steel containing Co and Al, transformation was very fast since these alloying elements accelerate the bainitic transformation.

(6) Hardness of the material decreases with the tempering time due to the increasing bainitic transformation. With respect to isothermal temperature, it has been found that the hardness decreases as the isothermal temperature is raised farther from the M_s temperature. However, beyond a certain value of the isothermal temperature, a further increase in the temperature results in an increase in the material hardness. This is due to the reducing volume fraction of bainite and a corresponding increase in the volume fraction of untransformed blocky austenite as the temperature approaches closer to the B_s temperature.

(7) From the compression tests it was concluded that different strain rates did not have a significant impact on the deformation behavior of the material. Further, it was found that Steel-2 has a good combination of strength and deformability. This is because of the fast bainitic transformation in this steel due to the presence of accelerating elements like Co and Al. While the large volume fraction of bainite contributes directly to the deformation ability of the steel, the fine microstructure in the nano-scale contributes to the strength of this steel. Additionally, due to the accelerated transformation in this steel, a large volume fraction of bainite can be obtained in a short isothermal transformation time.

(8) Three empirical correlation from the literature, relating hardness and yield strength, were applied to predict the yield strength of the current experimental data. It was observed that the

relative errors varied from 40% in the worst performing correlation to 14% in the best performing error.

(9) The thermostatistical model was validated with the experimental data on the volume fraction of retained austenite as well as volume fraction of ferrite which is obtained from XRD analysis. The neural network model for hardness was also evaluated with respect to the hardness data and it was able to predict the hardness of the present nanobainitic steels fairly accurately.

In summary, it can be stated that given the initial objective of developing computational tools to predict the bainitic transformation in terms of the volume fraction of bainite, analyze the microstructure and estimate material properties like hardness and yield strength, the models proposed in this thesis adequately address these requirements. The models have been well tested and can be applied with confidence to study isothermal heat treatment of bainitic steels.

8.2 Recommendations for Future Work

This thesis lays the foundations for the theoretical calculations for the kinetics of bainitic transformation and the mechanical properties of steels. The following aspects of this thesis could be studied further:

(1) Since Steel-2 undergoes a fast transformation, theoretical investigations can be initially conducted to determine an optimal chemical composition to minimize the transformation time as

well as cost of the alloying elements. This can be followed by an experimental investigation using the predicted optimal composition.

(2) The plate thickness in all three steels is in the nanometer range. This dimension is of interest due to superior quality of the material, in terms of its strength and toughness properties. Accordingly, the nanobainitc steel obtained after tempering can be investigated further for the microstructure characterization. In particular Transmission Electron Microscope (TEM) analysis can be conducted to study the microstructure of the bainitic steel that is in the nanometer range.

(3) The compression tests can be analyzed in further detail to understand the deformation and fracture mechanisms of the specimens and the existing theoretical models can be critically examined.

(4) Further mechanical testing can be conducted to understand the fracture toughness and fatigue properties of these nanobainitic steels to extend their applications.

Appendix A

Additional microstructures, verification of B_s and Dilatometry Curves

A.1 Verification of B_s Temperatures

As mentioned in Section 7.2 of Chapter 7, isothermal heat treatments were conducted at 200ºC, 250ºC, 300ºC and 350ºC. The SEM microstructures of the experiments at 200ºC and 300ºC are shown in Figure 7.17. The microstructures corresponding to the experiments at 250ºC and 350ºC are shown in Figures A1-A4. The experiments at 300ºC and 350ºC can be used to determine the accuracy of the theoretical B_s values of the three steels recorded in Table 7.1.

From Figures 7.17, A3 and A4, it is seen that in Steel-1 and Steel-3, there is evidence of bainitic transformation at 300ºC whereas there is no transformation at 350ºC. This implies that the theoretical B_s values of 309ºC and 302ºC for these two respective steels is close to 300ºC (taking into account a 3% experimental error). In case of Steel-2, there is evidence of bainitic transformation at 350ºC when the heat treatment is conducted for up to 96h (see Figure A4). However, at this temperature, for short isothermal transformation times (5h or so) there is only a very small fraction of bainite formation (see Figure A3). This is in contrast with the results at lower temperature (250ºC); where even for a short isothermal transformation time of 5h, there was a reasonable amount of bainite formation (See Figures A1). The small fraction at 350ºC and that too after prolonged heat treatment at 96h (Figure A4d) indicates that the temperature is close

to B_s value. Hence, it can be concluded that the theoretical B_s value of 358ºC must be fairly close to the true B_s temperature. It must be noted that the two temperature values (350ºC and 358ºC) are within 3% from each other.

(a) Steel 1, 5 h

(b) Steel-1, 48 h

(c) Steel-2, 5 h

(d) Steel-2, 48 h

(e) Steel-3, 5 h

(f) Steel-3, 48 h
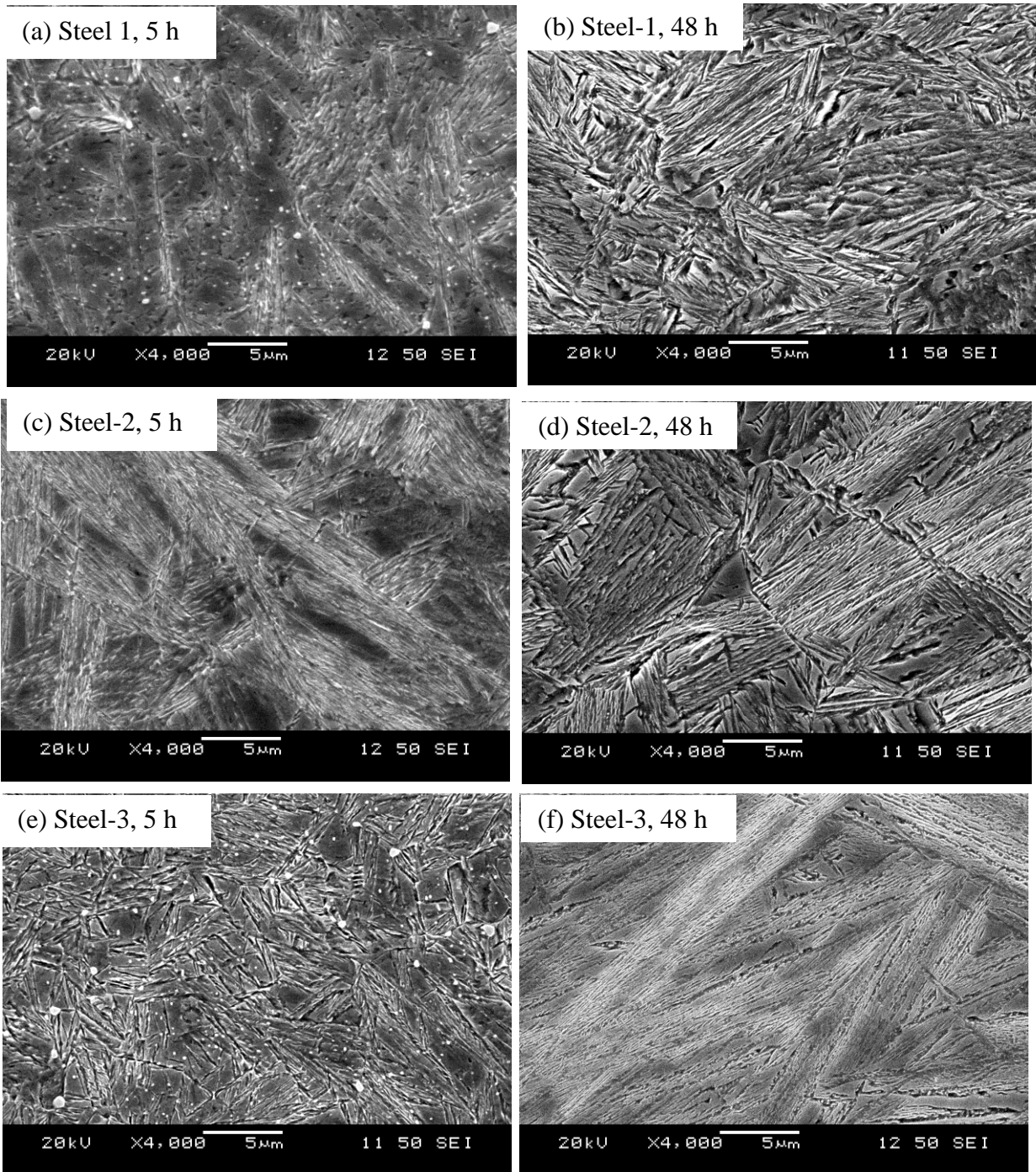
Figure A.1: SEM images of the three steels isothermally heat treated at 250°C.

(a) Steel 1, 144 h

(b) Steel-2, 144 h

(c) Steel-3, 144 h
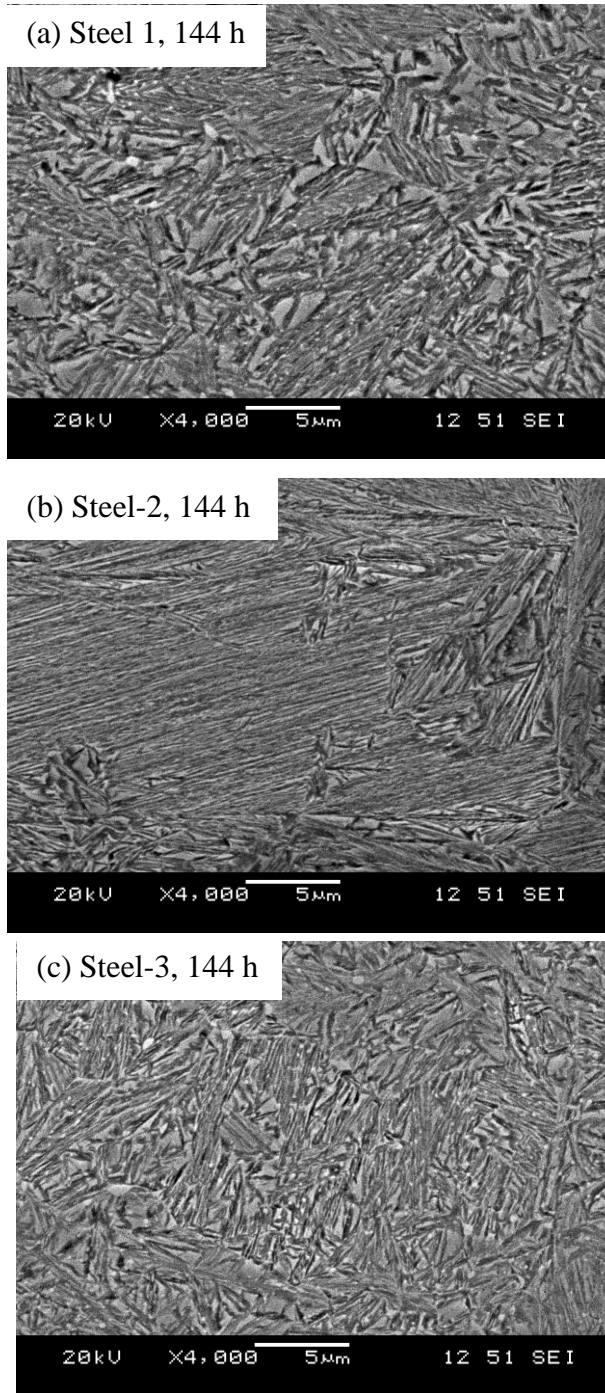
Figure A.2: SEM images of the three steels isothermally heat treated at 250 ℃.

(a) Steel 1, 5 h
20kV X4,000 5μm 11 50 SEI

(b) Steel-1, 24 h
20kV X4,000 5μm 12 50 SEI

(c) Steel-2, 5 h
20kV X4,000 5μm 11 50 SEI

(d) Steel-2, 24 h
20kV X4,000 5μm 11 50 SEI

(e) Steel-3, 5 h
20kV X4,000 5μm 13 51 SEI

(f) Steel-3, 24 h
20kV X4,000 5μm 12 51 SEI
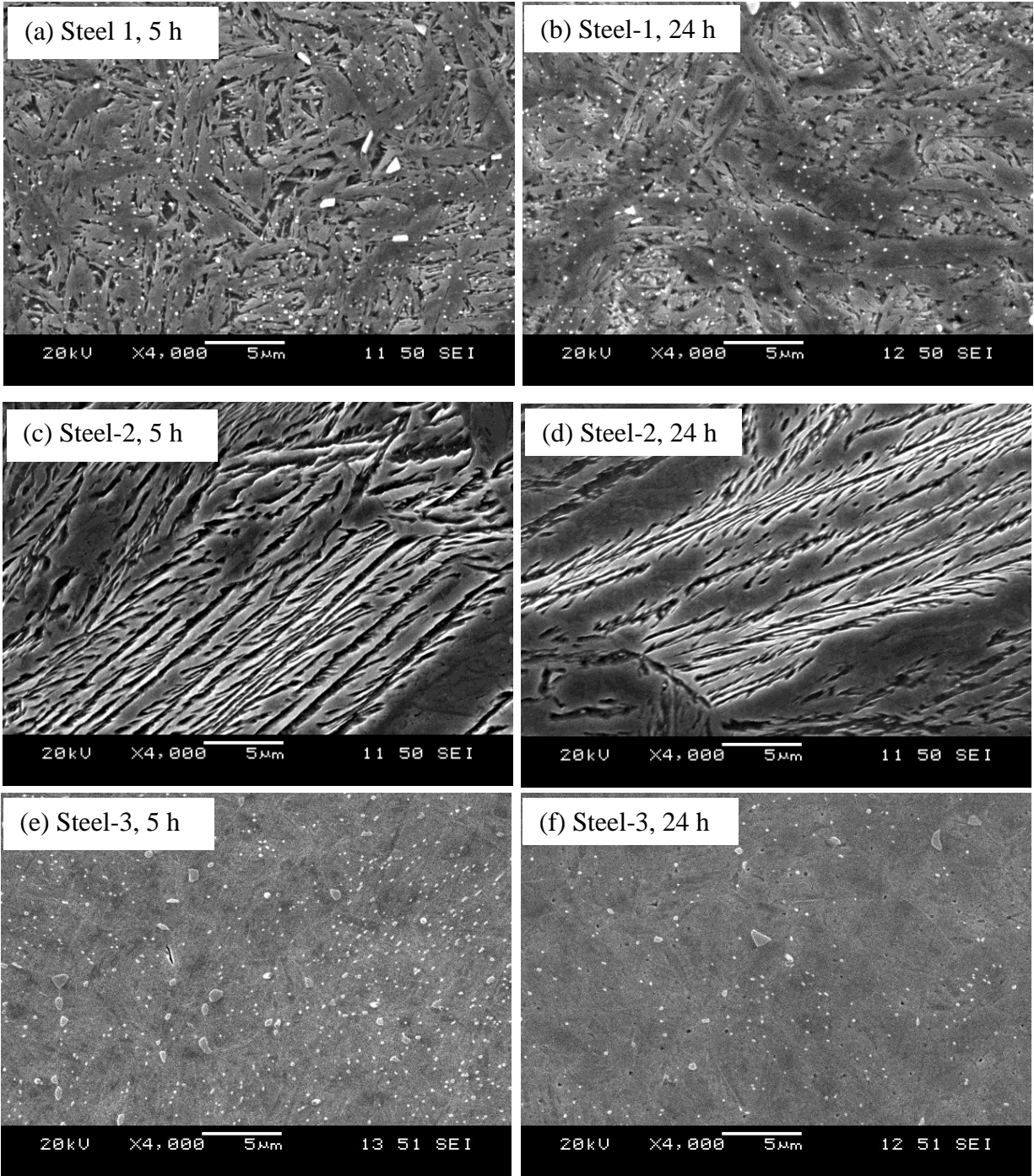
Figure A.3: SEM images of the three steels isothermally heat treated at 350℃.
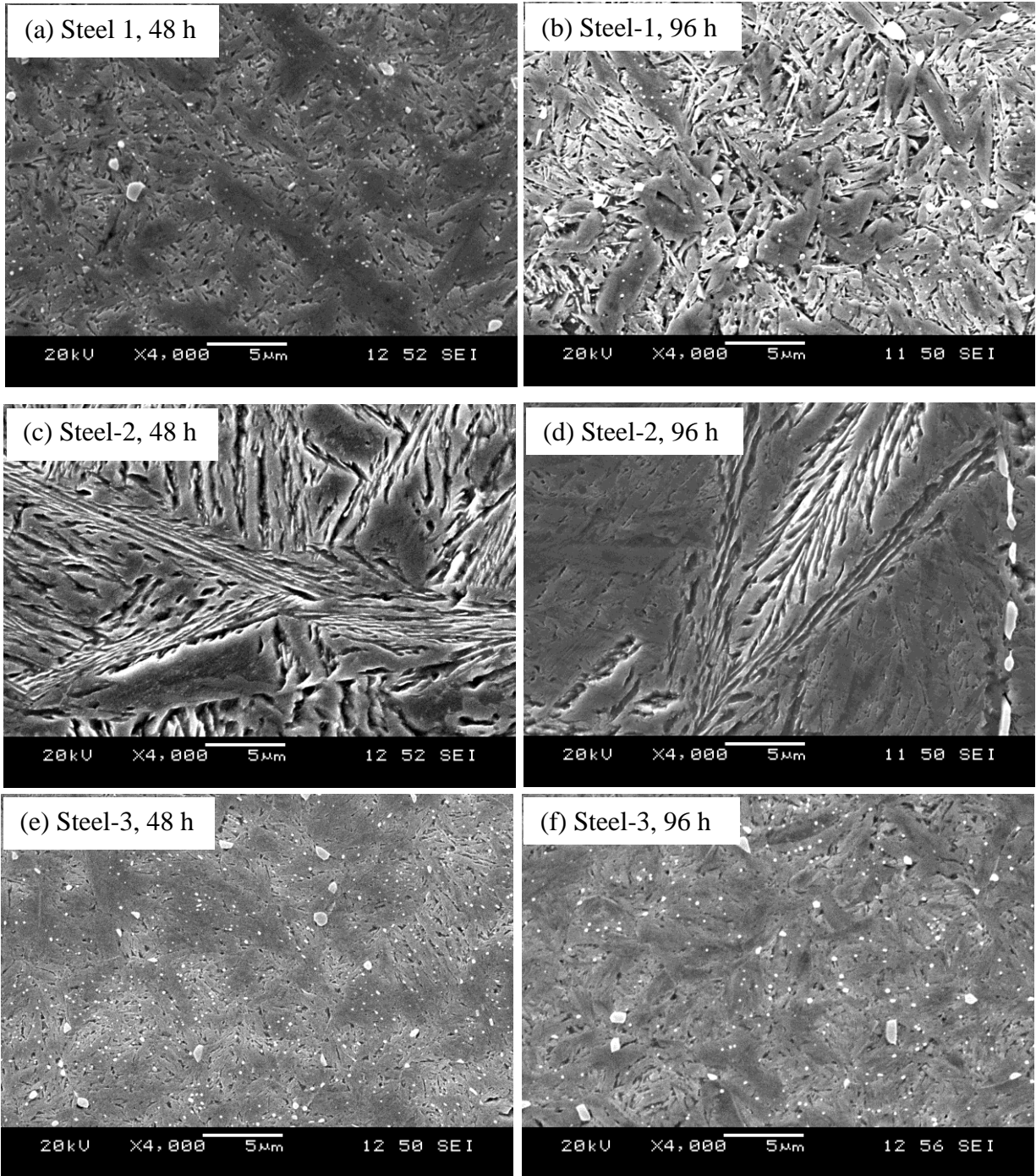
Figure A.4: SEM images of the three steels isothermally heat treated at 350°C.

A.2 Microstructures from Homogenization

(a) Steel 1

(b) Steel-2

(c) Steel-3
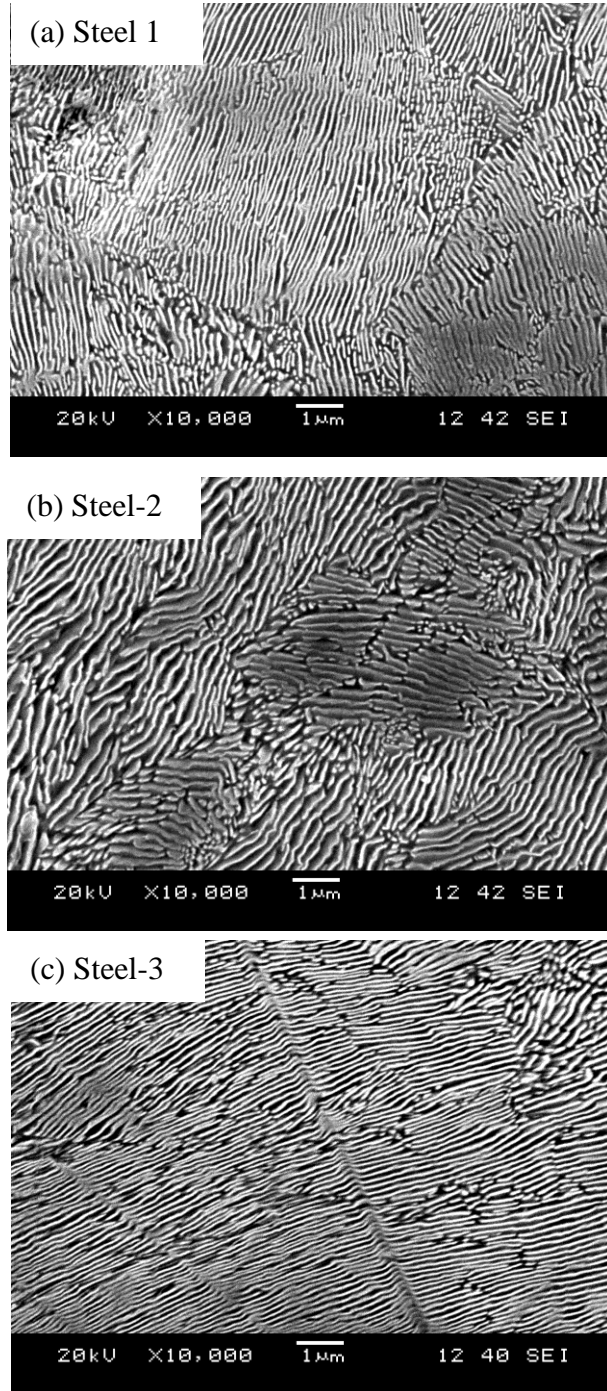
Figure A.5: SEM images of the three steels isothermally heat treated at 1200°C for 48h, indicating pearlite formation.

A.3 Dilatometry Curves
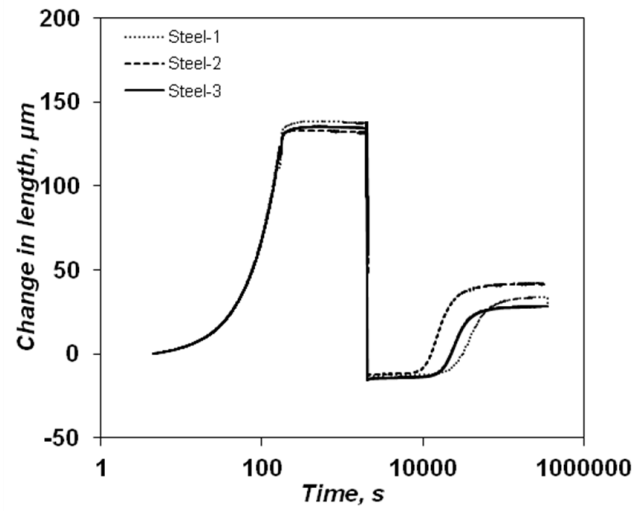
Figure A.6: Relative change in length for three steels at 250°C. Relative change in length in Steel-2 is much faster than the other two indicating a faster transformation.

Appendix B

A Fourier Method for Material Characterization at Micro, Nano and Angstrom Scales

B.1 Introduction

In this appendix, a new method based on the principles of Discrete Fourier Transform (DFT) [116] to study microstructure images in several applications to obtain the structural parameters is presented. The method presents several advantages: (a) it is fast, accurate and automated. (b) it does not require adjustment of image contrasts or colors. (c) in a non-uniform microstructure it is important to analyze the microstructure at various locations to get an accurate estimate of the average value of the microstructure parameter. In such cases, the application of the proposed method is quite time saving and fairly accurate.

The DFT based method can be employed to any image that exhibits a layered structure. For instance, it can be employed to obtain the interlamellar spacing (λ) in steels with a pearlitic microstructure or the plate thickness (t_p) from the microstructure of bainitic steels, lattice spacing (θ) in the selected area electron diffraction pattern of the ZnO nanorods in the semiconductor fabrication [117-119], etc.

B.2 Theoretical Foundation

The idea behind this approach is as follows: In the intensity images of microstructures of any material with layered structure, a narrow region appears as shown in the schematic in Figure B.1a. For example, in a microstructure of a pearlitic steel, the alternating dark and bright bands in this region (Figure B.1a) represent layers of ferrite (dark region) and cementite (bright region), respectively. Together they form the lamellar structure of pearlite. On the other hand, in bainitic microstructures, this region (Figure B.1a) represents adjacent bainitic plates, visible as bright bands, separated by the retained austenite (dark region).

Now, if scanning is done at the center of this image along the line shown in the schematic (Figure B.1a), a periodic pulse sequence of the intensity, similar to Figure B.1b is obtained. The length period (L) of the pulse corresponds to a frequency of f in the Fourier domain. More precisely, f is the frequency with which the pulse pattern repeats itself in the studied image. Now, depending upon the application, the interested in knowing either L or $L/2$. For instance, in a bainitic microstructure, the plate thickness is related to this frequency as $t_p=L/2=1/(2f)$. In pearlite, the interlamellar spacing, λ, is $\lambda=L=1/f$. In semiconductor fabrication, the lattice spacing, λ, is $\lambda=L=1/f$.

Mathematically, if the intensity recorded along the x direction in the line shown in Figure B.1a is denoted by the vector $\boldsymbol{i}$ with components $i(1), i(2), \ldots i(N)$, N being the number of pixels in the recorded line of the image, then a M-point Fourier transform of the intensity is

(a) (b) (c)
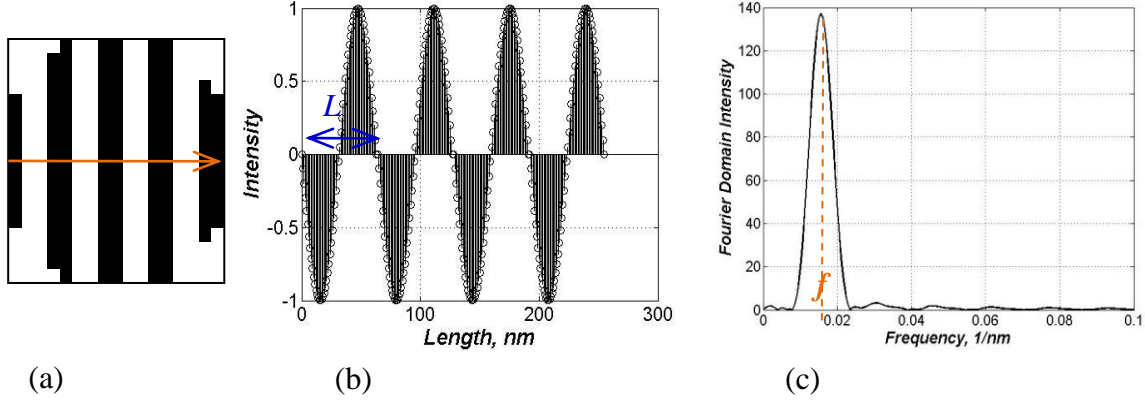
Figure B.1: (a) Schematic of a narrow region of a layered microstructure image. (b) The recorded intensity at the center of the image along the orange line in part (a) having a periodicity of L and (c) the DFT of this intensity, the frequency, f =1/L, in the Fourier domain corresponding to the oscillating intensity profile in (a).

$$I(m) = \sum_{n=0}^{N-1} i(n)e^{-j2\pi n m/N}, \quad m=1, 2, \ldots, M, \tag{B.1}$$

where $I(m)$ is the mth DFT output of the input vector $\boldsymbol{i}$. Further, the frequency resolution of the Fourier spectrum is $f_m=mf_s/N$, where, f_s is the sampling frequency, i.e., the number of pixels per unit length of the recorded image in the direction.

While the schematic in Figure B.1a represents a simple case for illustrative purposes, in practice, the thickness of the dark and bright regions in Figure B.1a can be different. For instance, in a bainitic microstructure, the thickness of retained austenite as well as the thickness of bainite plates can be different even in a small region of the microstructure. In such cases, the DFT of the intensity along the line at the center of the narrow region and in the direction orthogonal to the parallel plates (as before) will yield several distinct frequency peaks, f_k, in the Fourier domain (See Figure B.2a-B.2b). Assuming that the microstructure is composed of regions of this type,

the consequent periodic pattern is a summation of various sine and cosine functions. Put differently, the intensity profile of the microstructure image can be presented as a summation of two or more sinusoidal intensities as illustrated in the schematic in Figure B.2 (In this schematic, Figure B.2b is the sum of Figures B.2d and B.2f). The frequencies of these fundamental sinusoidal intensities (frequencies in Figure B.2d and Figure B.2f) are the relevant frequencies that determine the resulting microstructure.

Now, if there are p relevant frequencies, at which the Fourier intensity is reasonably high, then:

i) for a bainitic microstructure, the average plate thickness in this region can be calculated as

$$t_p = \frac{1}{p}\sum_{k=1}^{p}\frac{1}{2f_k}$$

(B.2)

ii) the interlamellar spacing in a pearlitic microstructure or the lattice spacing, λ, in semiconductor fabrication is

$$\lambda \text{ or } \theta = \frac{1}{p}\sum_{k=1}^{p}\frac{1}{f_k}.$$

(B.3)

Finally, keeping in mind the possibility of variations in the microstructure uniformity, it is appropriate to analyze several regions and determine the final value of t_p, λ, θ etc. as a statistical average of the calculations.

It must be noted that the accuracy of the method is likely to increase with M, the number of points in the DFT.
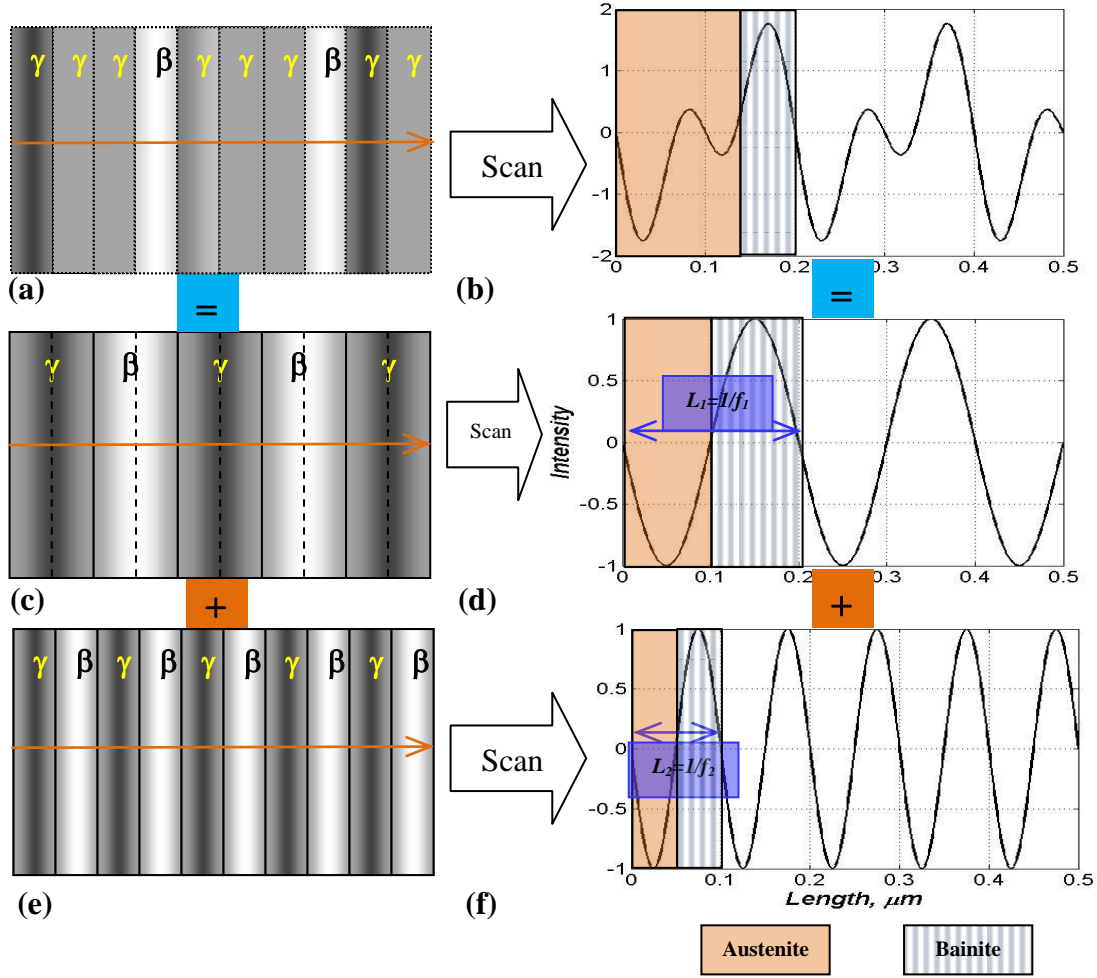
Figure B.2: An illustration of a lamellar structure with non-uniform dark and white region thickness as seen in a bainitic microstructure (γ is austenite region and β is bainite region).

The choice of a particular *M* for the investigated microstructures is discussed in the following section. Another factor that determines the accuracy of the method is the resolution of the original image. A higher resolution implies more information available for the same region and thereby more accurate processing.

B.3 Validation

The DFT approach presented above has been applied to the microstructures from different applications from the literature [45, 117-126] and illustrated for the steels with pearlitic and bainitic microstructures [45, 120-123] in Figure B.3. The Fourier spectrum of two sample regions randomly chosen in two pearlitic microstructures is shown in Figures B.3a and B.3b. Likewise, Figures B.3c and B.3d correspond to the Fourier spectrum of two bainitic microstructures. In these figures, the intensity peak at *f=0* corresponds to a background intensity level [116].

While in explaining the schematics, a rectangular window was used, applying a more appropriate windowing technique is necessary to minimize the spectral leakage and thereby the errors. Consequently, for the microstructures considered for the model validation in this section, Hamming window has been applied to the intensity values scanned from the microstructural images to minimize the maximum sidelobes and thereby the spectral leakage that can hinder the accuracy of the DFT output [116].

Also, in view of the fact that the number of points in the DFT spectrum can influence the accuracy, for each microstructure considered, the value of M for the M-point DFT was such that $M = 2^{a+4}$, where a is related to N (the number of pixels in recorded line scan of the image) as $2^a \geq N$. A larger M does not seem to have any further impact on the calculated results.
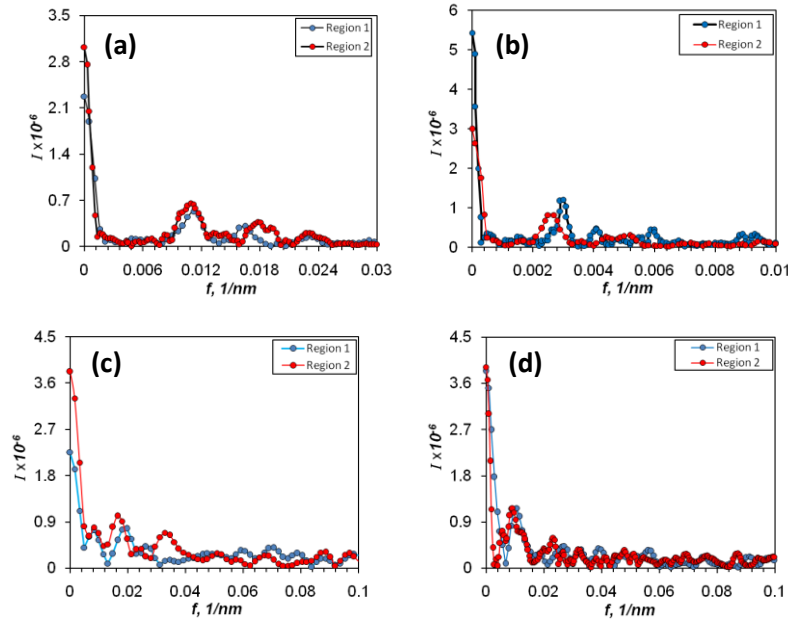
Figure B.3 DFT analysis of two pearlitic microstructures, viz., (a) Fig. 1b in [120], (b) Fig. 3a in [121], and two bainitic microstructures, viz., (c) Fig. 7 (bottom left) in [45] and (d) Fig. 4b in [123]. In each microstructure, analysis was done at various regions, two of which are shown for each experiment.

The microstructures analyzed, along with λ or t_p from the DFT method and the data from the literature are summarized in Table B.1.

The DFT values presented in this table have been obtained after analyzing five regions in each microstructure. Keeping in mind the uniformity of the microstructure in these cases, analysis of more regions is unlikely to impact the final average values significantly. Further, in Equations (B.2) and (B.3), a frequency, f_k, was included if the Fourier domain intensity at this frequency, I_k, was such that $I_k \geq 0.5\ I_{max}$, where I_{max} is the intensity of the most significant peak in the Fourier

Table B.1: Summary of the structural parameter values in various materials as calculated by the DFT method, in comparison with the data reported in the literature. The data in the literature are from the stereological method.

Length scale	Material	DFT value	Literature data	Source
Micron	Pearlite - Steels	0.208 μm	0.20 ± 0.03 μm	Ref. 120, Figure 1(a)
		0.073 μm	0.08 ± 0.01 μm	Ref. 120, Figure 1(b)
		0.239 μm	0.191 μm	Ref. 121, Figure 3(a)
		0.173 μm	0.177 μm	Ref. 121, Figure 3(b)
	Dendrites	2.7 μm	3.3 μm	Ref. 125, Figure 2(d)
Nanometer	Pearlite - Steels	49 nm	~50 nm	Ref. 122, Figure 3(a)
	Bainite - Steels	49 nm	<50 nm	Ref. 45, Figure 7 (bottom left)
		54 nm	49 ± 4 nm	Ref. 123, Figure 4(b)
	Polyethylene layer	10 nm	3-14 nm	Ref. 126, Figure 8(b)
	AlN layer	2.8 nm	2 nm	Ref. 124, Figure 3(a)
Angstrom	ZnO nanorods	5.5 Å	5.2 Å	Ref. 117, Figure 2(d)
	ZnO nanosheets	2.32 Å	2.67 Å	Ref. 118, Figure 2(c)
		2.93 Å	2.64 Å	Ref. 119, Figure 1(d)

domain. As seen in this table, in all cases, the proposed DFT method calculates λ or t_p fairly accurately.

The validation of the DFT method with respect to the other applications including, AlN layer thickness in solid state devices [124], ZnO nanorods and nanosheets in semiconductor fabrication [117-119], dendritic growths in composite materials [125], and polymer fabrication

[126], are also summarized in Table B.1. It clearly evident that the DFT method proposed in this study is able to predict the experimentally observed values fairly accurately. The disagreements between the present method and the experimental data are primarily due to the fact that the resolution of the images and the scale bars therein used for the validation of the present approach are those obtained from the published PDF articles.

Nevertheless, given that, even with such sources of inaccuracies, the method is able to quantitatively predict the structural parameters fairly accurately, the objective of realizing a simple, fast and reasonably accurate method to quantify the lamellar structures has been successfully achieved.

B.4 Summary

A simple DFT based method is proposed to study the structural parameters in the microstructural images of materials from various applications. The underlying principle is the fact that the optical intensity of the lamellar structure in narrow regions resembles a periodic pulse train. The discrete Fourier transform of such intensity yields wavelength-related frequencies from which the parameters of the lamellar structures at micro, nano and angstrom scales can be accurately determined. In addition to being fast and accurate, the method does not require any image manipulation such as brightness, contrast, binarization, etc. The method can be applied to several local regions in the microstructure to understand the general behavior of the structural parameters.

The method has been tested on structures that show a very simplistic and uniform variation as well as more complicated microstructures like that of pearlitic and bainitic steels. It has been shown to accurately evaluate the desired parameters in the investigated scales. The disagreements are attributed to the fact that the images obtained from the literature are from the PDF articles published online which lack high resolution. Nevertheless, given the excellent performance of this method, it has been employed in Chapter 7 to determine the plate thickness from the microstructural images of the heat treated bainitic steels in this thesis.

References

[1] H.K.D.H. Bhadeshia, Bainite in steels, IOM communications ltd, London, second edition, 2001.

[2] H.K.D.H. Bhadeshia, "New bainitic steels by design", Displacive phase transformations and their applications in Materials Engineering, eds K. Inoue, K. Mukherjee, K. Otsuka and H. Chen, *The Minerals, Metals and Materials Society*, Warrendale, Pennsylvania, U.S.A., 1998, pp. 69-78.

[3] H.K.D.H. Bhadeshia, and R.W.K. Honeycombe, Steels microstructure and properties, third edition, 2006.

[4] E.S. Davenport and E.C. Bain, "Transformation of austenite at constant subcritical temperatures", *Transactions of Metallurgical Society, AIME*, 90, 1930, pp. 117–144.

[5] E.C. Bain, Functions of the alloying elements in steel. American Society for Metals, Metals Park, Ohio, USA, 1939.

[6] A. Hultgren. *J. Iron Steel Inst.,* 114, 1926, pp. 421–422.

[7] J.M. Robertson, "The microstructure of rapidly cooled steel", *Journal of the Iron and Steel Institute*, 119, 1929, pp. 391–424.

[8] F.Z. Wever, "On the transformation in the case of the hardening of steel", *Metallkunde*, 1932, pp. 270.

[9] F. Wever and W. Jellinghaus, "Transformation kinetics of austenite .II. dilatometry investigations of austenite decomposition", Mitt.Kaiser–Wilhel Inst. Eisenforschung, 1932, pp. 14-85.

[10] K. Tsuzaki and T. Maki, "Some aspects of bainite transformation in Fe-based alloys", *Journal De Physique IV, Colloque C8, supplement au Journal de Physique III*, 5, 1995, pp. 61-70.

[11] M. Hillert, "Paradigm shift for bainite", *Scripta Materialia*, 47, 2002, pp. 175-180.

[12] J.R. Vilella, G.E. Guellich. and E.C. Bain, "On naming the aggregate constituents in steel", *Transactions of ASM*, 24, 1936, pp. 225–261.

[13] E.C. Bain, and H.W. Paxton, Alloying Elements in Steel, American Society for Metals, Cleveland, Ohio, 1966.

[14] H.K.D.H. Bhadeshia, and J.W. Christian, "Bainite in steels", *Metallurgical Transactions A*, 21, 1990, pp. 767–797.

[15] H.K.D.H. Bhadeshia, and D.V. Edmonds, "The Bainite transformation in silicon steel", *Metallurgical Transaction. A*, 10, 1979, pp. 895–907.

[16] H.K.D.H. Bhadeshia, and D.V. Edmonds, "Bainite in silicon steels: a new composition-property approach. Part I", *Metal Science*, 17, 1983, pp. 411–419.

[17] M. Takahashi and H.K.D.H. Bhadeshia, "Model for transition from upper to lower bainite", *Material Science and Technology*, 6, 1990, pp 592–603.

[18] H.I. Aaronson , The Decomposition of austenite by diffusional processes, ed. Zackay V F and Aaronson H I, Interscience Publishers, New York, 387-546, 1962.

[19] H.I. Aaronson, The Mechanism of Phase Transformations in Crystalline Solids, The Institute of Metals, London, 270, 1969.

[20] H.I. Aaronson, G. Spanos and W.T. Reynolds Jr, "A progress report on the definitions of bainite", *Scripta Materialia*, 47, 2002, pp.139-144.

[21] David Quidort and Yves J.M. Brechet, "A model of isothermal and non isothermal transformation kinetics of bainite in 0.5%C steels", *ISIJ International*, 42, no. 9, 2002, pp. 1010-1017.

[22] H.K.D.H. Bhadeshia, and D.V. Edmonds, "The Mechanism of Bainite Formation in Steels", *Acta Metallurgica*, 28, 1980, pp. 1265-1273.

[23] H.K.D.H. Bhadeshia, "BCC-BCC Orientation relationships, Surface Relief and Displacive Phase Transformations in Steel", *Scripta Metallurgica*, 14, 1980, pp.821-824.

[24] H.K.D.H. Bhadeshia, "A rationalization of shear transformation of steels", *Acta Metallurgica,* 29, 1981, pp. 1117-1130.

[25] J. Speer, D.K. Matlock, B.C. De Cooman, and J.G. Schroth, "Carbon partitioning into austenite after martensite transformation", *Acta Materialia*, 51, 2003, pp. 2611-2622.

[26] J.G. Speer, D.V. Edmonds, F.C. Rizzo, and D.K. Matlock, "Partitioning of carbon from supersaturated plates of ferrite, with application to steel processing and fundamentals of the bainite transformation", *Current Opinion in Solid State and Materials Science*, 8, 2004, pp. 219-237.

[27] B.C. Muddle and J.F. Nie, "Formation of bainite as a diffusional-displacive phase transformation", *Scripta Materialia*., 47, 2002, pp. 187-192.

[28] A. Saha, G. Ghosh, and G.B. Olson, "An assessment of interfacial dissipation effects at reconstructive ferrite-austenite interfaces", *Acta Materialia*, 53, 2005, pp. 141-149.

[29] C. Zener, "Kinetics of the decomposition of austenite", *Trans. AIME*, 167, 1946, pp. 50-595.

[30] C. Zener, "Equilibrium relations in medium–alloy steels", *Trans AIME*, 167, 1946, pp.513–534.

[31] F. Wever and H. Lange, "The transformation kinetics of austenite. I. magnetic investigations of the decomposition of austenite", *Mitt.Kaiser–Wilhelm Inst. Eisenforschung*, 14, 1932, pp. 71–83.

[32] G.I. Rees and H.K.D.H. Bhadeshia, "Bainite Transformation Kinetics, Part I, Modified Model, *Material Science and Technology,* 8, 1992, pp. 985-993.

[33] N. Chester and H.K.D.H. Bhadeshia, "Mathematical modeling of bainite transformation kinetics", *Journal de Physique IV, Colloque C5*, 7, 1997, pp. 41-46.

[34] S.B. Singh, Phase transformations from deformed austenite, Ph.D. Thesis, University of Cambridge, UK 1998.

[35] P. Opnedaker, The rate of the bainite transformation, Ph.D. Thesis, University of Cambridge, UK 2001.

[36] H. Matsuda and H.K.D.H. Bhadeshia, "Kinetics of bainitic transformation", *Proceeding Royal Society London A,* 460, 2004, pp. 1707-1722.

[37] S.M.C. Van Bohemen and J. Sietsma, "Modeling of isothermal bainite formation based on the nucleation kinetics", *International Journal Materials Research*, 7, 2008, pp. 739-747.

[38] S.M.C. Van Bohemen and J. Sietsma, "Kinetics of bainite and martensite formation in steels during cooling", *Material Science and Engineering A*, 527, 2010, pp. 6672-6676.

[39] Maria Jesus Santofimia, F.G. Caballero, C. Capdevila, C. Garcia-Mateo, and C. Garcia De Andres, "New model for all the overall transformation kinetics of bainite, part-1: the model", *Materials Transaction*, 47, 2006, pp. 2465-2472.

[40] Maria Jesus Santofimia, F.G. Caballero, C. Capdevila, C. Garcia-Mateo, and C. Garcia De Andres, "New model for all the overall transformation kinetics of bainite, part-2: validation", *Materials Transaction*. 47, 2006, pp. 2473-2479.

[41] Maria Jesus Santofimia, F.G. Caballero, C. Capdevila, C. Garcia-Mateo, and C. Garcia De Andres, "Evaluation of Displacive Models for bainite transformation kinetics in steels", *Materials Transaction* ,47, No.6, 2006, pp. 1492-1500.

[42] C. Garcia-Mateo, F.G. Caballero and H.K.D.H. Bhadeshia, "Development of hard bainite, *ISIJ International*, 43, No. 8, 2003, pp. 1238-1243.

[43] C. Garcia-Mateo, F.G. Caballero and H.K.D.H. Bhadeshia, "Acceleration of low temperature bainite, *ISIJ International,* 43, No. 11, 2003, pp. 1821-1825

[44] C. Garcia-Mateo, F.G. Caballero and H.K.D.H. Bhadeshia, "Mechanical properties of low temperature bainite", *Material Science forum*. 500-501, 2005, 495-502.

[45] F.G. Caballero, H.K.D.H. Bhadeshia, , K.J.A. Mawella, D.G. Jones, and P. Brown, "Very strong low temperature bainite", *Material Science and Technology*, 18, 2002, pp. 279-284.

[46] F.G. Caballero, C. Garcia-Mateo, C. Capdevila, and C. Garcia De Andres, "Advanced ultra high strength bainitic steels", *Materials and Manufacturing Processes*, 22, 2007, pp. 502-506.

[47] F.G. Caballero, M.K. Miller, S.S. Babu, and C. Garcia-Mateo, "Atomic scale observations of bainite transformation in a high carbon high silicon steel", *Acta Materialia*, 55, 2007, pp. 381-390.

[48] F.G. Caballero, C. Garcia-Mateo, M.J. Santofimia, M.K. Miller, and C. Garcia De Andres, "New experimental evidence on the incomplete transformation phenomenon in steel", *Acta Materialia*, 57, 2009, pp. 8-17.

[49] M. Peet, S.S. Babu, M.K. Miller and H.K.D.H. Bhadeshia, "Three-Dimensional Atom Probe Analysis of Carbon Distribution in Low-Temperature Bainite", *Scripta Materialia*, 50, 2004, pp. 1277-1281.

[50] L.C. Chang, "Bainite transformation temperatures in high-silicon steels", *Metallurgical and Material Transaction A*, 30, 1999, pp. 909-916.

[51] J. Gordine and I. Codd, "The influence of silicon up to 1.5 wt% on the tempering characteristics of a spring steel", *Journal of Iron and Steel Institute*, 1968, pp. 461–467.

[52] W. S. Owen, "Effect of silicon on the kinetics of tempering", *Transactions ASM*, 46, 1954, pp. 812–829.

[53] A.G. Alten and P. Payson. Transactions ASM, 45 (1953) 498–531.

[54] L. Zhu, D. Wu, and X. Zhao, "Effect of silicon content on the austenite decomposition", *Journal of Iron and Steel Research International*, 13, 2006, pp. 57–60.

[55] E. Kozeschnik and H.K.D.H. Bhadeshia, "Influence of silicon on cementite precipitation in steels", *Materials Science and Technology*, 24, No. 3, 2008, pp. 343–347.

[56] R.L. Houillier, G. Begin, and A. Dube, "A study of the particularities of austenite during the formation of bainite", *Metallurgical Transactions*, 2, 1971, pp. 2645–2653.

[57] H.K.D.H. Bhadeshia, "Bainite in silicon steels: new composition-property approach part 2", *Metal Science*, 17, 1983, pp. 420–425.

[58] J. Mahieu, Contribution to The Physical Metallurgy of Crash-resistant Galvanized TRIP-assisted Steel for Automotive Structures. PhD thesis, Ghent University, 2003.

[59] P.J. Jacques, E. Girault, A. Mertens, B. Verlinden, J. van Humbeeck, and F. Delannay, "The developments of cold-rolled TRIP-assisted multiphase steels. Al-alloyed TRIP-assisted multiphase steels", *ISIJ International*, 41, 2001, pp. 1068-1074.

[60] A. Mertens, P. J. Jacques, L. Zhao, S. O. Kruijver, J. Sietsma, and F. Delanna, "On the inuence of aluminium and silicon contents on the kinetics of bainite transformation of intercritical austenite", *Journal of Phys. IV*, 112, 2003, pp. 305-308.

[61] M. Bouet, J. Root, E. Es-Sadiqui, and S. Yue. In 40th MWSP conference proceedings, *Iron and Steel Society/AIME*. 36, 1998, pp. 675-684.

[62] M. Bouet, J. Root, E. Es-Sadiqui, and S. Yue. *Material Science Forum*, 284-286, 1998, pp. 319-326.

[63] G. Poulachen, M. Dessoly, C. Le Calvez, J.L. Lebrun, V. Prunet, and I.S. Jawahir, "An investigation of the influence of sulphide inclusions on tool-wear in high speed milling of tool steels", *Wear*, 250, 2001, pp. 334–343.

[64] G. King, R. A. Jarman, and P. Judson, "The effect of manganese and nickel on the room temperature tensile characteristics of ferritic weld metal," *Technical report, Thames Polytechnic Report*, April, 1989.

[65] J.R. Davis, editor. "Alloying: understanding the basics", ASM International, Materials Park, OH, first edition, December 2001.

[66] K. Sugimoto, N. Usui, M. Kobayashi, and S. Hashimoto, "Effects of volume fraction and stability of retained austenite on ductility of TRIP-aided dual phase steels", *ISIJ International*, 32, 1992, pp. 1311–1318.

[67] M. Takahashi and H.K.D.H. Bhadeshia, "A model for the microstructure of some advanced bainitic steels", *Transactions Japan Institute of Metals*, 32, 1991, pp. 689–696.

[68] H.K.D.H. Bhadeshia, "Review, Nanostructured bainite", *Proceeding Royal Society London A,* 466, 2010, pp. 3–18.

[69] K. He and D.V. Edmonds, "Formation of acicular ferrite and influence of vanadium alloying", *Material Science. and Technology*, 18, 2002, pp. 289-296.

[70] S.V. Parker: PhD thesis, Modeling of phase transformations in hot-rolled steels, University of Cambridge, UK 1997.

[71] A. Ali and H. K. D. H. Bhadeshia, "Nucleation of Widmanst¨atten ferrite", *Material Science and Technology*, 6, 1990, pp. 781-784.

[72] G. Sidhu, S.D. Bhole, D.L. Chen and E. Essadiqi, "An improved model for bainite formation at isothermal temperatures", *Scripta Materialia*, 64, 2011, pp. 73-76.

[73] M. Avrami, "Kinetics of phase change. I. General theory", *Journal of chemical Physics*, 7, 1939, pp. 1103-1112.

[74] M. Avrami, "Kinetics of phase change. II. Transformation-time relations for random distribution of nuclei", *Journal of Chemical Physcs*, 8, 1940, pp. 212-224.

[75] M. Avrami, "Kinetics of phase change. III. Granulation, phase change, and microstructure", *Journal of Chemical Physics*, 9, 1941, pp 177-184.

[76] J.W. Christian, The Theory of Transformations in Metals and Alloys, *part-1* (Pergamon press), 2002.

[77] H.K.D.H. Bhadeshia, www.msm.cam.ac.uk/map/steel/programs/mucg83.html; 1982.

[78] G. Sidhu, S.D. Bhole, D.L. Chen and E. Essadiqi, Reply to comments on "An improved model for bainite formation at isothermal temperatures", *Scripta Materialia,* 65, 2011, pp. 373-375

[79] S.M.C. Van Bohemen, "Modeling Start Curves of Bainite Formation", *Metallurgical and Material Transactions A*, 41, 2009, pp. 285-296.

[80] L.C. Chang, "Microstructures and Reaction Kinetics of Bainite Transformation in Si-rich Steels", *Material Science. and Engineering A,* 368, 2004, pp. 175-182.

[81] H.K.D.H. Bhadeshia, "Neural networks in materials science", *ISIJ International*, 39, 1999, pp. 966-979.

[82] J. Trzaska, A. Jagiello, L. A. Dobrzanski, "The calculation of CCT diagrams for engineering steels", *Archives of Materials Science and Engineering*, 39 , 2009, pp. 13-20.

[83] O. Tugrul, K. Yigit, "Predictive modeling of surface roughness and tool wear in hard turning using regression and neural network", *International Journal of Machine Tools and Manufacture* , 45 , 2005, pp. 467-479.

[84] N.B. Fredj, R. Amamou, "Ground surface roughness prediction based upon experimental design and neural network models", *International Journal of Advance Manufacturing Technology*, 31, 2006, pp. 24-36.

[85] A. Brahme, M. Winning, D. Raabe, " Prediction of cold rolling texture of steels using an Artificial Neural Network", *Computational Material Science*, 46, 2009, pp. 800-804.

[86] Hwang, Y. Chen, H. Huang, "Artificial intelligent analyzer for mechanical properties of rolled steel bar by using neural networks", *Expert Systems with Applications*, 37, 2010, pp. 3136-3139.

[87] J.C.F. Pujol, J.M.A. Pinto, "A neural network approach to fatigue life prediction", *International Journal of Fatigue*, 33, 2011, pp. 313-322.

[88] S.K. Singh, K. Mahesh, A.K. Gupta, " Prediction of mechanical properties of extra deep drawn steel in blue brittle region using Artificial Neural Network" , *Materials and Design*, 31, 2010, pp. 2288-2295.

[89] C. Capdevila, C. Garcia-Mateo, F.G. Caballero, C. Garcia de Andres, "Neural network analysis of the influence of processing on strength and ductility of automotive low carbon sheet steels", *Computational Material Science,* 38, 2006, pp. 191-201.

[90] J. Trzaska, L.A. Dobrzanski, "Application of neural networks for designing the chemical composition of steel with the assumed hardness after cooling from the austenitising

temperature", *Journal of material Processing and Technology*, 164-165, 2005, pp. 1637-1643.

[91] H. Monajati, D. Asefi, A. Parsapour, S. Abbasi, " Analysis of the effects of processing parameters on mechanical properties and formability of cold rolled low carbon steel sheets using neural networks", *Computational Material Science*, 49, 2010, pp. 876-881.

[92] T. Parthiban, R. Ravi, G.T. Parthiban, S. Srinivasan, K.R. Ramakrishnan, M. Raghavan, "Neural network analysis for corrosion of steel in concrete", *Corrosion Science*, 47, 2005, pp. 1625-1642.

[93] T. Rolich, I. Rezic, L. Curkovic, "Estimation of steel guitar strings corrosion by artificial neural network, *Corrosion Science*, 52, 2010, pp. 996-1002.

[94] M. Mukherjee, S.B. Singh, "Strain induced transformation of retained austenite in TRIP aided steels: a neural network model", *Materials and Manufacturing Processes*, 24, 2009, pp. 198-208.

[95] H.K.D.H. Bhadeshia, R.C. Dimitriu, S. Forsik, J.H. Pak, J.H. Ryu, "Performance of neural networks in materials science" , *Material Science and Technology*, 25 , 2009, pp. 504-510.

[96] R. Rojas, Neural Networks, Berlin: Springfer-Verlag; 1996.

[97] T. Suzuki, Y. Ono, G. Miyamoto, T. Furuhara, "Effects of Si and Cr on Bainite Microstructure of Medium Carbon Steels", *ISIJ International*, 50, 2010, pp. 1476-1482.

[98] O. Yakubovsky, N. Fonstein, C. Cheng, D. Bhattacharya, "Effect of alloying elements on mechanical properties and coatability of multi phase steels with ferrite-bainite and ferrite-bainite plus retained austenite microstructure", *Galvatech '04: 6th International Conference on Zinc and Zinc Alloy Coated Steel Sheet - Conference Proceedings*, 2004, pp. 547-558.

[99] H. Hillert, L. Hoglund, J. Agren, "Role of Carbon and Alloying Elements in the Formation of Bainitic Ferrite", *Metallurgical and Material Transactions A*, 35, 2004, pp. 3693-3700.

[100] N. Radovic, A. Koprivica, D. Glisic, A. Fadel, D. Drobnjak, " Influence of Cr, Mn and Mo on structure and properties of V microalloyed medium carbon forging steels", *Metalurgija*, 16, 2010, pp. 1-9.

[101] Vander Voort GF. Atlas of time temperature diagrams for irons and steels, editor, 1991.

[102] M.N.Yoozbashi, S. Yazdani, "Mechanical properties of nanostructured, low temperature bainitic steel designed using a thermodynamic model", *Material Science & Engineering A* 527, 2010, pp. 3200-3205.

[103] Zou Q, "Binary regression investigate on composition tempering temperature and hardness (HRC) of common steel", *Advanced Material Research* , 204-210, 2011,pp. 1362-1365.

[104] Standard test methods of Compression testing of metallic materials at room temperature, E9-09.

[105] W. Steven and A.G. Haynes, "The temperature formation of martensite and bainite in low alloy steels, *JISI*, 183, 1956, pp. 349-359.

[106] B.D. Cullity and S.R. Stock, Elements of X-ray diffraction. Upper Saddle River, NJ, third edition, 2001.

[107] Feng Hu and Kaiming Wu, "Isothermal transformation of low temperature super bainite", *Advanced Materials Research*, 146-147, 2011, pp. 1843-1848.

[108] Y.K. Lee, H.C. Shin, Y.C. Jang, S.H. Kim, C.S. Choi, " Effect of isothermal transformation on amount of retained austenite and its thermal stability in a bainitic Fe-3%Si-0.45%C-X steel", *Scripta Materialia*, 47, 2002, pp. 805-809.

[109] Cheng Liu, Zhenbo Zhao, S.D. Bhole, "Lathlike upper bainite in a silicon steel", *Material Science and Engineering A*, 43-34, 2006, pp. 289-293.

[110] O.O. Miller, "Influence of austenization time and temperature on austenite grain size of steel", *Transaction ASM*, 43, 1951, pp. 260–289.

[111] W. Sitek and L.A. Dobrzanski, "Application of genetic methods in materials design", J*ournal of Materials Processing Technology*, 164-164, 2005, pp. 1607–1611.

[112] H.K.D.H. Bhadeshia, "Matensite and bainite in steels: Transformation mechanism and mechanical properties", *Journal of Physics IV France,* 7, 1997, pp. C5-367-C5-376.

[113] S. Curtze, M. Kundu, V.T. Kuokkala, S. Datta and P.P. Chattopadhyay, "Dynamic properties of new generation high-strength steels for armoring applications", *Proceedings of the XI th Intern. Congress and Exposition*, June 2-5, 2008.

[114] P. Zhang, S.X. Li and Z.F. Zhang, "General relationship between strength and hardness", *Materials Science and Engineering A*, 529, 2011, pp. 62-73.

[115] E.J. Pavlina and C.J. Van Tyne, "Correlation of yield strength and tensile strength with hardness of steels", *Journal of Materials Engineering and Performance*, 17, 2008, pp. 888-893.

[116] R.G. Lyons, Understanding Digital Signal Processing, Addison Wesley Pub. Co., 1992.

[117] Xiurong Qu, Wen Wang, Wei Liu, Zhihua Yang, Xiaoming Duan, Dechang Jia, "The growth and optical property of ZnO rods evolved from layered basic zinc acetate in humid atmosphere", *Material Science Semiconductor. Processing,* 14, 2011, pp. 241-246.

[118] Jinghai Yang, Xue Li, Jihui Lang, Lili Yang, Maobin Wei, Ming Gao, Xiaoyan Liu, Hongju Zhai, Rui Wang, Yang Liu, Jian Cao, "Synthesis and optical properties of Eu-doped

ZnO nanosheets by hydrothermal method", *Material Science Semiconductor, Processing,* 14, 2011, pp. 247-252.

[119] D.D. Wang, G.Z. Xing, J.H. Yang, L.L. Yang, M. Gao, J. Cao, Y.J. Zhang, B. Yao, "Dependence of energy transfer and photoluminescence on tailored defects in Eu-doped ZnO nanosheets-based microflowers", *Journal of Alloys Compound,* 504, 2010, pp. 22-26.

[120] F.G. Caballero, C. Capdevila and C.G. de Andres, "Modeling of the interlamellar spacing of isothermally formed pearlite in a eutectoid steel", *Scripta Materialia,* 42, 2000, pp. 537-542

[121] J.Q. Xu, Y.Z. Liu and S.M. Zhou, "Calculation models of interlamellar spacing of pearlite in high speed 82B rod", *Journal of Iron and Steel Research*, 15, No. 4, 2008, pp. 57-60

[122] R. A. Jaramillo, S. S. Babu, G. M. Ludtka, R. A. Kisner, J. B. Wilgen, G. Mackiewicz-Ludtka, D. M. Nicholson, S. M. Kelly, M. Murugananth and H.K.D.H. Bhadeshia, "Effect of 30 Tesla magnetic field on transformations in a novel bainitic steel", *Scripta Materialia,* 52,2004, pp. 461-466.

[123] C. Garcia-Mateo, F.G. Caballero and H.K.D.H. Bhadeshia, "Low temperature bainite", *Journal de Physique IV*, 112, 2003, pp. 285-288.

[124] Youxing Yu, Yasuaki Hodumi, Ji Shi, and Yoshio Nakamura, "Effects of AlN layer thickness on magnetic anisotropy and transport phenomena of CoPt/AlN layered structures", *Vacuum*, 84, 2010, pp. 158-161.

[125] Jian Kong, Zhi-Tao Ye, Fang Lv, "Non-equilibrium solidification character of $Zr_{56.2}Ti_{13.8}Nb_{5.0}Cu_{6.9}Ni_{5.6}Be_{12.5}$ bulk metallic glass composites containing ductile dendrite phase", *Journal of Alloys Compound,* 478, 2009, pp. 202-205.

[126] F. Ania, F.J. Balta Calleja, R.K. Bayer, A.Tshmel, I. Naumann and G.H. Michler, "Comparative study of size and distribution of lamellar thicknesses and long periods in polyethylene with a shish-kebab structure", *Journal of Material Science,* 31*,* 1996, pp. 4199-4206.